Lithosphere

Structural analysis of the Valles Marineris fault zone: Possible evidence for large-scale strike-slip faulting on Mars

An Yin

Lithosphere 2012;4;286-330
doi: 10.1130/L192.1

Notes

Structural analysis of the Valles Marineris fault zone: Possible evidence for large-scale strike-slip faulting on Mars

An Yin*
DEPARTMENT OF EARTH AND SPACE SCIENCES AND INSTITUTE FOR PLANETS AND EXOPLANETS (iPLEX), UNIVERSITY OF CALIFORNIA, LOS ANGELES, CALIFORNIA 90095-1567, USA, AND STRUCTURAL GEOLOGY GROUP, CHINA UNIVERSITY OF GEOSCIENCES (BEIJING), BEIJING 100083, CHINA

ABSTRACT

Despite four decades of research, the origin of Valles Marineris on Mars, the longest trough system in the solar system, remains uncertain. Its formation mechanism has been variably related to rifting, strike-slip faulting, and subsurface mass removal. This study focuses on the structural geology of Ius and Coprates Chasmata in southern Valles Marineris using THEMIS (Thermal Emission Imaging System), Context Camera (CTX), and HiRISE (High Resolution Imaging Science Experiment) images. The main result of the work is that the troughs and their plateau margins have experienced left-slip transtensional deformation. Syntectonic soft-sediment deformation suggests the presence of surface water during the Late Amazonian left-slip tectonics in Valles Marineris. The total left-slip motion of the southern Valles Marineris fault zone is estimated to be 150–160 km, which may have been absorbed by east-west extension across Noctis Labyrinthus and Syria Planum in the west and across Capri and Eos Chasmata in the east. The discovery of a large-scale (>2000 km in length and >100 km in slip) and rather narrow (<50 km in width) strike-slip fault zone by this study begs the question of why such a structure, typically associated with plate tectonics on Earth, has developed on Mars.

LITHOSPHERE; v. 4; no. 4; p. 286–330. | Published online 4 June 2012. doi: 10.1130/L192.1

INTRODUCTION

Although the 4000-km-long Valles Marineris trough zone is the longest canyon system in the solar system (Fig. 1A), its origin remains elusive. The following hypotheses have been proposed: (1) rifting (e.g., Carr, 1974; Blasius et al., 1977; Frey, 1979; Sleep and Phillips, 1985; Masson, 1977, 1985; Banerdt et al., 1992; Lucchitta et al., 1992, 1994; Peulvast and Masson, 1993; Schultz, 1991, 1995, 1998, 2000; Mège and Masson, 1996a, 1996b; Schultz and Lin, 2001; Anderson et al., 2001; Mège et al., 2003; Golombek and Phillips, 2010), (2) subsurface removal of dissolvable materials or magma withdrawal (e.g., Sharp, 1973; Spencer and Fanale, 1990; Davis et al., 1995; Tanaka and MacKinnon, 2000; Montgomery and Gillespie, 2005; Adams et al., 2009), (3) massive dike emplacement causing ground-ice melting and thus catastrophic formation of outflow channels (McKenzie and Nimmo, 1999), (4) interaction among Tharsis-driven activity and an ancient Europe-sized basin (Dohm et al., 2001a, 2009), and (5) large-scale right-slip or left-slip faulting related to plate tectonics, lateral extrusion, or continental-scale megalandslide emplacement (Courtillot et al., 1975; Purucker et al., 2000; Anguita et al., 2001, 2006; Webb and Head, 2001, 2002; Bistacchi et al., 2004; Montgomery et al., 2009). Some combination of these processes and the role of preexisting weakness in controlling its developmental history have also been proposed (Lucchitta et al., 1994; Schultz, 1998; Borraccini et al., 2007; Dohm et al., 2009). The purpose of this study is to test the above models by analyzing satellite images across two of the longest and most linear trough zones in the Valles Marineris system: Ius Chasma in the west and Coprates Chasma in the east across the southern Valles Marineris region (Figs. 1B and 1C). As shown here, the two trough zones are dominated by trough-parallel normal and left-slip faults; left-slip zones are associated with en echelon folds, joints, bookshelf strike-slip faults, and thrusts typically seen in a left-slip simple shear zone on Earth. In total, this study indicates that the Valles Marineris fault zone is a left-slip transtensional system and its development was similar to that of the Dead Sea left-slip transtensional fault zone on Earth. The magnitude of the left-slip motion across the Valles Marineris fault zone is estimated to be ~160 km. The lack of significant distributed deformation on both sides of the Valles Marineris fault zone suggests that rigid-block tectonics is locally important for the crustal deformation of Mars.

*E-mail: yin@ess.ucla.edu.

DATA AND METHODS

Satellite Data

The main objective of this study was to use the shape, orientation, spatial association and crosscutting relationships to infer fault kinematics and the deformation history of the linear and continuous Ius-Melas-Coprates trough system in the southern Valles Marineris region (Fig. 1). To achieve this goal, the following data, available publically via web access at http://pds.jpl.nasa.gov, were used for reconnaissance and detailed mapping: (1) Thermal Emission Imaging System (THEMIS) satellite images obtained from the *Mars Odyssey* spacecraft with a typical spatial resolution of ~18 m/pixel (Christensen et al., 2000), (2) the Context Camera (CTX) images (spatial resolution of ~5.2 m/pixel), (3) High-Resolution Imaging Science Experiment (HiRISE) (spatial resolution of 30–60 cm/pixel) satellite images collected by the *Mars Reconnaissance Orbiter* spacecraft (Malin et al., 2007; McEwen et al., 2007, 2010), (4) Mars Obiter Camera (MOC) images from *Mars Global Surveyor* spacecraft with a spatial resolution of 30 cm/pixel to 5 m/pixel (Malin and Edgett, 2001), and (5) High-Resolution Stereo Camera (HRSC) satellite images obtained from the *Mars Express*

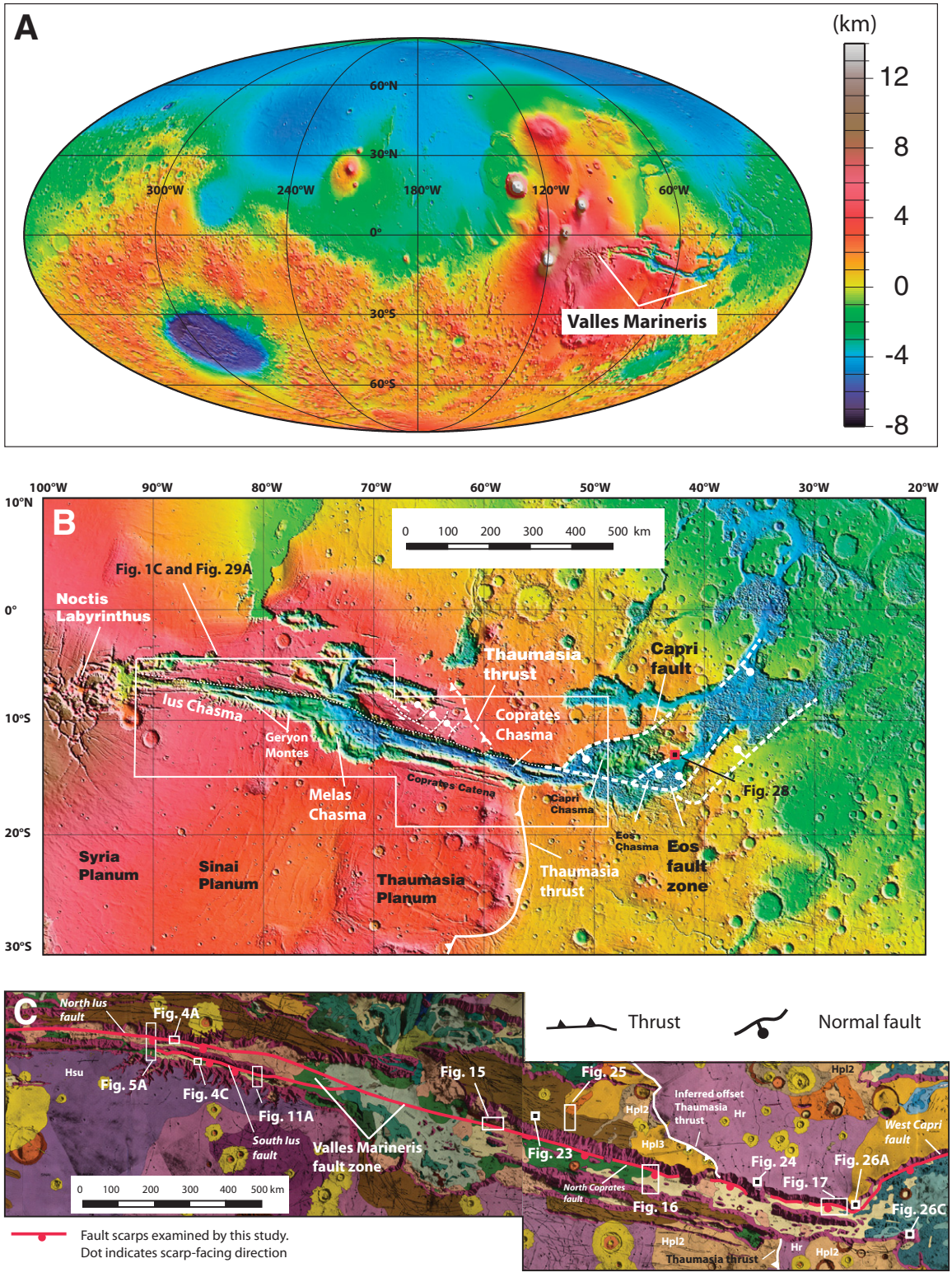

Figure 1. (A) Global topographic map of Mars and location of Valles Marineris. (B) Topographic map of Valles Marineris and locations of Figures 1C, 28, and 29A. The Ius-Melas-Coprates (IMC) trough zone is bounded by a continuous and nearly linear fault system at the bases of the trough walls. The fault system terminates at northeast-striking normal faults bounding Capri and Eos Chasmata in the east and a complexly extended region across Noctis Labyrinthus and Syria Planum. The Ius-Melas-Coprates trough zone also terminates the north-striking Thaumasia thrust in the south and may have offset the thrust to the north for 150–160 km in a left-lateral sense (see text for detail). Note that Melas Chasma is much wider and its southern rim is higher than the surrounding region. Also note that the eastern part of the Melas depression has a semicircular southern rim. (C) Geologic map of southern Valles Marineris from Witbeck et al. (1991). Locations of detailed study areas described in this study are also shown. Note that the location of the Thaumasia thrust, not mapped by Witbeck et al. (1991), is defined by the Hesperian plain deposits (units Hpl2 and Hpl3) in the west and the Hesperian wrinkle ridge terrane (unit Hr) in the east. This contact, truncated by the Ius-Melas-Coprates trough zone, corresponds to the Thaumasia thrust belt shown in Figure 1B.

spacecraft with a typical spatial resolution of ~12–13 m/pixel (Neukum et al., 2004). The utility of these data in planetary geologic mapping can be found in an excellent review by Schultz et al. (2010). Following the approach of Fueten et al. (2008, 2011) and Schultz et al. (2010), the THEMIS and HRSC images were used for reconnaissance to locate key regional structures. This was followed by the use of high-resolution CTX and HiRISE images for detailed mapping and structural analysis. Mapping on HRSC images has been carried out by geologists with the aid of HRSC digital terrain models (DTM) using ORION software available from Pangaea Scientific (http://pangaeasci.com/) (Fueten et al., 2005). This approach allows determination of attitudes of planar structural features such as bedding and faults (Fueten et al., 2006, 2008, 2010, 2011). Because mapping conducted in this study used mostly high-resolution CTX images, for which digital topographic maps are not widely available to the public, the "rule of V's" was applied for inferring the bed dip directions. This is a general practice of structural geologists mapping on Earth; it can be done because the shading of the images, particular with low incident angles of sunlight, provides a general sense of topography (i.e., locations of ridges and depressions) (Tanaka et al., 2009).

Photogeologic Mapping

Photogeologic mapping is inherently uncertain due to the lack of direct field checks. As such, it is important to separate observations from interpretations. To do so, each interpreted geologic map is presented in companion with an uninterpreted satellite image used for map construction. Key features are also marked on the uninterpreted images so that the readers can easily see how the suggested interpretations in this study were reached. In addition, assumptions and mapping criteria are listed when presenting geologic maps. Finally, the strengths and weaknesses of competing interpretations of the same set of observations are compared, and, when possible, their predictions for future investigations are discussed.

The mapping presented in this study focuses mainly on the trough-wall and trough-floor structures. Identifying structures on trough walls is difficult in places, as young talus deposits and screens of dusts obscure bedding attitudes. Mapping structures in Valles Marineris trough floors is equally challenging, as they are generally covered by young landslides and recent trough fills (mostly sand and dust deposits) (Witbeck et al., 1991; Quantin et al., 2004). Given that landslide emplacement, possibly triggered by impacts, climate change, and tectonics, can also generate faults and folds similar to those caused by tectonic processes involving deformation of the entire lithosphere (e.g., Okubo et al., 2008; Metz et al., 2010; Okubo, 2010), care must be taken to separate the two types of structures. Criteria used in this study for identifying, mapping, and characterizing tectonically induced features include: (1) structural features not restricted to a single unit, (2) deformation patterns that can be explained by a uniform stress field across the studied region with a sufficient arterial coverage (e.g., across a segment of the whole trough zone), and (3) structural patterns involving recent strata in the trough zones and their association with those observed in older bedrock of the trough walls and plateau margins.

Map Symbols

For map symbols in the geologic maps generated by this study, I followed the standard naming practice employed by the U.S. Geological Survey. Capital letters N, H, and A denote the geologic time of Noachian, Hesperian, and Amazonian during which the map units were deposited or emplaced. Units with lowercase names are informal, with the intention of being descriptive. For example, trough-fill, gully-fill, and surface deposits of dust and talus with unknown ages may be designated as units tf, gf, and sd. When two trough-fill units are mapped, subscripts "y" and "o" (i.e., tf_y, tf_o) are used to denote the younger and older fill units. For multiple landslides, subscripts of 1, 2, 3, …, are used to indicate the older-to-younger sequence (e.g., ls_1, ls_2).

Methods and Procedure of Structural Analyses

An important procedure in the structural analysis of folds adopted in this study is that the first-order structures at the scale of the trough width are mapped first. This is followed by systematic mapping of smaller secondary structures within the first-order features. For example, a large flexural-slip fold may contain numerous secondary parasitic folds, which typically fan out from the main fold axial plane (Fig. 2). In such a case, the trends of the secondary folds could differ significantly from that of the main fold axis. A statistic tabulation of all fold trends without a clear differentiation of their actual structural positions and size-order relationships could lead to grossly wrong interpretations, such as an inference of multiple phases of shortening under variable regional stress states. That approach is most effective for a simple structural system that formed under a single stress regime. However, for structures formed by superposition of several tectonic events under different stress regimes, a holistic approach of analyzing structures at various scales independently without assuming any genetic linkages was considered in this study.

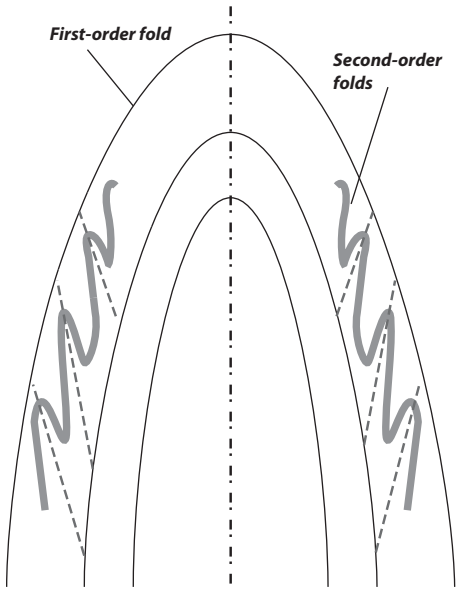

Figure 2. Relationship between trends of minor parasitic fold axes and the main fold axis. Note that the orientation of minor folds could vary as much as 90°. Thus, using fold trends for inferring regional shortening directions without a structural context can be misleading.

GEOLOGIC BACKGROUND

The formation of Valles Marineris started in the Late Noachian (Dohm and Tanaka, 1999; Dohm et al., 2001a, 2001b, 2009) and lasted after the end of the Hesperian (Schultz, 1998) or as late as the Late Amazonian (younger than 0.7 Ga) (Witbeck et al., 1991). The base of the trough walls is commonly marked by linear and high-angle escarpments interpreted as fault scarps (Sengör and Jones, 1975; Blasius et al., 1977; Witbeck et al., 1991; Lucchitta et al., 1992; Schultz, 1998) (Figs. 1B and 1C). Blasius et al. (1977) considered that the inferred faults may still be active as some of the scarps cut recent sediments and landslides. This argument was corroborated in a recent study by Spagnuolo et al. (2011).

The existing hypotheses for the origin of Valles Marineris may be divided into (1) those related to erosion, (2) those related to tectonic processes, and (3) those related to gravity-driven processes (Table 1). In the erosion models, the Valles Marineris trough system was induced by surface collapse via mass withdrawal from below (magma, ice, or carbonate rocks) (e.g., Sharp, 1973; Spencer and Fanale, 1990; Davis and Golombek, 1990; Tanaka and MacKinnon,

TABLE 1. EXISTING MODELS AND THEIR PREDICTIONS FOR THE ORIGIN OF VALLES MARINERIS (VM)

Model types	Erosion (submodels below)		Tectonics (submodels below)				Gravity-driven (submodels below)	
List of predicted features (below)	Collapse (Ref. 20–26)	Antecedent (This study)	Simple rift (Ref. 1–11)	Complex rift (Ref. 12–13)	Right-slip (Ref. 14–16)	Left-slip (Ref. 17–19)	Spreading (Ref. 18)	Megaslide (Ref. 19)
1. Relation btw troughs and faults	None	Could be related to preexisting joints	Steep trough-bounding faults	Steep trough-bounding faults	Vertical trough-bounding faults	Vertical trough-bounding faults	Vertical trough-bounding faults	Vertical trough-bounding faults
2. Fault or trough-edge geometry in map view	Highly irregular trough margins	N/A	Curvilinear, discontinuous, overlapping fault traces	Curvilinear, discontinuous, overlapping fault traces	Straight and continuous linear fault traces	Straight and continuous linear fault traces	Straight and continuous linear fault traces	Straight and continuous linear fault traces
3. Normal faulting	Locally developed	N/A	Only structures	Required	NW-striking en echelon normal faults	NE-striking en echelon normal faults	NE-striking en echelon normal faults	NE-striking en echelon normal faults
4. Strike-slip faulting	Not required	N/A	Not required	Not required	Required	Required	Required	Required
5. Along-strike variation of fault motion	Localized extension across collapse sites	N/A	Decrease laterally	Decrease laterally	Variable extension along releasing bends	Variable extension along releasing bends	Variable extension along releasing bends	Variable extension along releasing bends
6. Attitude of trough-margin beds	Inward dipping	Flat	Outward dipping due to rift-shoulder uplift	Inward tilt predating VM rifting	No need for bed tilt	No need for bed tilt	No need for bed tilt	No need for bed tilt
7. Secondary structures	Normal faults	N/A	Normal faults	Normal faults	Normal, reverse, strike-slip and folds	Normal, reverse, strike-slip and folds	Normal, reverse, strike-slip and folds	Normal, reverse, strike-slip and folds
8. Relation btw VM faults and NNE-trending grabens	Not required	Not required	Not required	Not required	Possible, with strike-slip faults as transfer structures	Possible, with strike-slip faults as transfer structures	Possible, with strike-slip faults as transfer structures	Not required
9. Relation between VM faults and Thaumasia thrust belt	No relation	No relation	No relation	No relation	VM faults must have outlasted thrusting	VM faults must have outlasted thrusting	VM faults terminate at thrust belt	VM faults terminate at thrust belt
10. Predict closed basins	Yes	No	No	No	Possible by forming pull-apart basins	Possible by forming pull-apart basins	Possible by forming pull-apart basins	Possible by forming pull-apart basins
11. Linking structures at ends of the VM trough zone	Not required	Not required	Not required as extension vanishes	Not required as extension vanishes	Fault zone terminates at NNE-trending contractional structures at two ends	Fault zone terminates at NNE-trending extensional structures at two ends	Fault zone terminates at NNE-trending extensional structures in the east and a thrust belt in the west	Fault zone terminates at NNE-trending extensional structures in the east and a thrust belt in the west

Note: References: (1) Blasius et al. (1977), (2) Masson (1977, 1985), (3) Frey (1979), (4) Wise et al. (1979), (5) Melosh (1980), (6) Plescia and Saunders (1982), (7) Lucchitta et al. (1992), (8) Peulvast and Masson (1993), (9) Schultz (1998), (10) Peulvast et al. (2001), (11) Schultz and Lin (2001), (12) Lucchitta et al. (1992), (13) Schultz (1998), (14) Courtillot et al. (1975), (15) Anguita et al. (2001), (16) Bistacchi et al. (2004), (17) Purucker et al. (2000), (18) Webb and Head (2002), (19) Montgomery et al. (2009), (20) Sharp (1973), (21) Spencer and Fanale (1990), (22) Davis and Golombek (1990), (23) Tanaka and MacKinnon (2000), (24) Montgomery and Gillespie (2005), (25) Adams et al. (2009), and (26) Jackson et al. (2011).

2000; Montgomery and Gillespie, 2005; Adams et al., 2009; Jackson et al., 2011) or development of an antecedent drainage system. The tectonic hypotheses may be divided into (1) the right-slip model (Courtillot et al., 1975; Anguita et al., 2001; Bistacchi et al., 2004) (Fig. 3A), (2) the left-slip model (Purucker et al., 2000; Webb and Head, 2002; Montgomery et al., 2009) (Fig. 3B), (3) the simple-rift model (e.g., Blasius et al., 1977; Masson, 1977, 1985; Frey, 1979; Wise et al., 1979; Plescia and Saunders, 1982; Lucchitta et al., 1992; Peulvast and Masson, 1993; Schultz, 1998; Peulvast et al., 2001; Schultz and Lin, 2001) (Fig. 3C), and (4) the complex-rift model (i.e., the ancestral basin model) (see Lucchitta et al., 1992; Schultz, 1998). Finally, the gravity-driven hypotheses consist of (1) the thick-skinned gravitational spreading model of Webb and Head (2001, 2002) and (2) the thin-skinned megalandslide model of Montgomery et al. (2009).The contrasting predictions by the competing models for the development of the Valles Marineris trough zone are summarized in Table 1.

The 2400 km linear trough zone consisting of Ius-Melas-Coprates Chasmata is the most dominant feature in southern Valles Marineris (Fig. 1B). Overall, the elevation of the trough zone floor decreases from west to east. Ius Chasma has two linear subtrough zones separated by a linear ridge. The central ridge terminates in the westernmost part of Ius Chasma where two subtrough zones merge. In the east, the central ridge terminates at much wider Melas Chasma. The overall width of Ius Chasma increases gradually eastward. Melas Chasma has an irregular southern margin marked by two spoon-shaped scarps; the eastern scarp is about two times wider than that in the west. The trough-floor elevation of Melas Chasma decreases northward, reaching the maximum depth against the broadly curved northern trough margin (Fig.1). Coprates Chasma is the longest linear trough zone in Valles Marineris. Its width decreases systematically from west to east, opposite to the width-variation trend of Ius Chasma. Discontinuous and trough-parallel linear ridges with various lengths are present within the trough zone (Fig. 1).

GEOLOGY OF IUS CHASMA

Trough-Bounding Structures

The Geryon Montes separate Ius Chasma into the northern and southern trough zones. Two

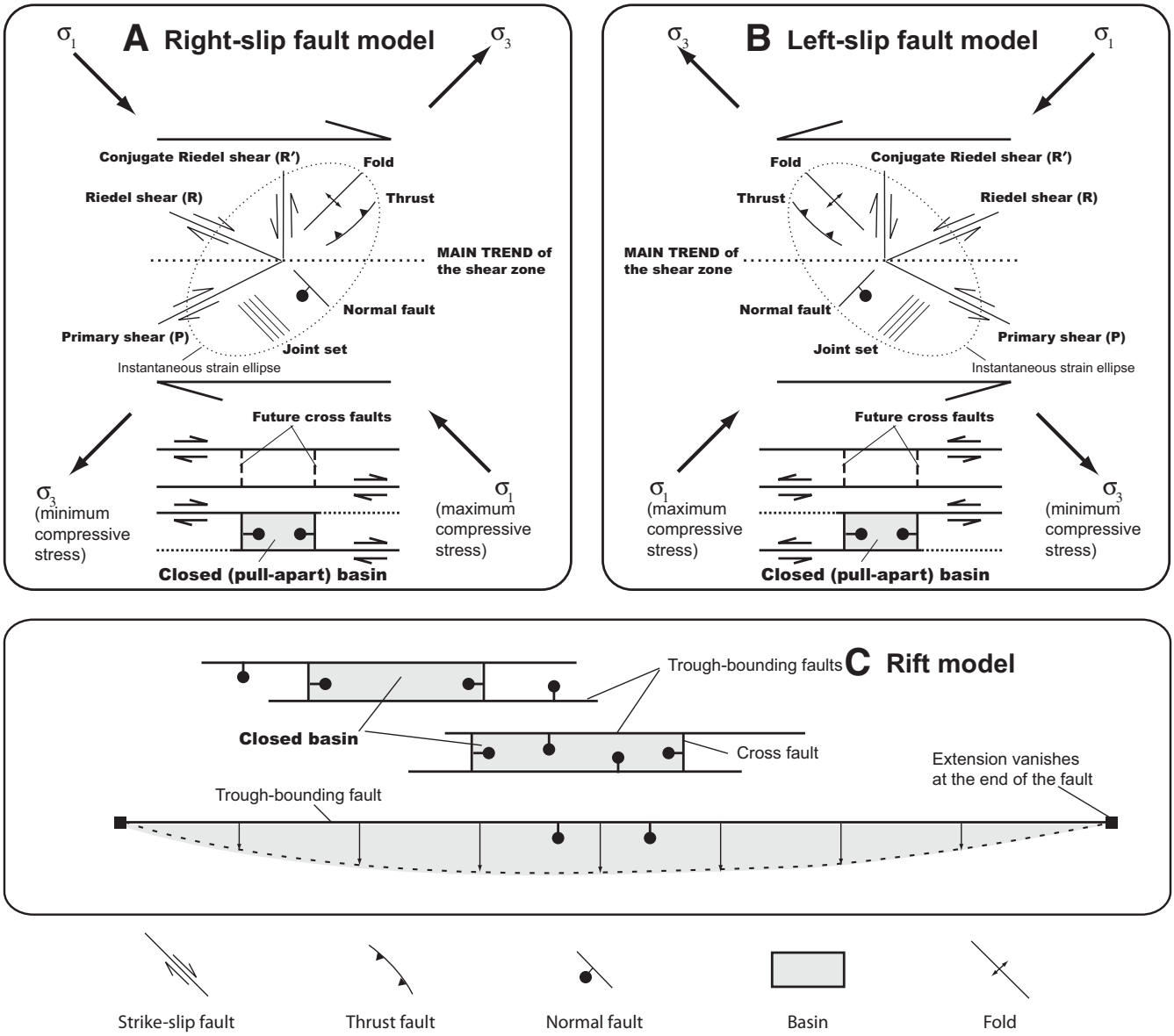

Figure 3. Three end-member structural models for the formation of Valles Marineris and their predicted structural associations and basin development: (A) right-slip fault zone model, (B) left-slip fault zone model, and (C) rift zone model. Note that box-shaped closed basins may be explained as pull-apart basins in strike-slip fault models, whereas the rift model requires orthogonal development of coeval normal faults. Symbols σ_1 and σ_3 represent the maximum and minimum compressive-stress directions.

main linear traces of escarpment were mapped along the north side of the two subtrough zones by Witbeck et al. (1991) (Fig. 1C). Along the north-wall base of the northern subtrough, the linear escarpment typically truncates spurs and gullies and is expressed by prominent rocky cliffs with their bases covered by unconsolidated talus cones. This can be seen from a CTX image (CTX: B03_010713_1739_XN_06S082W) shown in Figures 4A and 4B. The talus cones commonly exhibit multiphase slump structures with sharp semicircular breakaway scarps in the upslope source regions and crescent-shaped toes at the downslope distal edges (Fig. 4B). Head scarps are mostly buried by younger talus deposits coming from above, leaving the toes of the older slumping structures sticking out at the base of younger talus slopes (Fig. 4B).

Some of the debris flows coming out of the channel together with large fan deposits at the base of the escarpment are cut by fault scarps (see the lower-right corner of Fig. 4B). The young fault scarp in turn is buried by younger slump structures to the west (Fig. 4B). Since sediments cut by the fault scarp appear unconsolidated, the scarp marking the trace of a trough-bounding fault may be still active, as postulated by the classic study of Blasius et al. (1977). Because no strike-slip offsets are apparent across local short fault scarps and the regional escarpment, the trough-bounding structure of this segment of Ius Chasma appears to be a normal fault.

A prominent escarpment is also well developed along the base of the north wall of the southern subtrough, as seen from a CTX image (CTX: P12_005795_1730_XI_07S082W) in Figure 4C. Landslides and talus deposits were derived from spurs, whereas long-runout debris flows originated from canyons cutting the trough wall. These deposits were emplaced onto the trough floor, which is dominated by consolidated layered sediments (Fig. 4C). The

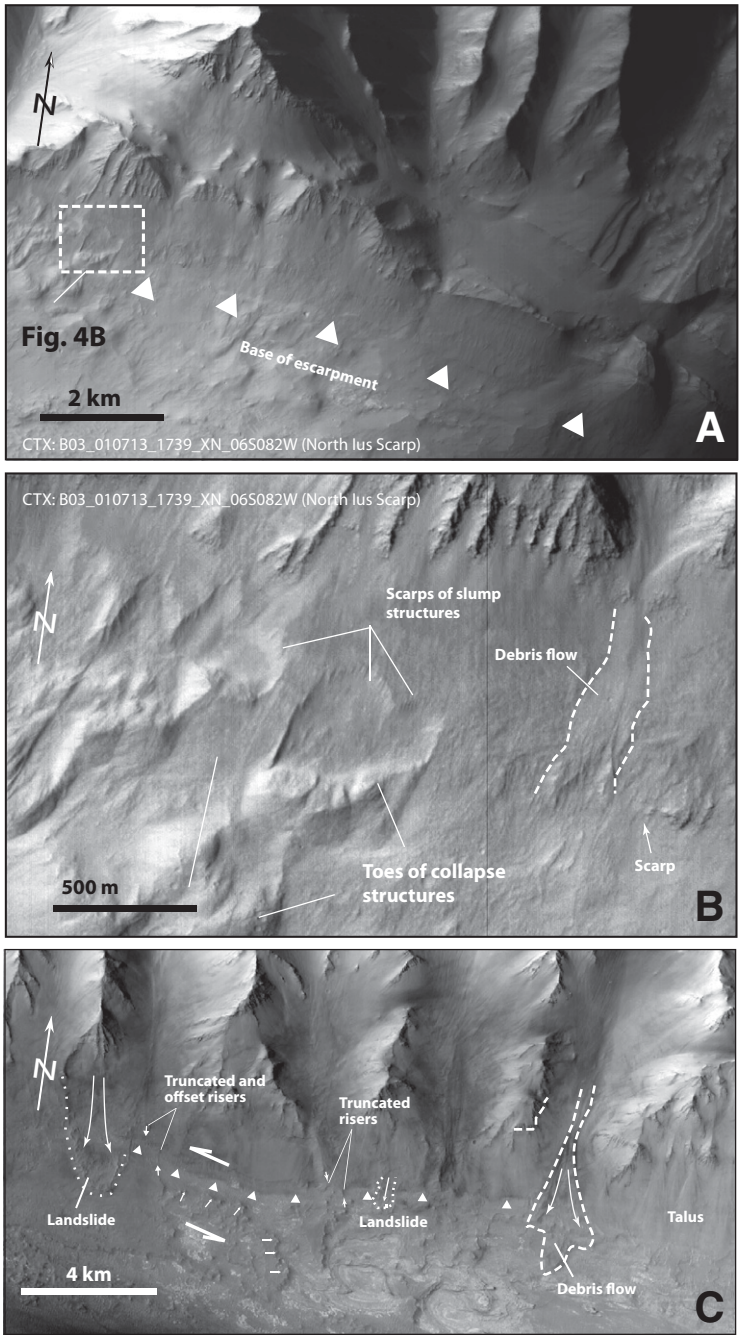

Figure 4. (A) Context Camera (CTX) image B03_010713_1739_XN_06S082W shows a linear scarp bounding the north trough wall of the northern Ius subtrough zone. The location of the escarpment is marked by white triangles. See Figure 1C for location. (B) Close-up view of scarps at the base of the north wall of the northern Ius subtrough zone. Numerous recent slump structures are present on talus slopes. Their presence requires the operation of geologic processes that have continuously built up the basal talus slope, causing it to exceed the angle of repose periodically and thus occurence of slumping. Alternatively, slumping may have been triggered by seismic activity on nearby faults. (C) Context Camera (CTX) image P12_005795_1730_XI_07S082W shows a linear topographic scarp bounding the north trough wall of the southern Ius subtrough zone. See Figure 1C for location. Two south-flowing channels display steep risers on the west sides that are truncated and offset left laterally by the escarpment. The offset risers are indicated by white arrow pairs pointing in opposite directions. Also note that the highly eroded drainage channel on the trough floor has an apparent left-lateral deflection, curving progressively eastward from north to south. The south side of this inferred channel is marked by a series of thin and long white arrows. Several landslides originating from the north trough wall overlie the trace of the escarpment, indicating that the formation of the escarpment predates the emplacement of the landslides.

landslides and debris flows appear to be much older than those seen in the northern subtrough in that their surfaces are highly incised and irregular in comparison to the smooth surfaces seen in the northern subtrough (cf. Fig. 4B). Because the sunlight was shed from the left side of the image in Figure 4C, the left banks of canyons on the trough wall and trough floor are well defined by the shade (Fig. 4C). The banks of the trough-wall canyons are nearly linear, whereas the banks of the trough-floor canyons have rather irregular shapes (thin white arrows in Fig. 4C). An interesting observation is that the west banks of linked trough-wall and trough-floor canyons are not continuous but appear to be offset by the basal escarpment (indicated by thick white arrows in Fig. 4C). If the trough-floor canyon banks (i.e., risers as defined in tectonic geomorphology; see Burbank and Anderson, 2001) were once continuous and linear, the misalignment of the trough-wall and trough-floor risers may indicate a left-slip sense of offset along the trough-bounding fault. Alternatively, the trough-floor canyons may have originated by a different mechanism such as wind erosion rather than flowing water. The third possibility is that the trough-wall and trough-floor canyons were parts of a large drainage system. In this case, stream channels bend westward coming out of the mountain range as a result of tributaries merging with the eastward-flowing main stream along the axis of the trough floor; this may have caused an apparent left-lateral stream deflection (e.g., Burbank and Anderson, 2001). This latter explanation seems unlikely because the discontinuities of canyon banks are abrupt and occur at the exact location of the escarpment. Also, the truncation of the canyon banks by the escarpment is consistent with the presence of a fault offsetting the risers. The fault-offset interpretation implies ~500 m of left-slip motion after the formation of the risers as seen from two canyon systems (Fig. 4C). As debris flows and landslides are not offset by the escarpment (i.e., the trough-bounding fault), the inferred left-slip fault motion must have occurred before the emplacement of these units.

Trough-Floor Structures: The Western Traverse

In order to understand the structural evolution of Ius Chasma, two traverses were mapped via photogeologic analysis across the trough zone. The eastern structural transect is ~45 km long in the north-south direction and ~30 km wide in the east-west direction (Fig. 5A). This overall trough zone is bounded by flat plateau margins in the north and south. In detail, it is

divided by the Geryon Montes into the northern and southern subtrough zones (Fig. 5A). The northern subtrough floor exposes a large landslide complex derived from the north trough wall in the north and a narrow strip of layered trough-fill sediments in the south. The southern subtrough exposes several smaller landslides that were originated from the south trough wall and layered trough-fill strata display a northwest-trending fold complex associated with complex minor secondary and tertiary folds (see details in the following sections). The geology of the northern and southern subtrough zones is described separately later herein.

Northern Subtrough Zone

A narrow strip of thinly bedded unit (gf_o in Figs. 5B and 5C) lies in the north across a transition zone between the north trough wall and the main landslide (unit As of Witbeck et al., 1991). To the south, a narrow strip of folded trough-fill strata is exposed along the southern margin of the northern subtrough (units Atf_1 and Atf_2 in Figs. 5B and 5C). Unit gf_o is separated from the main landslide by a zone of unconsolidated and fine-textured unit (sd_y in Figs. 5B and 5C). This unit is interpreted as surface deposits of windblown dust and talus. Beds in unit Atf_2 are composed of flat-lying, light-toned layers that can be traced into two deep-cut valleys across the south wall (Figs. 5B and 5C). This relationship suggests that unit Atf_2 lies depositionally on top of preexisting topography of the south wall. Embayment relationships indicate that folded strata of unit Atf_1 are younger than the mapped landslide complex (unit As in Figs. 5B and 5C). Thus, landslide emplacement predated deposition of unit Atf_1 and folding.

Trough-floor structures. In order to decipher the effect of tectonic deformation across the northern trough zone, one must first establish the primary structures related to the emplacement of the large landslide complex. For landslides that occur in Valles Marineris without postemplacement deformation, their surfaces commonly display continuous grooves and ridges with rounded geometry in cross-section views (e.g., Lucchitta, 1979; also see fig. 6a *in* Barnouin-Jha et al., 2005). Fractures associated with emplacement of landslides typically trend perpendicular to the landslide transport directions (see fig. 2 *in* McEwen, 1989). In contrast to these expectations, the northeast-trending and north-northeast–trending ridges with rounded morphology within the landslide block are highly broken and are systematically cut by northwest-trending fractures. In addition to having rounded top morphology (Figs. 6A–6D), the interpreted primary ridge surfaces exhibit characteristic (1) rough surface morphology possibly induced by erosion

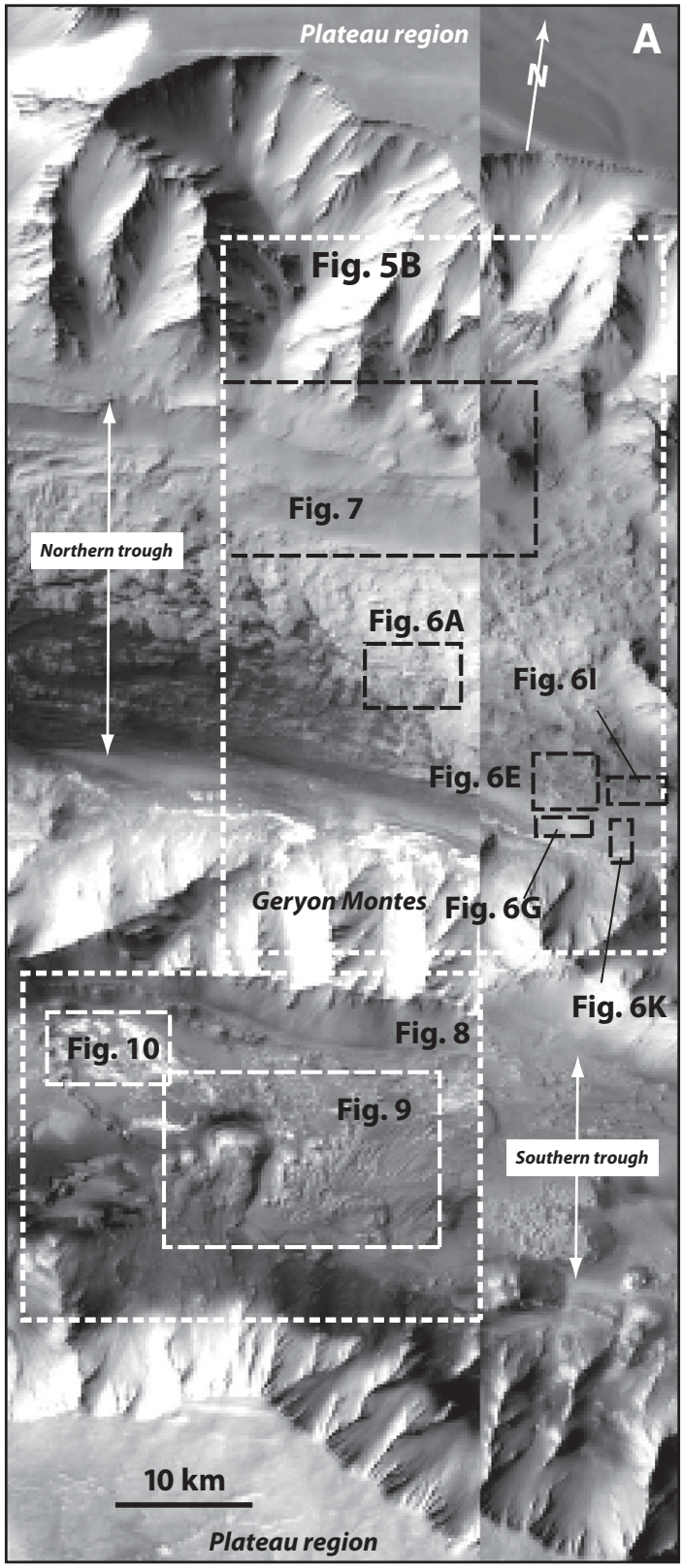

Figure 5. (A) Index map across a segment of western Ius Chasma based on Context Camera (CTX) image P05_002815_1720_XN_08S084W. The Ius trough can be divided into the northern and southern subtrough zones divided by the Geryon Montes. See Figure 1C for location. (*Continued on following page.*)

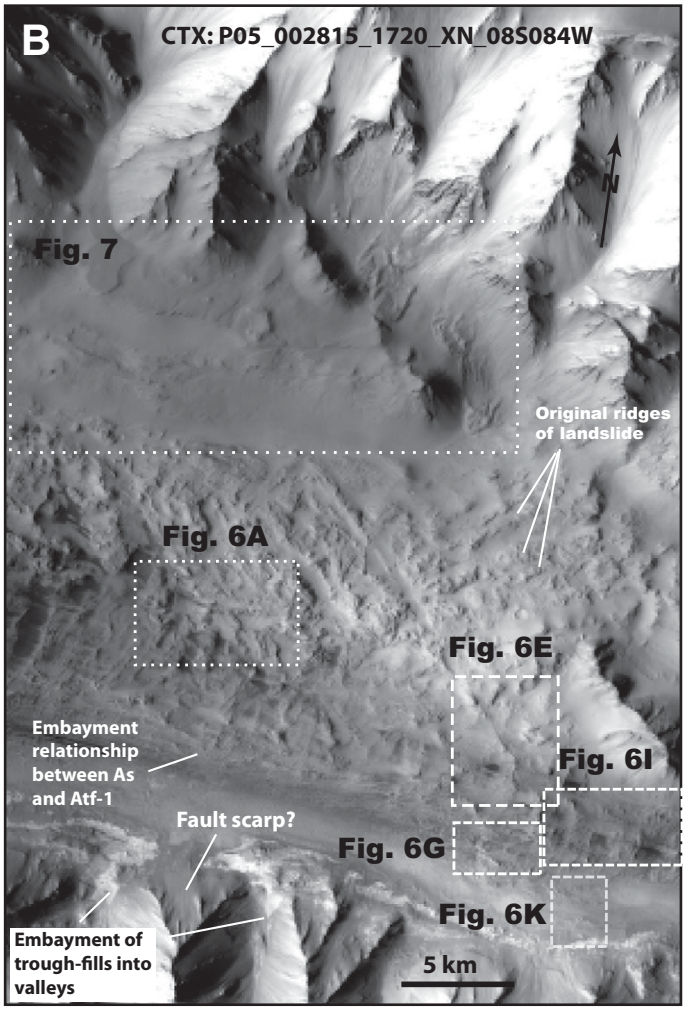

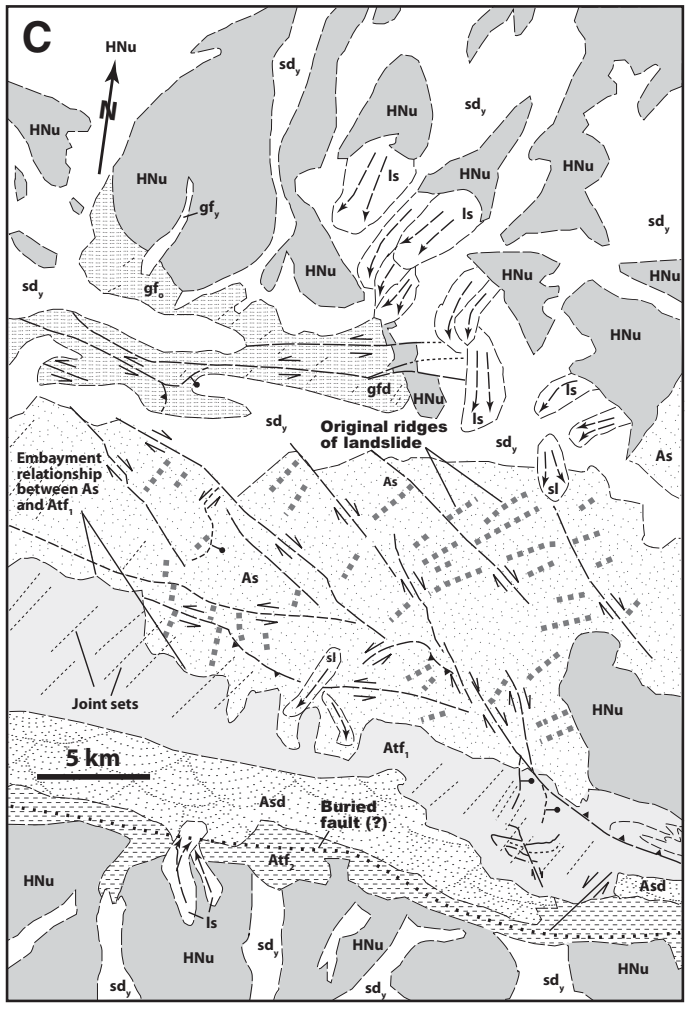

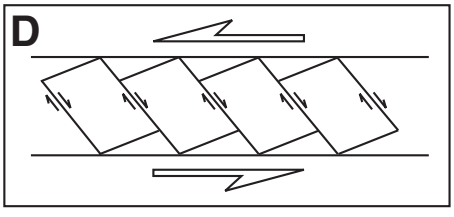

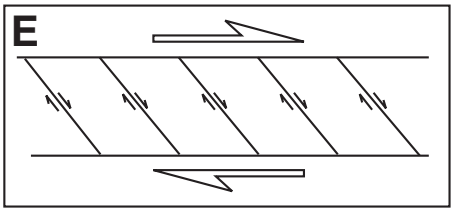

ls	Young landslide deposits derived from steep cliffs in mountainous regions; surface morphology is well preserved.
sd_y	Young unconsolidated surficial deposits (dust and talus), fine-textured surface and lack of bedding.
Asd	Sand dune fields
gf_y	Young gully fills restricted in narrow valleys in trough walls.
gfo	Thinly bedded and consolidated sedimentary strata at the base of north trough wall. Beds can be traced into deep-cut valleysand form mesas in places. They are interpreted as older valley and trough fill deposits.
As	Landslide sheet covering most northern trough floor.
Atf_2	Younger trough-fill strata, light-toned and fine-textured on surface. Beds are not folded.
Atf_1	Older trough-fill strata, dark-toned and rougher textured than Atf_2. Beds are folded.
HNu	Trough-wall rock, thickly bedded.

Ridge formed during emplacement of the landslide block

Inferred fault contact now buried below young sediments

Strike-slip fault

Fold

Joints

Normal fault

Thrust

Landslide, rock avalanche, or debris flow

Figure 5 (*continued*). (B) A portion of uninterpreted CTX image P05_002815_1720_XN_08S084W. See A for location. (C) Interpreted geologic map of the northern lus trough zone based on image shown in B. Detailed lithologic division is shown in map legend and also described in detail in the text. (D) Development of northwest-striking right-slip faults interpreted as a result of bookshelf faulting. (E) Development of northwest-striking right-slip faults interpreted as a result of formation of Riedel shears. See text for details.

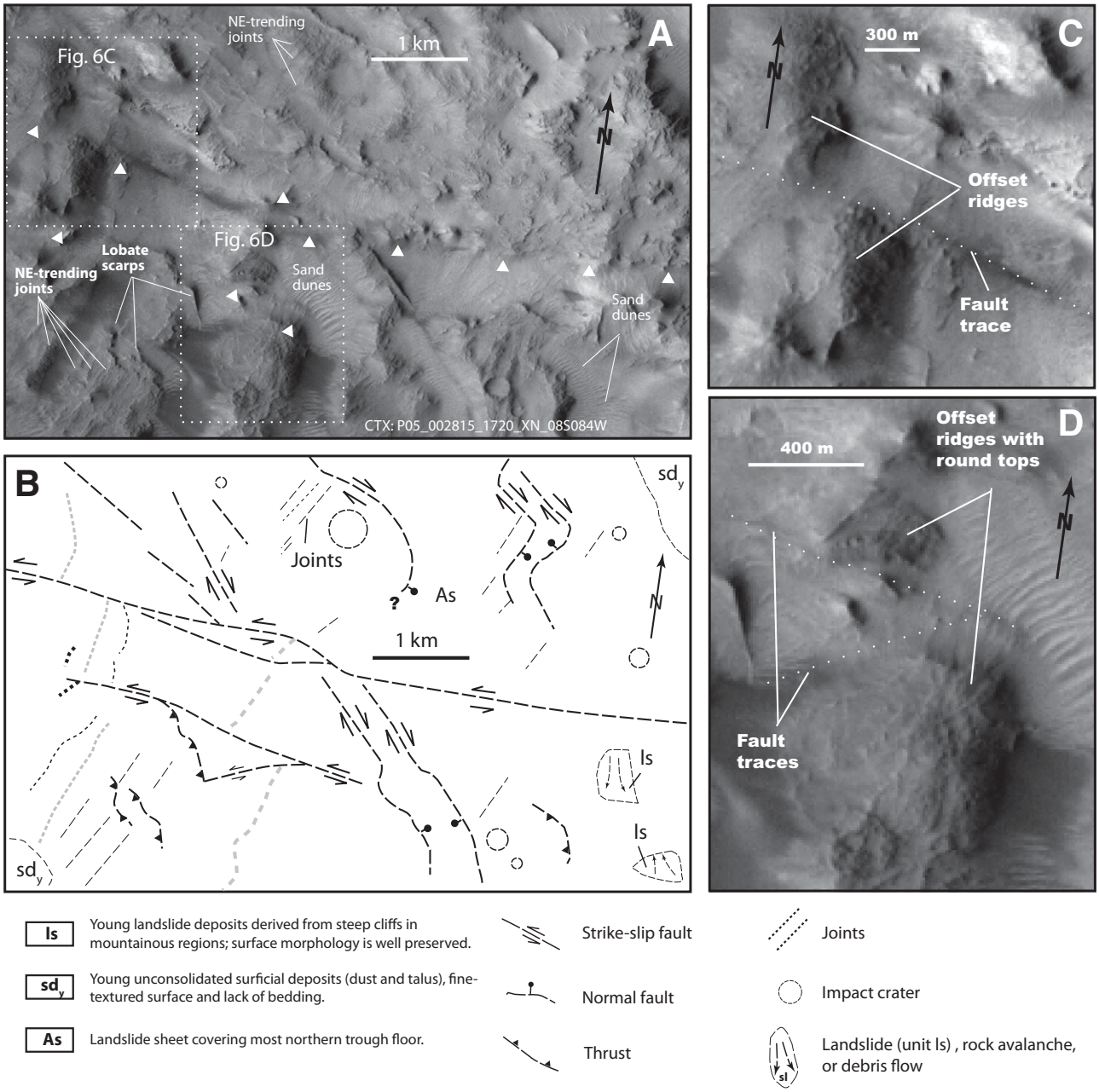

Figure 6. (A) Uninterpreted Context Camera (CTX) image P05_002815_1720_XN_08S084W. See Figure 5B for location. (B) Interpreted geologic map based on image shown in A. (C) Close-up image showing possible left-lateral offset of a ridge across an interpreted fault. See A for location. (D) Close-up view showing possible left-lateral offset of a ridge across a fault. See A for location. (*Continued on following page.*)

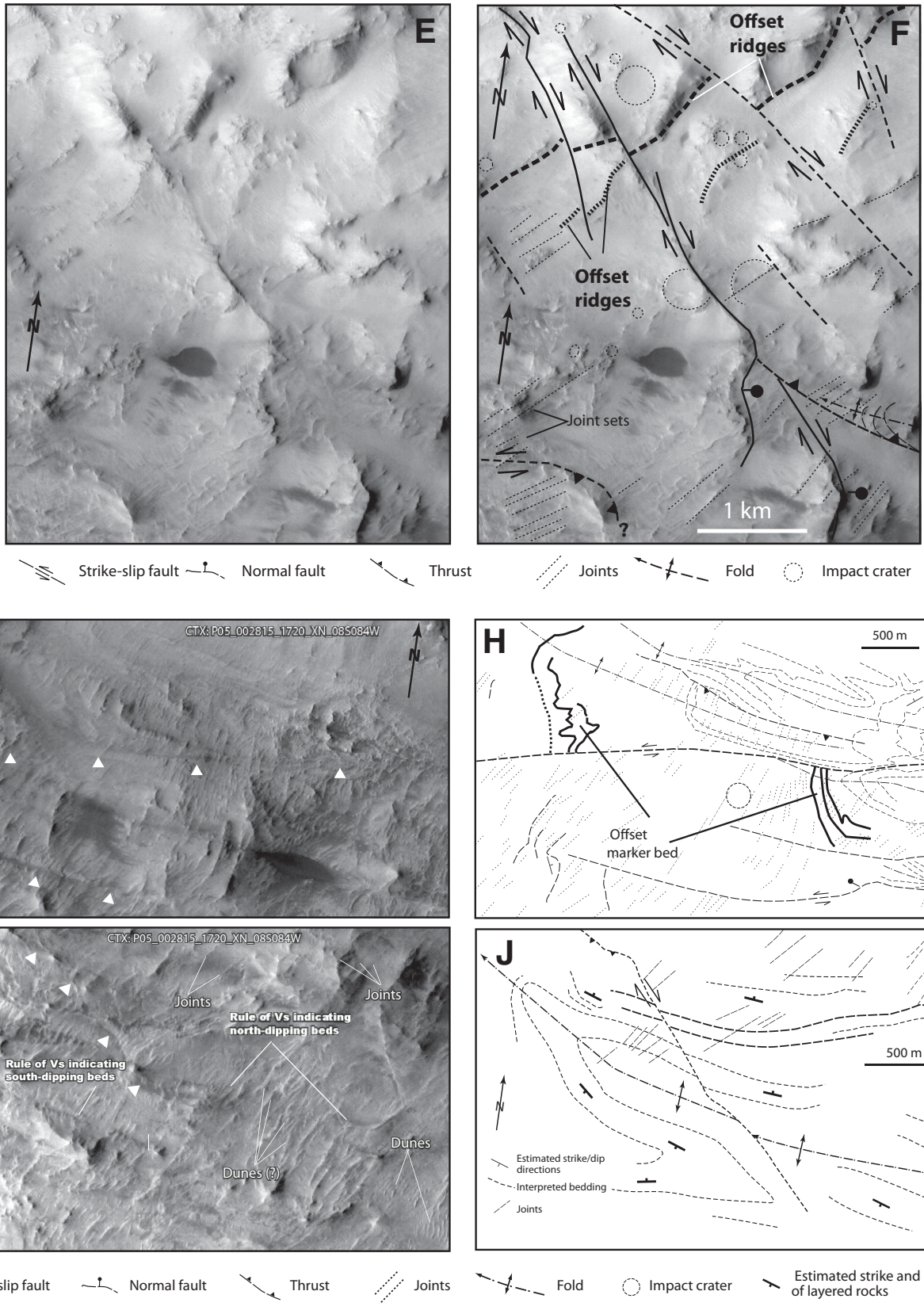

Figure 6 (*continued*). (E) Uninterpreted CTX image; see Figure 5B for location. White triangles point to the traces of left-slip faults. (F) An interpreted fault map corresponding to image shown in E. (G) Uninterpreted CTX image; location shown in Figure 5B. (H) Interpreted geologic map showing relationships between a left-slip fault and a series of oblique folds. (I) Uninterpreted CTX image; location shown in Figure 5B. (J) Interpreted geologic map showing relationships between a right-slip fault and a fold. (*Continued on following page.*)

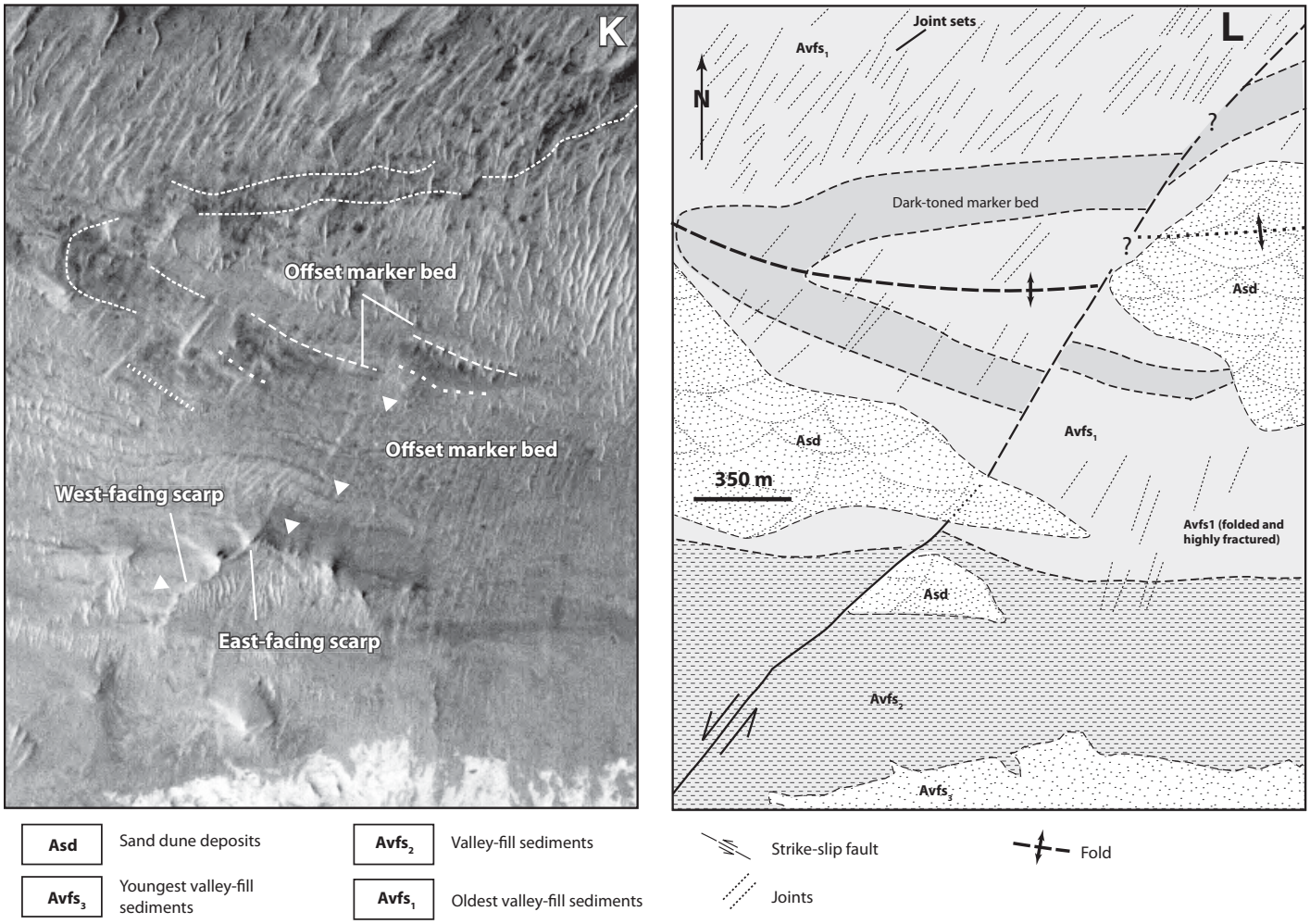

Figure 6 (*continued*). (K) Uninterpreted CTX image indicating the traces of a folded marker bed and a linear scarp interpreted as a fault; location shown in Figure 5B. (L) Interpreted geologic map showing relationships between a left-slip fault and a fold.

after landslide emplacement (Figs. 6B–6D) and (2) a gradual change in ridge trends (Figs. 6B and 6C). The latter is in sharp contrast to the northwest-trending linear and smooth scarps interpreted as post-landslide fractures in this study. The observation that the rounded ridges display curved geometry is common for all landslides in Valles Marineris due to lateral spreading of the landslide materials (e.g., Lucchitta, 1979).

The recognition of originally continuous ridges induced by landslide emplacement allows determination of fault kinematics. First, the offsets of north-northeast–trending ridges in the western part of the landslide require left-slip faulting on several east-striking fractures (Figs. 6A–6D). Second, the offset of northeast-trending ridges in the eastern part of the landslide requires right-slip faulting along northwest-striking fractures (Figs. 6E–6D). The strongest evidence for the tectonic origin of the northwest-striking fractures is that they cut not only the landslide itself but also younger unit Atf_1 in the south (Figs. 6B and 6C). They also offset the contact between the landslide and unit sd_y right laterally along the northern margin of the trough zone (Figs. 6B and 6C). The northwest-striking right-slip faults and east-trending left-slip faults must have occurred simultaneously, as indicated by their mutual crosscutting relationship shown in Figures 6B and 6C. Thus, interpretation of the origin of any one set of the fractures must take this relationship into account.

The northwest-striking right-slip faults display an en echelon fault pattern, typically related to the initiation of strike-slip fault zones (e.g., Naylor et al., 1986) (Figs. 6F and 6G). The observed right-slip faults may have normal-slip components, as they all bound linear basins parallel and adjacent to the faults. The northwest-striking faults terminate at north-striking normal faults at their southern ends (Figs. 6F and 6G). The evidence for the interpreted normal faults includes (1) their irregularly curved fault traces, and (2) fault scarps dying out in scarp height away from their intersections with strike-slip faults indicating diminishing normal-slip motion (Figs. 6F and 6G). In contrast, the east-striking left-slip faults terminate at northwest-striking thrusts that are expressed by lobate scarps (see Figs. 5A and 6B).

The northwest-striking right-slip faults across the northern subtrough margin exhibit nearly regular spacing at 3.5–4 km. This structural arrangement is quite similar to the classic bookshelf fault pattern in a broad shear zone. That is, northwest-striking right-slip faults were generated by east-trending left-slip shear (Fig. 6D). Alternatively, the northwest-striking right-slip faults may have been generated as Riedel shears in a broad east-trending right-slip shear zone (Fig. 6E). This interpretation, however, contradicts the observation that east-striking left-slip faults were active at the

same time as right-slip faulting. The junctions between the trough zone and the northwest-striking right-slip faults, with angles ranging from 45° to 50°, are also too large to be Riedel shears, as Riedel shear fractures typically form at ~15°–25° from the main trend of the shear zone (Sylvester, 1988). As shown in the following, the right-slip interpretation for trough-floor deformation shown in Figure 5E is also inconsistent with the west-northwest trend of folds in the trough zone, which indicate left-slip shear (Fig. 5B) (see more details in the following sections).

The west-northwest–trending folds involving unit Atf_1 are expressed by the distribution of several weathering-resistant layers (Figs. 6G–6J). The antiformal and synformal fold shapes can be inferred from the dip directions of the fold limbs using the "rule of V's" and the fold shapes in map view can be inferred from the distribution of marker beds with distinctive tones (e.g., dark-toned bed in Fig. 6I). The fold in Figure 6I could have been offset by a left-slip fault trending northeast. This inferred fault has clearly defined scarps in the south; its southern segment faces to the west, whereas its northern segment faces to the east, as inferred from the shading of the topographic scarps. Such geometry implies along-strike changes in the sense of relative vertical motion across the fault that can only be associated with strike-slip faults. Although this inferred fault appears to offset a dark-toned bed defining the southern fold limb, its extent to the north is unclear.

The northeast-striking linear ridges and elongate depressions are prominent morphological features across the folds (Figs. 6G–6J). These features could either be erosional or depositional features such as linear sand ridges or expression of joints. The joint interpretation is favored here as the linear ridges have remarkably even spacing and are distributed across major topographic highs forming narrow resistant bends, possibly due to fluid flow and mineralization along the joint fractures (Okubo and McEwen, 2007). Thus, the formation of the folds and joints in the area is interpreted to have occurred during the same phase of tectonic deformation. An additional piece of evidence to support the joint interpretation is that the northeast-trending linear ridges occur in all trough-floor units except the youngest unconsolidated deposits, unit gf_y (Figs. 6B and 6C).

In the southeastern corner of Figure 6B, a northeast-striking fault offsets two sets of marker beds in a left-lateral sense (Figs. 6I and 6J). As this fault is subparallel to nearby joint sets, it is interpreted here as a normal fault. However, the northern extent of the fault also offsets or deflects the northern fold limb in a left-lateral sense, suggesting that this structure has moved left laterally. Together, these observations suggest that the fault may have been reactivated from a preexisting joint fracture. Notice that the linear sand dunes in this area can be clearly distinguished from the northeast-striking linear ridges interpreted as joints in bedrock; the sand dunes are restricted to topographic depressions, have variable ridge trends, and display curvilinear geometry along individual ridges (Figs. 6G and 6I).

Northern trough margin. Three linear fracture-scarp zones are recognized across the northern margin of the northern subtrough zone (Figs. 7A and 7B). The northern scarp zone has an east strike in the east and a west-northwest strike in the west. The two segments are linked by a northwest-striking right-step bend. The southern scarp zone strikes mostly to the east except along its westernmost segment, where it strikes in a west-northwest direction. Finally, the western scarp zone trends dominantly in the west-northwest direction.

Figures 7A and 7B (CTX image P05_002815_1720_XN_08S084W) show two scarp zones along the base of the north trough wall of the northern Ius subtrough zone. Small black and white triangles in Figure 7 show the traces of interpreted left-slip faults. A right-bank riser of a trough-wall canyon appears to be offset left laterally (Fig. 7). This interpretation implies that the curved segments of the faults (labeled as right-step bend) trending northwest are thrust faults. Also note that both the northern and southern fault scarps truncate stream channels in their hanging walls. No corresponding channels can be found in the footwalls, which may have been buried. The large white triangles in Figure 7A also indicate an oblique northwest-trending scarp in the western part of the image. In close-up view, both the northern and southern scarp zones consist of an en echelon array of short fractures (Figs. 7C and 7D), which are interpreted as high-angle extensional fractures as they only display dip-slip offset and have straight surface traces. The latter imply high angles of fracture dips. The arrangement of the extensional fractures implies left-slip motion on the scarps that are interpreted as faults. The left-slip interpretation is consistent with the interpreted possible left-slip offset of canyon banks.

Interpreted geologic relationships adjacent to the western scarp in Figure 7A are shown in Figures 7E and 7F in which two units (gf_{o1} and gf_{o2}) are recognized. The older unit gf_{o1} has a ripple-like surface morphology and locally high albedo. In contrast, the younger unit gf_{o2} displays a smooth surface morphology, is well layered, and is resistant to weathering as expressed through cliff-forming morphology. It also has a lower albedo, contrasting with unit gf_{o1}. An anticline trending west-northwest was recognized based on bedding dip directions determined by the use of the rule of V's. The anticline is bounded by the western scarp along its northern edge. This fault is interpreted to have offset a thin and light-toned marker bed left laterally. This same marker bed is folded into a smaller anticline to the north and is itself in turn offset by a curved fault interpreted as a thrust, because its geometry in map view indicates a low dip angle.

Southern trough margin. The presence of a linear alignment of north-facing scarps along the southern edge of the northern subtrough wall in Ius Chasma indicates that the trough-wall boundary may be controlled by a buried fault below unit Atf_2 (Figs. 5B and 5C). The shape of the scarp indicates north side down, and thus implies a normal-slip component across this inferred fault. However, this observation alone does not preclude the fault from having strike-slip motion (i.e., it could be a transtensional structure).

Southern Subtrough Zone

From younger to older ages, the following major lithologic units are recognized in the southern trough zone (Figs. 8A and 8B): (1) young surface deposits of mostly dust (unit sd_y), (2) recent landslides (unit ls), (3) sand dune deposits (unit Asd), (4) two phases of postfolding landslide deposits (units $ptf\text{-}sl_1$ and $ptf\text{-}sl_2$), (5) flat-lying postfolding trough fills (unit pst-fd), (6) pre- and synfolding sediments (unit pre/syn-fd), and (7) thickly bedded strata exposed on the north trough wall (unit HNu) (Figs. 8A and 8B).

The pre- and synfolding strata consist of highly fragmented broken beds in the eastern part of the main depression, which has been incised by erosion. The broken blocks vary from a few hundreds of meters to less than 15 m in the longest dimension (Figs. 8C and 8D). Most large blocks have rounded edges, and their internal beds are folded (Figs. 8C and 8D). This observation suggests that folding occurred before the fragmentation of the beds. Individual broken beds appear to have slid from the margins to the center of the depression, as they commonly display long and straight lateral ridges marking the edges of transport flows linking with lateral spreading heads in the interior of the depression (Figs. 8E and 8F).

Similar broken bed units were also observed by Metz et al. (2010) in many parts of Valles Marineris. These authors suggested that they were induced by emplacement of landslides from trough walls, and thus were unrelated to

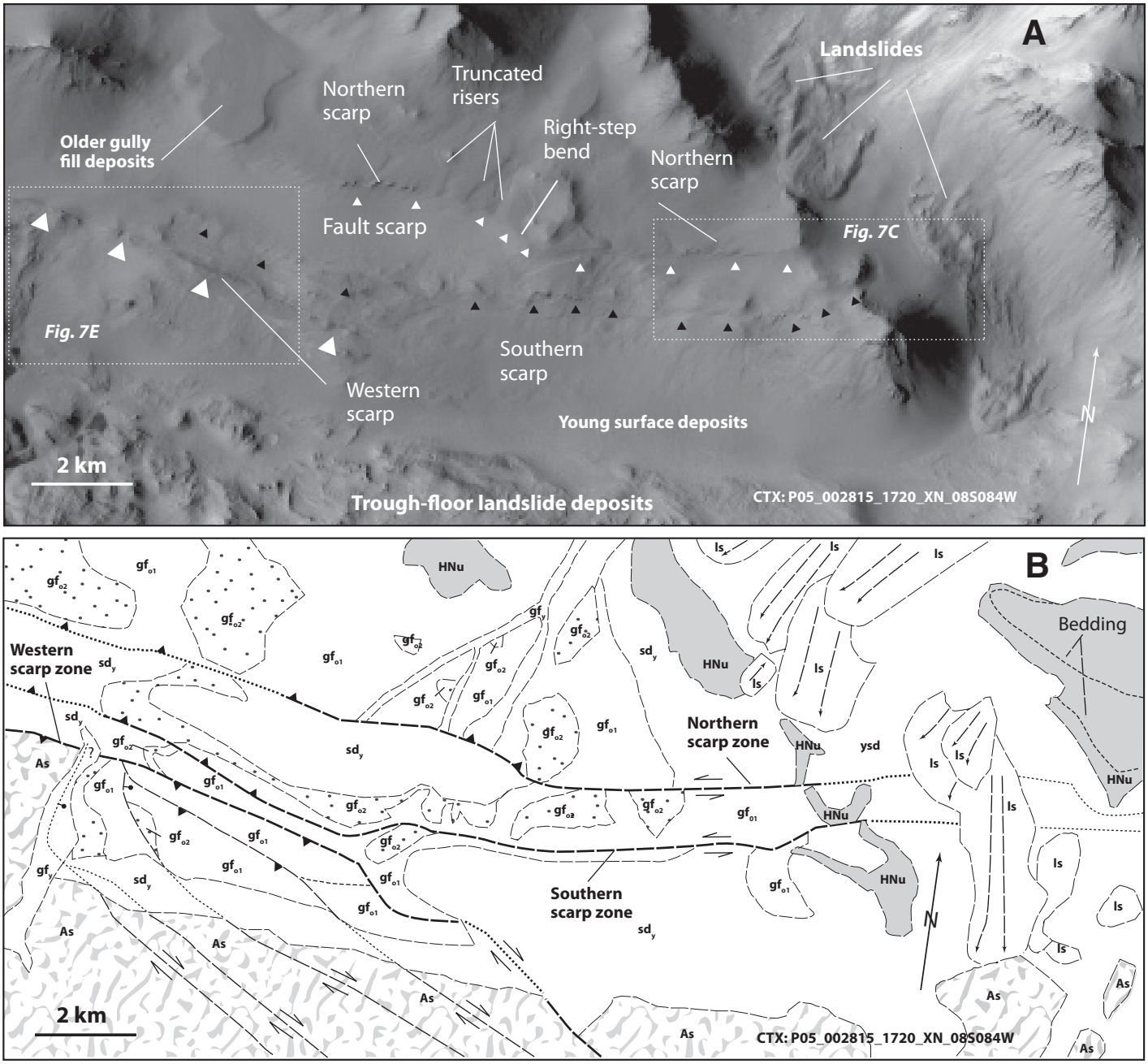

Figure 7. (A) An uninterpreted Context Camera (CTX) image (P05_002815_1720_XN_08S084W) along the northern margin of the northern lus trough zone. See Figure 5B for location. Small black and white triangles indicate the traces of interpreted left-slip faults. Note that the right-bank risers of a trough-wall canyon on the west side of the image appear to be offset left laterally. This interpretation implies that the curved segments of the faults (i.e., the labeled right-step bend in the figure) trending northwest are thrust faults. Also note that both the northern and southern fault scarps truncate risers in their hanging walls. No corresponding risers can be found in the footwall, which may have been buried by the interpreted thrust or younger sediments in the thrust footwall. The large white triangles also indicate an oblique northwest-trending scarp in the western part of the image. (B) A detailed geologic map based on interpretation of the CTX image shown in A. (*Continued on following page.*)

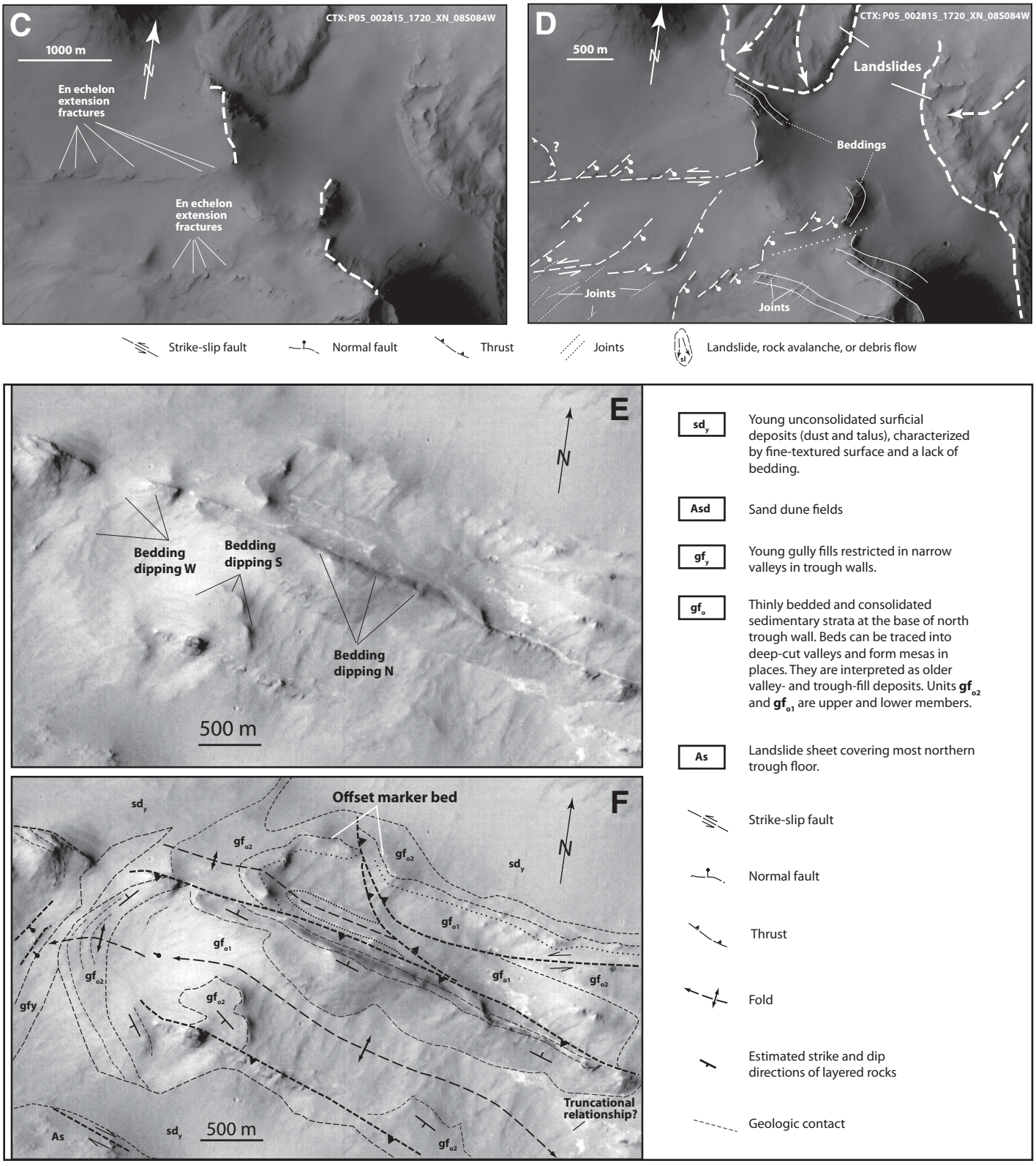

Figure 7 (*continued*). (C) Uninterpreted image to show a close-up view of the scarp zones along the northern margin of Ius Chasma. See A for location. (D) Interpreted fault map based on image shown in C. Note that the scarp zones consist of an en echelon array of faults, which are interpreted as an extensional fracture implying left-slip motion. (E) Uninterpreted image, with location shown in A. (F) Interpreted geologic relationships adjacent to the western scarp. A west-northwest–trending anticline was recognized based on bedding-dip directions using the rule of V's. The anticline is bounded by the western scarp along its northern edge. This fault appears to offset a thin and light-toned marker bed left laterally. This same marker bed is offset to the north by a curved fault trace, which is interpreted as a thrust as its fault geometry in map view indicates a low dip angle.

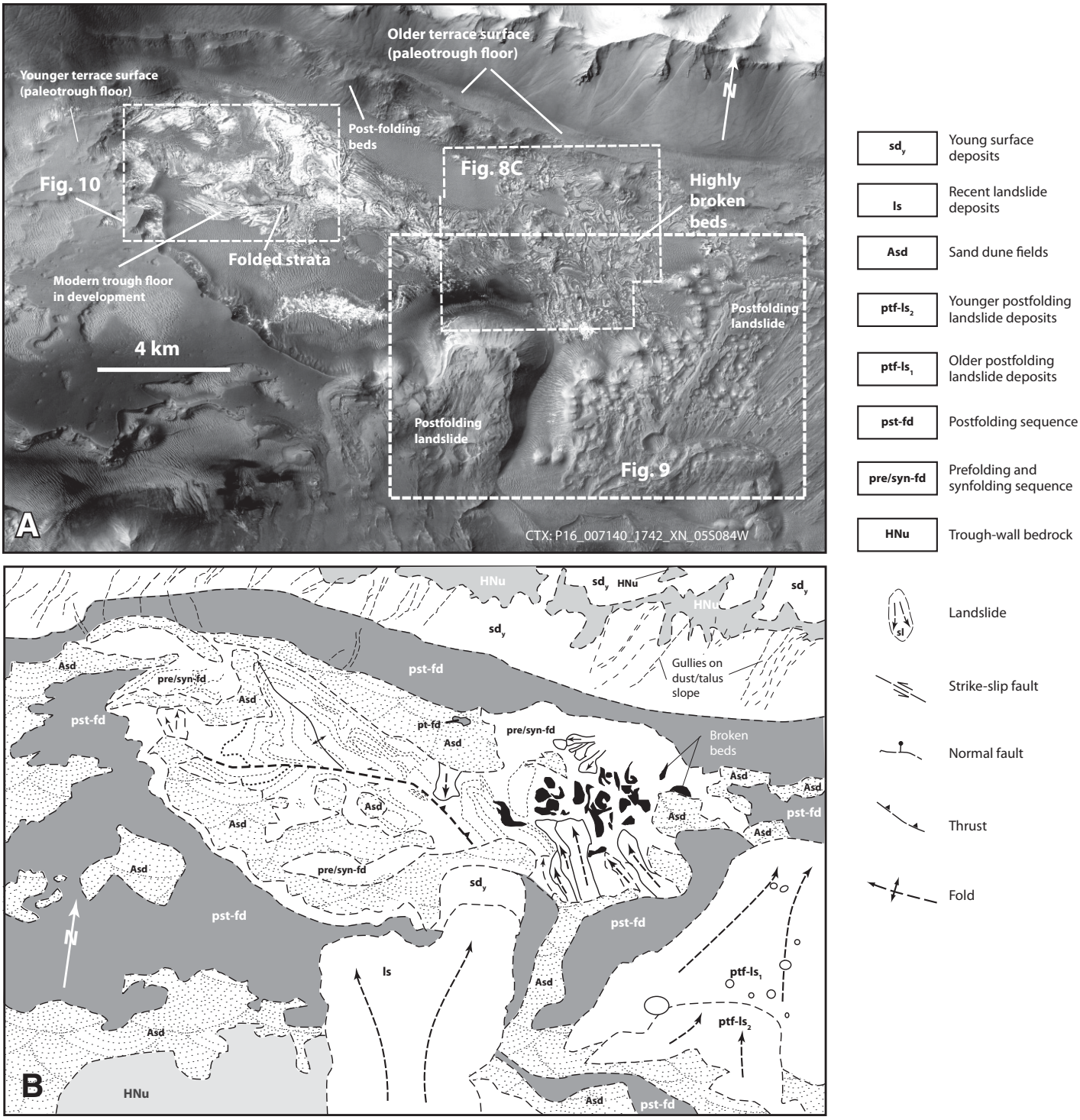

Figure 8. (A) Uninterpreted Context Camera (CTX) image P16_007140_1742_XN_05S084W. See Figure 5A for location. (B) Detailed geologic map of the southern Ius trough zone based on interpretation of CTX image shown in A. (*Continued on following page.*)

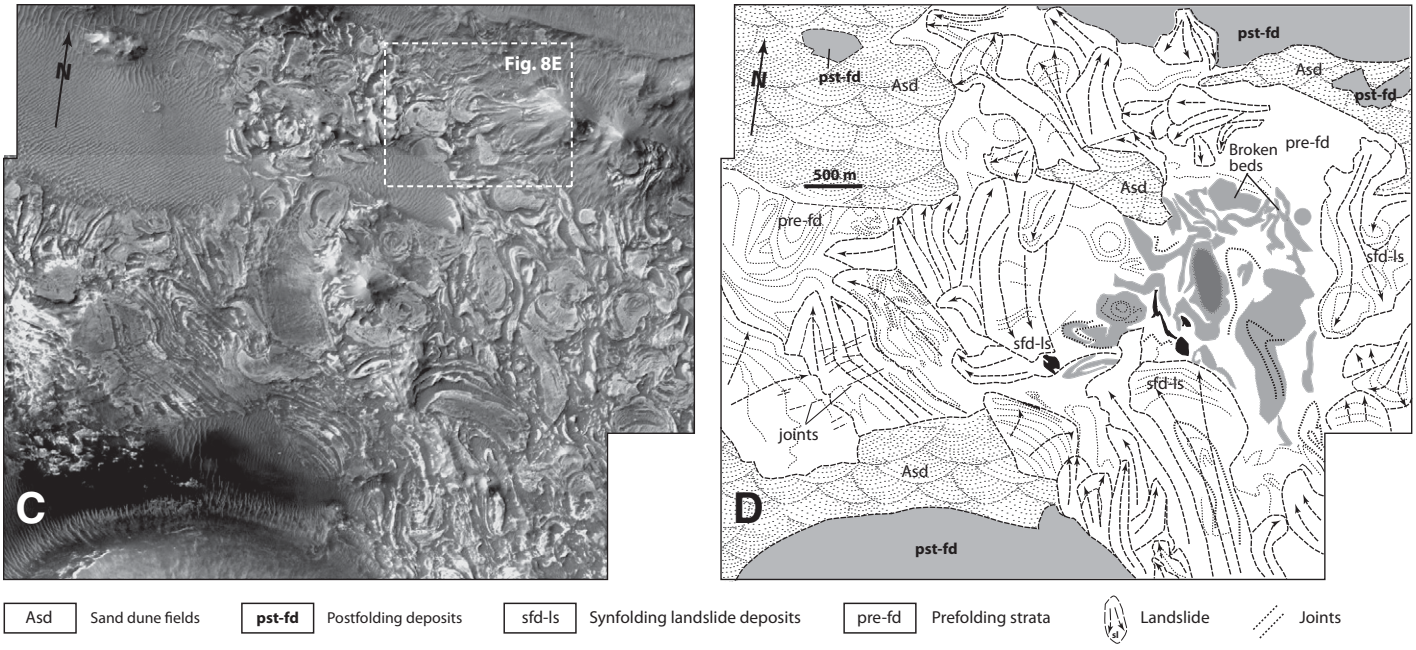

Figure 8 (*continued*). (C) Uninterpreted CTX image with location shown in A. (D) Interpreted geologic map of slump structures based on image shown in C.

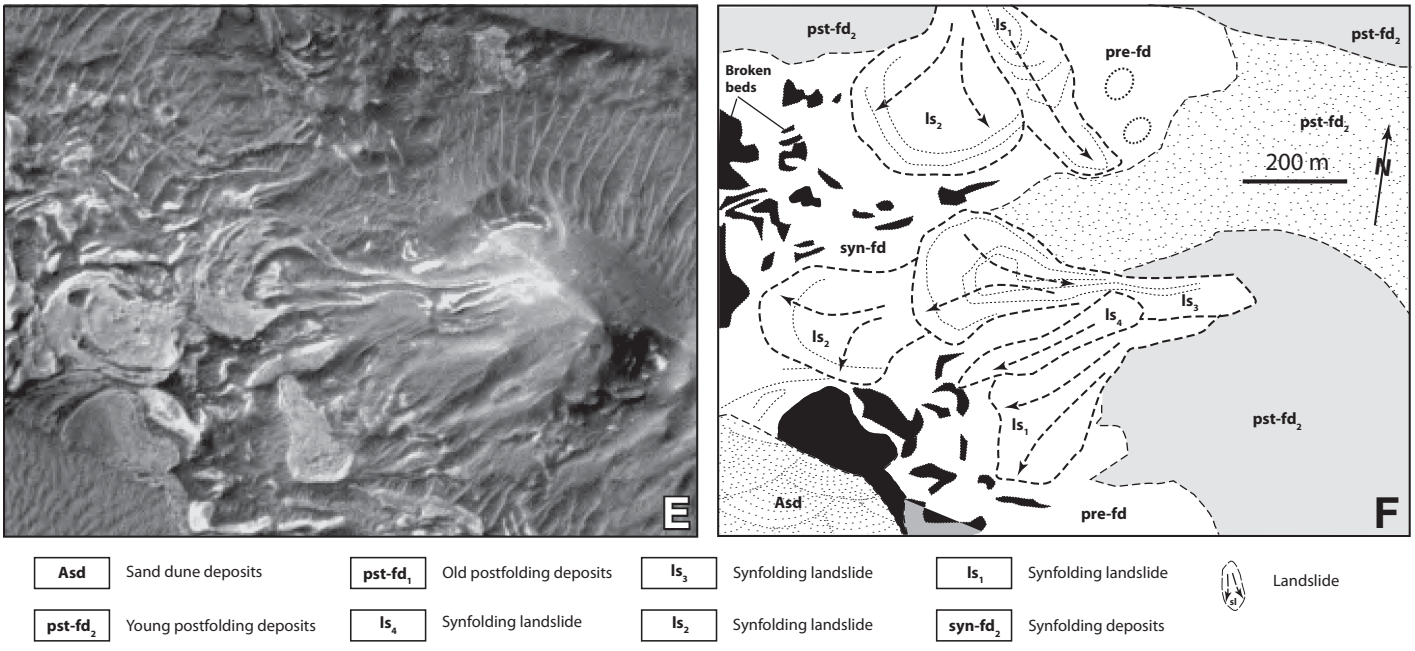

Figure 8 (*continued*). (E) Uninterpreted CTX image P16_007140_1742_XN_05S084W, with location shown in C. (F) Detailed geologic map of slump structures based on interpretation of image shown in E. Note that their narrow transport channel and expanding head region indicate fluid-like transport and spreading.

tectonic processes. In Figure 9, the traces of several landslides can be recognized. They display linear striations in thin sheets. Bedding below the striated landsliding surfaces can be clearly recognized and is flat-lying and not deformed. These flat-lying beds in turn were deposited on top of the folded strata (i.e., unit pst-fd in Fig. 8B). These relationships suggest the following sequence of events: (1) deposition of prefolding strata, (2) folding, (3) deposition of postfolding strata, and (4) emplacement of thin landslide sheets. Note that a landslide sheet in the lower-left corner of the image appears to be resistant to weathering. As a result, beds below the landslide layer were protected from erosion; the shape of the underlying beds is clearly shown by morphology of the thin draping landslide sheet.

In the western part of the southern subtrough, the first-order folds (i.e., the largest folds) dominantly trend northwest and are oblique to the trend of the trough walls (Figs. 8A and 8B). A broken-bed unit is interlayered within a well-bedded and intensely folded sequence in the western mapped area (Fig. 10). This relationship suggests that deformation causing fragmentation of the beds occurred at the same time as deposition of the folded sequence. The northwest-trending fold complex and the broken-bed unit are offset by an east-striking, left-slip fault (Fig. 10). The aforementioned slumping structures in the eastern part of the depression may have been induced by seismicity during motion on trough-bounding faults, as suggested by Metz et al. (2010) for the occurrence of similar structures in Valles Marineris.

Trough-Floor Structures of Ius Chasma: The Eastern Traverse

Northern Subtrough

The northern subtrough is bounded by Noachian–Hesperian wall rocks in the north and south (Witbeck et al., 1991). The contact between the north wall and trough-fill deposits is covered by dust and talus deposits superposed by small slump structures. No prominent scarps cutting these young deposits are observed. The contact between the southern wall and trough-fill units is also covered by young sediments, and no escarpment is exposed in the mapped area. Thus, the nature of the contacts at the base of the north and south walls is unclear.

The floor of the northern subtrough zone is dominated by two large landslide sheets (units Als_1 and Als_2) that have complex surface textures characteristic of landslides in the Valles Marineris region (e.g., Lucchitta, 1979) (Fig. 11). The large landslide complexes are in turn overlain by younger and much smaller landslides (unit Als_3 and Als_4) originating from the north and south walls of the trough zone (Fig. 11). Note that the units shown in Figure 11 are defined in more detail in close-up maps of the area presented later herein.

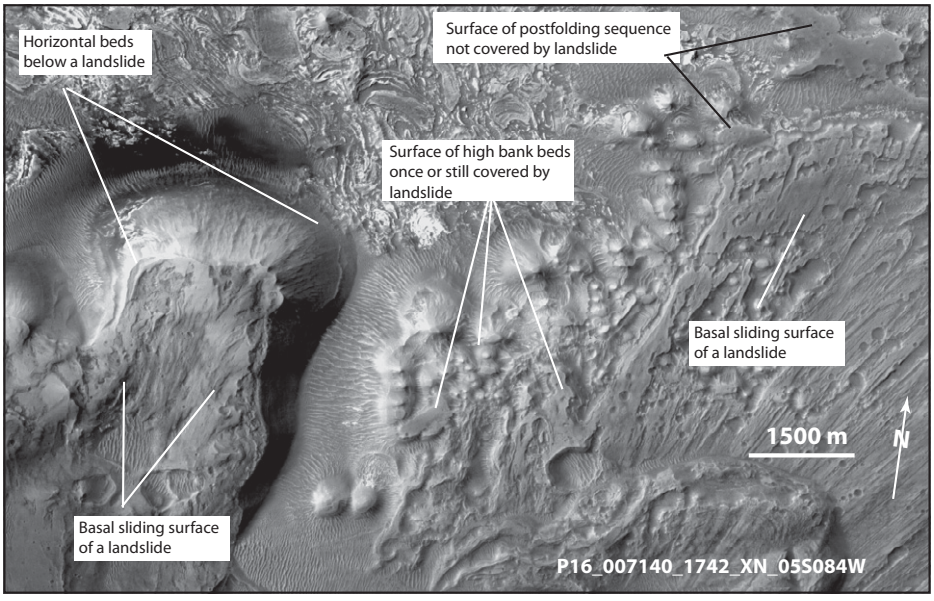

Figure 9. Context Camera (CTX) image P16_007140_1742_XN_05S084W showing the relationship between landslides and older slump structures. Note that the beds below a thin landslide sheet in lower-left corner are subhorizontal, which suggests deposition after folding and formation of slump structures. See Figure 8A for location.

Southern Subtrough

The southern subtrough zone in the eastern traverse of Ius Chasma exposes Noachian–Hesperian strata, as mapped by Witbeck et al. (1991), and trough-fill strata. The latter consist of a folded unit, a broken-bed unit, and a flat-lying post-folding unit (Fig. 12A). The broken-bed unit occurs mostly along the margin of the topographic depression, with fragments ranging in size from >300 m to <15 m. Their geometry includes rounded patches (Fig. 12C), U-shaped patches (Fig. 12C), elongated patches (Fig. 12D), highly angular blocks with internal folds (Fig. 12E), and angular breccia (Fig. 12F). The rounded and elongate patches appear to be induced by the formation of load structures, whereas the breccia may have resulted from downslope transport. The presence of folds in consolidated angular blocks requires folding to have predated fragmentation of the beds, regardless if the process was induced by slumping or not. A likely setting for the formation of the broken-bed unit is that they were located on the banks of a water-saturated basin; folding occurred first, and the folded strata were later transported into the basin by a gravity or seismically driven mechanism as suggested by Metz et al. (2010).

Figure 13 is a detailed geologic map of a layered unit bounding the broken-bed unit in the south. The most striking features in the map area are a series of fold-like structures defined by alternating white-toned and dark-gray–toned beds. This pattern could be induced by mesa-like topography draping over flat-lying strata. This explanation can be tested by examining the topography around the fold-like features. In the image shown in Figure 13A, the sun-lit angle is from northwest to southeast, as indicated, and thus sunlight would have cast dark shadows on the southeastern edges of the fold-like structures. The lack of predicted shades around the fold-like features suggests that there is hardly any topography across these structures. Some light-toned layers pinch out completely along the southwestern limbs of two northwest-trending fold-like features (Fig. 13A). The lack of shadows suggests that the missing beds cannot be explained by the presence of nearly vertical cliffs. A simple explanation is that this is induced by deformation, and the fold-like features are indeed structures imprinted over a rather flat topographic surface.

Because of the flatness of the topography, it is difficult to differentiate anticlines from synclines. Only in three locations where topographic reliefs are sufficiently large was I able to determine the directions of dips and strikes of bedding applying the rule of V's. From the determination of this anticlinal structure, the rest of the fold geometry can be inferred and is shown in Figure 13B.

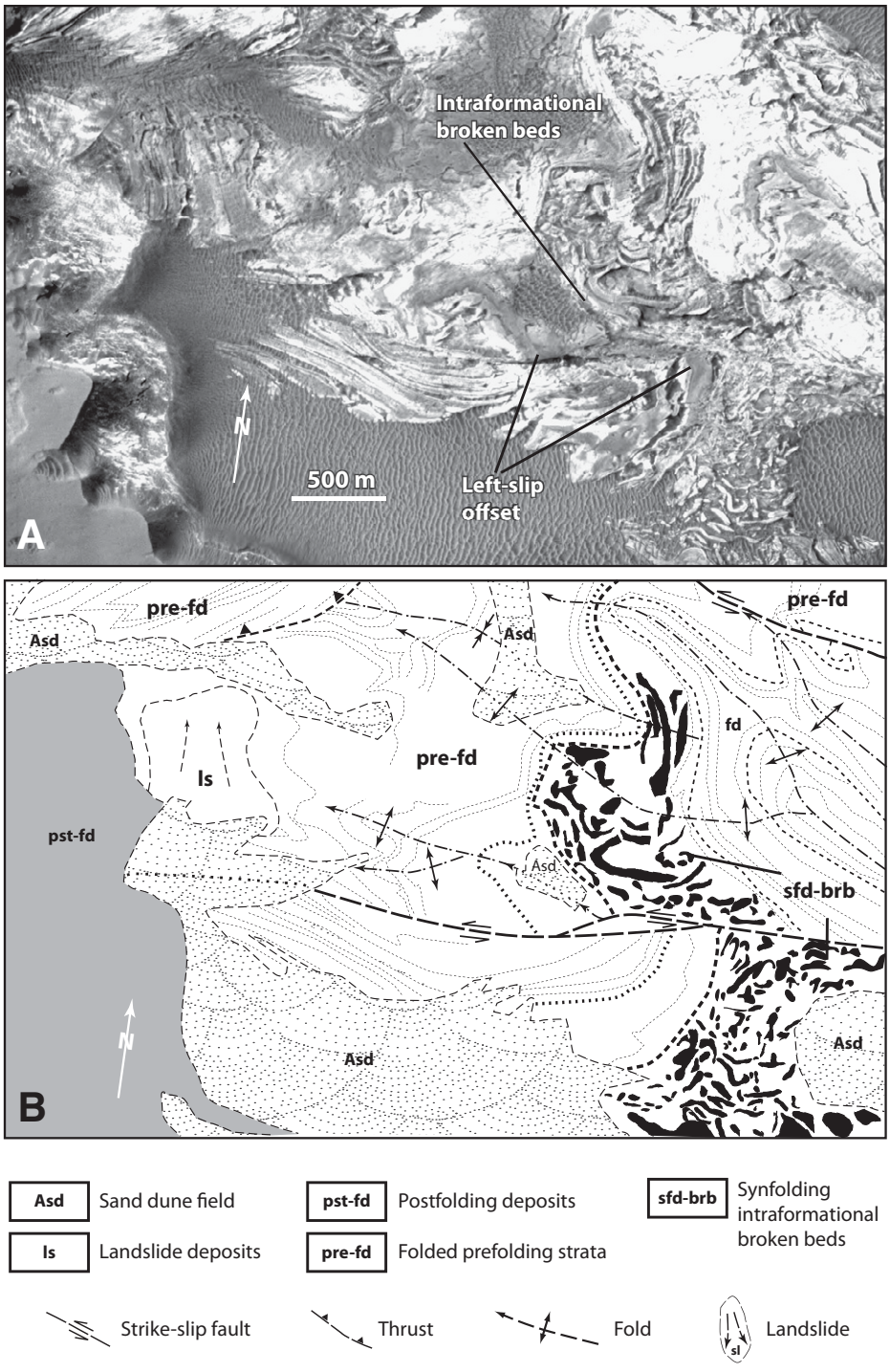

Figure 10. (A) Uninterpreted Context Camera (CTX) image P16_007140_1742_XN_05S084W. See Figure 8A for location. (B) Interpreted geologic map based on interpretation of image shown in A. The fold limb and an intraformational broken bed unit are offset by an east-striking left-slip fault.

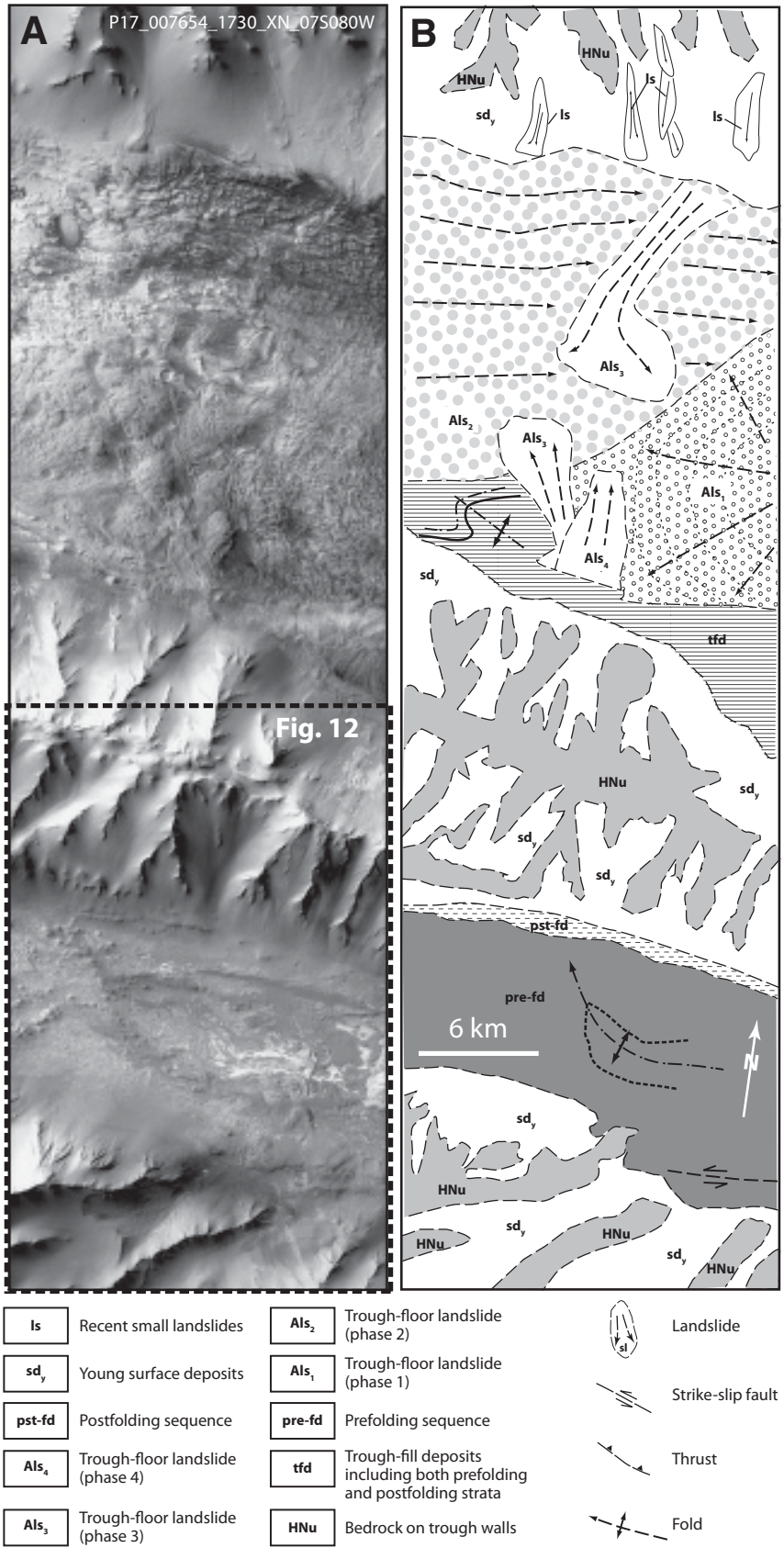

Figure 11. (A) Uninterpreted Context Camera (CTX) image P17_007654_1730_XN_07S080W. See Figure 1C for location. (B) Interpreted geologic map based on image in A.

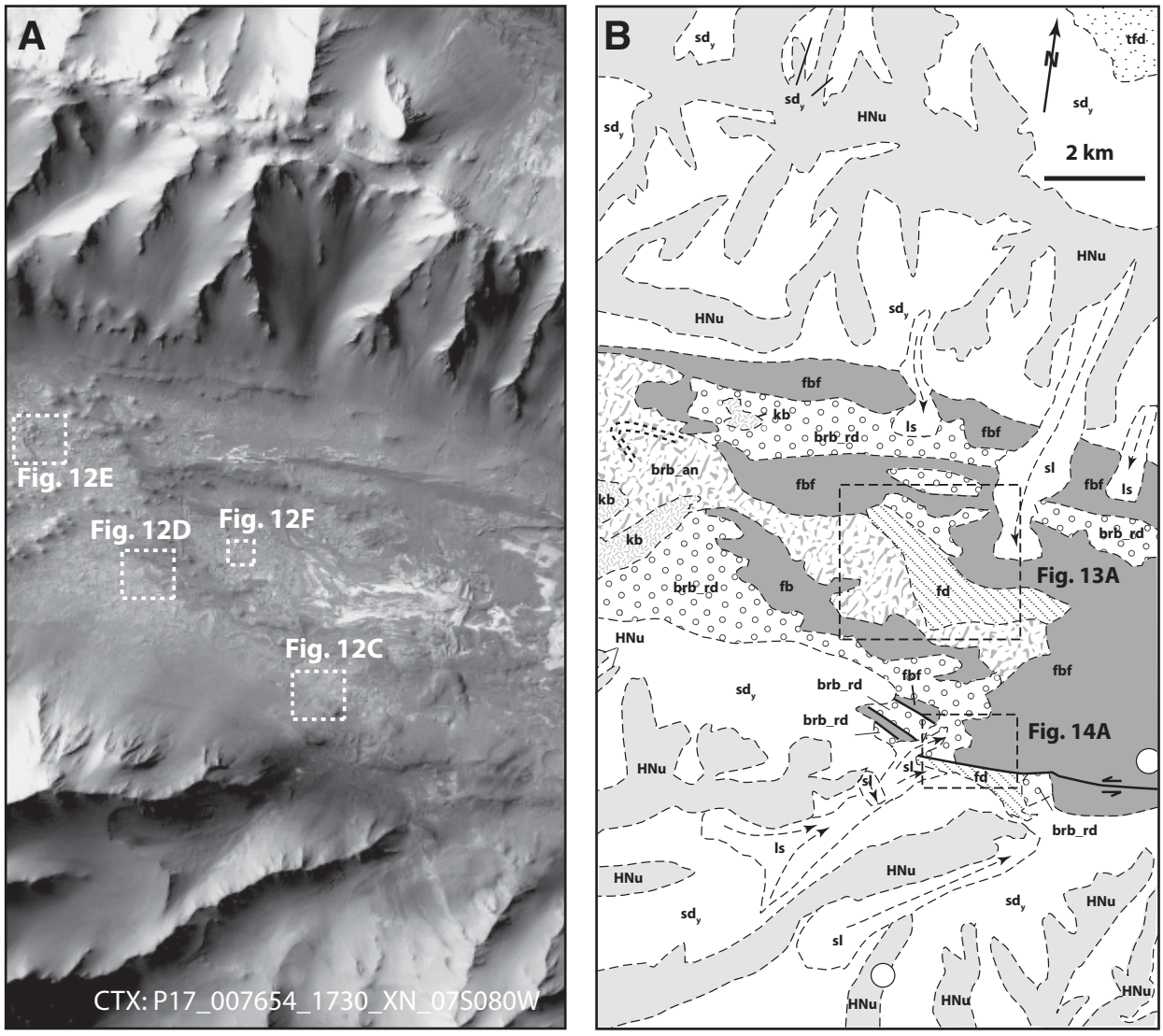

Map legend

ls	Landslide, rock avalanche, or debris-flow deposits derived from gullies of steep bedrock trough walls.
sd_y	Young surface deposits interpreted as talus and dust deposits.
tfd	Trough-floor deposits, northern Ius trough.
fbf	Flat-lying, layered basin fills.
kb	Layered beds expressed morphologically as rounded knobs. Interpreted as relicts of unit **fbf**.
fd	Folded, thickly bedded and weathering-resistant layers interbedded with thinly bedded layers.
brb_an	Broken beds with angular blocks.
brb_rd	Broken beds rounded patches, interpreted as load structures.
HNu	Noachian–Hesperian bedrock on trough walls.

Strike-slip fault

Thrust

Fold

Landslide (sl)

Figure 12. (A) Uninterpreted Context Camera (CTX) image P17_007654_1730_XN_07S080W from the southern trough zone of Ius Chasma. See Figure 11A for location. Also shown are locations of C, D, E, and F. (B) Interpreted geologic map based on image shown in A. (*Continued on following page.*)

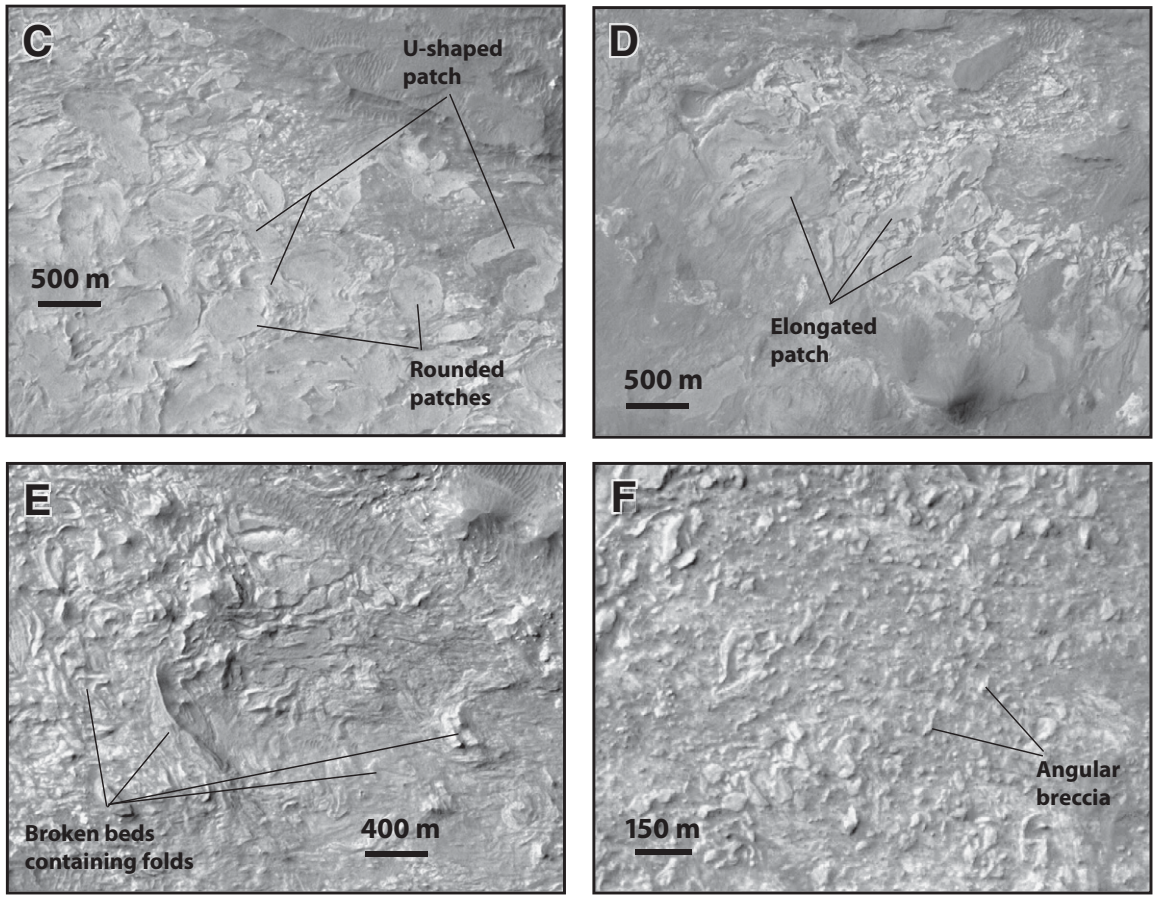

Figure 12 (*continued*). (C) Rounded patches of broken beds, possibly induced by formation of load structures. (D) Elongated patches, possibly related to fluidized slump structures derived from basin margins. (E) Broken bed blocks in which folded strata are present. This indicates folding occurred before slumping. (F) Angular breccia in the broken bed unit.

The traces of the interpreted fold structures are dominantly northwest-trending. However, they make a sharp turn to the south with an east-west strike (Fig. 13). It can also be seen that a white-toned marker bed is offset by a fault with a left-lateral sense of separation (Fig. 13A). Folds change trend progressively from east to northwest, exhibiting an oroclinal pattern indicative of left-slip shear (Fig. 13A). Thrusts parallel to the traces of fold axial surfaces are also exposed in the area (Fig. 13B). From the topographic relationships, the folded beds in the south appear to lie above the broken-bed unit to the north.

Strata in the southwestern part of the mapped area also appear to be folded, and they are in turn truncated by a fault in the north (Fig. 14). This fault juxtaposes three units in the north: (1) a bright and massive-looking unit with a smooth surface (unit tfd_1), (2) a ridge-forming unit (unit tfd_2), and (3) a broken-bed unit that can be traced to a basin to the north (unit brb) (Fig. 14). Three units are mapped south of the fault: (1) the interpreted folded strata unit (unit fd), (2) the ridge-forming unit (unit tfd_2), and (3) sand dune deposits (Asd). Gully-fill deposits (unit gf) extend across the interpreted fault and represent postfaulting deposits.

From its relatively straight trace, the interpreted fault appears to be nearly vertical, but its kinematics are difficult to deduce. Determining the shape of the apparently folded strata is equally challenging due to the lack of valleys cutting across the folded beds. Because of this, the assigned synformal fold shape is highly tentatively, requiring verification when detailed topographic maps are available in this area.

GEOLOGY OF COPRATES CHASMA

Like Ius Chasma, Coprates Chasma can also be divided into the northern and southern subtrough zones divided by a central mountain belt. Unlike Ius Chasma, however, its southern subtrough is much narrower, less continuous, and extensively filled by recent sediments and landslides in comparison to the southern subtrough of Ius Chasma. In fact, the southern trough of Coprates Chasma at its eastern end disappears altogether before reaching Capri Chasma (Fig. 1). For these reasons, this study focuses only on the structures exposed in the northern subtrough zone across its western, central, and eastern segments (Fig. 1).

Western Area

A detailed geologic map was constructed based on a CTX image across the trough-bounding fault zone at the base of the north wall in western Coprates Chasma (Fig. 15). The following units, from youngest to oldest, are recognized in the map area (Fig. 15): (1) modern sand dune deposits (unit Asd), (2) young surface deposits comprising talus and deposits with smooth surfaces (unit sd_y), (3) old surface deposits comprising talus and dust deposits with their surfaces locally incised by recent erosion (unit sd_o), (4) landslide deposits on trough wall and its transition zone to the trough floor (units ls and $ls_{1,2,3}$), (5) a landslide complex with long, smooth, and slightly curved ridges and grooves

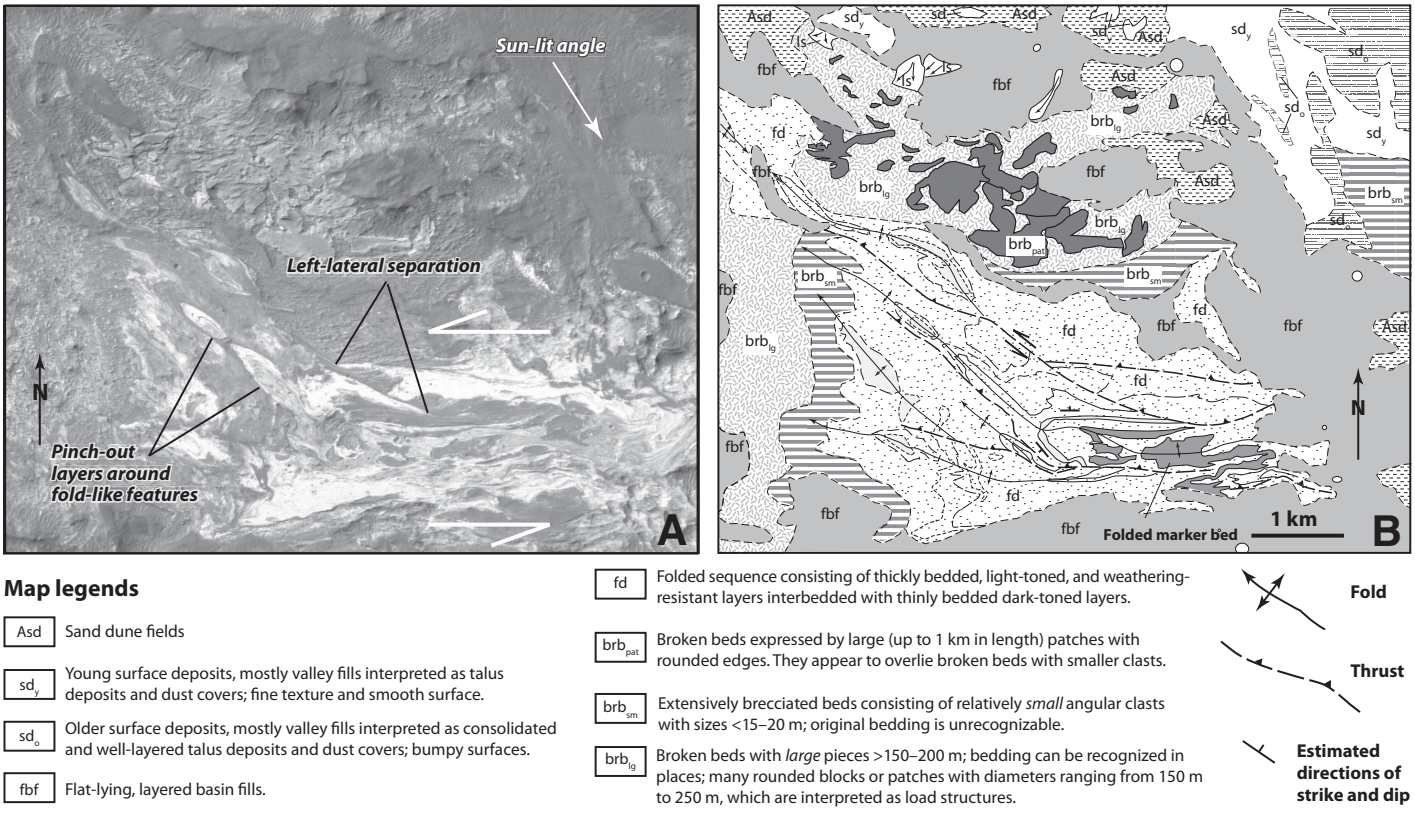

Figure 13. (A) Uninterpreted Context Camera (CTX) image P17_007654_1730_XN_07S080W of the southern trough zone of Ius Chasma. See Figure 12B for location. (B) Detailed geologic map based on interpretation of image in A. Note that the fold train exhibits an oroclinal drag pattern that is indicative of distributed left-slip shear.

that are cut by evenly spaced north-northeast–trending fractures (unit As), (6) trough-fill deposits having smooth surfaces and irregular contacts, appearing to lie below the landslide unit As (unit ifd), (7) layered trough-fill deposits at the base of the trough wall (unit tfd), and (8) undifferentiated Noachian–Hesperian wall rocks (unit HNu).

Among all the mapped units, unit tfd stands out in that it is well layered, as defined by weathering-resistant beds. The bedding appears to be folded, displaying asymmetric fold geometry with the long limb parallel to the trough margin (Fig. 15). The short limb of the interpreted fold is truncated by a sharp and discrete linear feature that is interpreted to be a fault. The interpreted fault juxtaposes the folded strata with a dark tone in the north against gray-toned materials that do not have obvious layering. The straight trace of the interpreted fault requires a nearly vertical fault orientation.

From the image shown in Figure 15, another nearly vertical fault can also be observed on a steep cliff at the western side of a landslide-generated canyon on the trough wall. There, the fault juxtaposes a thinly bedded and light-toned unit in the south against a thickly bedded and dark-toned unit to the north (Fig. 15). The light-toned unit has been interpreted to be Amazonian trough-fill deposits (equivalent to unit tfd of this work), whereas the dark-toned unit was assigned as the undivided Noachian–Hesperian unit of Witbeck et al. (1991).

The same fault that truncates the fold also forms a scarp, labeled as main fault trace in Figure 15. Across the fault scarp, the fault abruptly juxtaposes two very different landslide deposits. Landslide deposits in the north are clearly derived from the north wall and have a bumpy surface with many rounded knobs (unit ls$_{kb}$ in Fig. 15). In contrast, the landslide deposits in the south display closely spaced, long, curved, and smooth grooves and ridges (unit ls$_{gr}$ in Fig. 15), indicating a different emplacement mechanism. East of the high fault scarp, the fault juxtaposes the same landslide unit with the rough and bumpy surface. Surface offset indicates that the fault motion had caused downward movement of the south side. North of this fault, the western edge of the landslide is clearly truncated by the fault in the south, and its southern tip cannot be found directly south of the fault. The only possible counterpart south of the fault that marks the western edge of the rough-surface landslide block in the trough floor is the contact between unit ls$_{gr}$ and unit ls$_{kb}$ in the east. This interpretation requires a left-slip of about 5 km after the emplacement of the rough-surface landslide block. This fault also has a minor component of down-to-the-south motion. The left-slip interpretation is consistent with the fold geometry that is cut by the fault, as its asymmetry also indicates a left-slip sense of shear, should it be considered as a drag fold.

Central Area

A geologic map was constructed using a CTX image across the central segment of the northern subtrough of Coprates Chasma (Fig. 16). The following units from youngest to oldest are recognized by interpreting the image: (1) recent landslides mostly concentrated along gullies (unit ls$_y$), (2) older landslides mostly distributed across the trough floor (unit ls$_o$), (3) younger surface sediments comprising mostly talus and dust deposits displaying smooth surface (unit sd$_y$), (4) older surface deposits comprising mostly talus and dust deposits with incised surfaces due to erosion (unit sd$_o$), (5) trough-fill deposits that can be further divided into a knob-forming subunit and a smooth-floor subunit (the former appears to be older based on mapped structural relationships; see following discussion) (unit

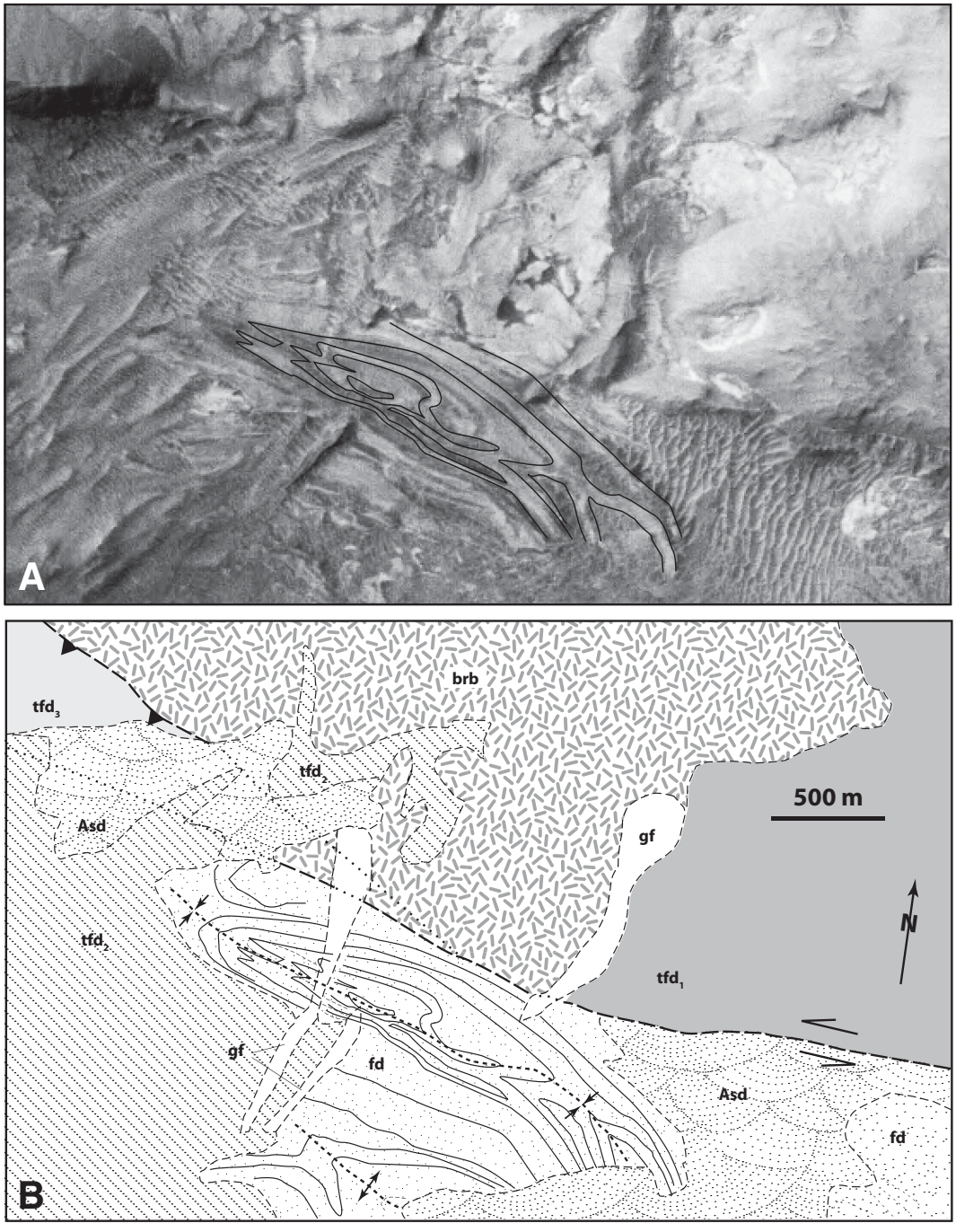

Figure 14. (A) Uninterpreted image and (B) interpreted image from an area across an interpreted fault. See Figure 12B for location.

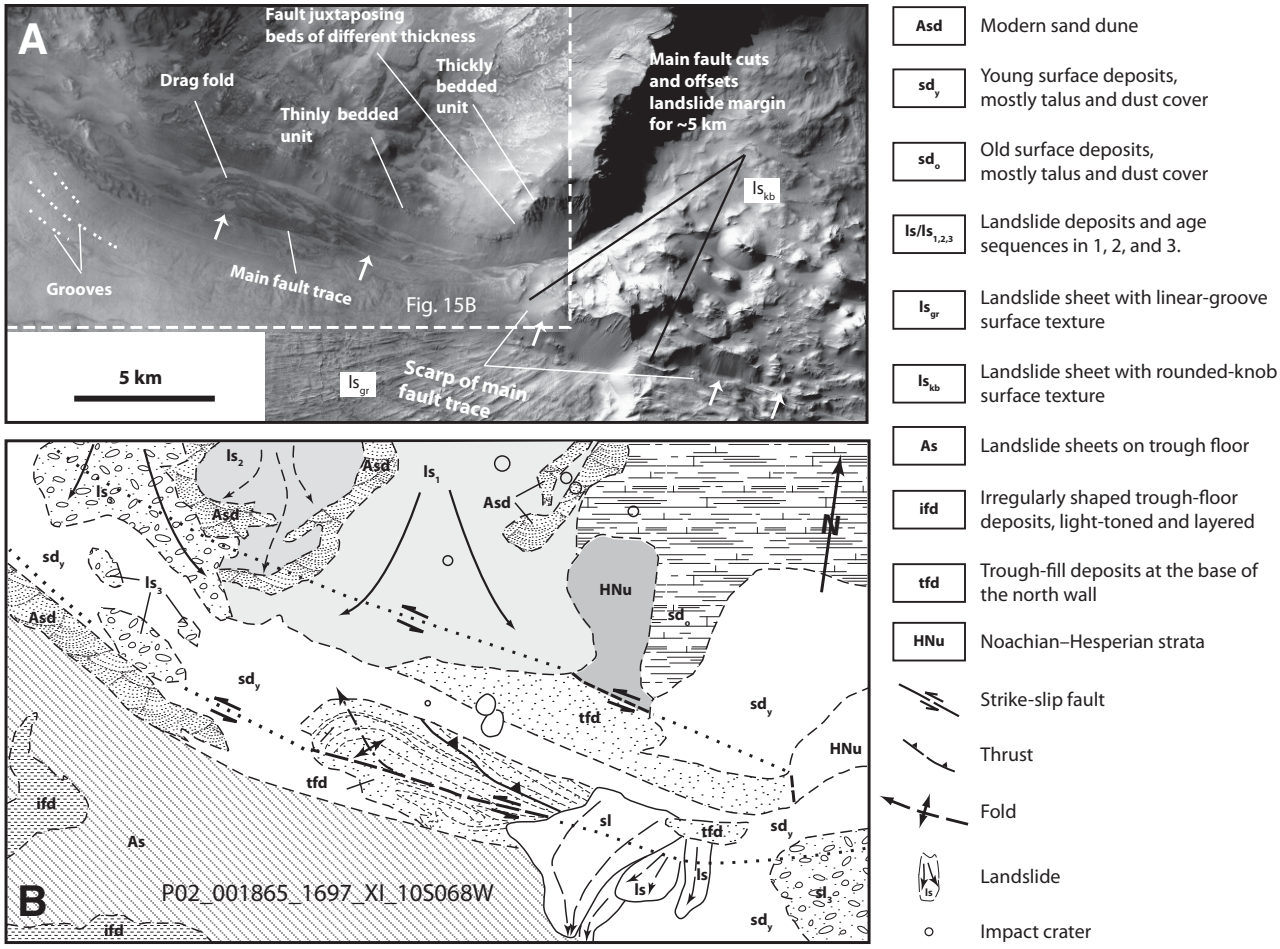

Figure 15. (A) Uninterpreted mosaic from Context Camera (CTX) images P02_001865_1697_XI_10S068W and P19_008616_1689_XI_11S068W. Note that the drag fold is cut by the same fault along its southern edge as the fault scarp that cuts and offsets a landslide with massive lithology. The offset distance of the western margin of this landslide is ~3–6 km. (B) Interpreted detailed geologic map based on image shown in A.

tfd), and (6) undivided Noachian–Hesperian bedrock exposed on the trough wall (unit HNu).

The mapped segment of the trough is remarkably "clean" in that it is nearly free of any large landslide deposits distributed across nearly the whole trough floor as seen in the west and east of Coprates Chasma and in Ius Chasma. At a first glance, the trough floor is smooth with a few small craters and mesa-like knobs (Fig. 16). In detail, however, one can see numerous small-scale structures such as west-northwest– and northwest-trending lobate scarps and northeast-trending fractures. Following the common practice in planetary geologic mapping (e.g., Schultz et al., 2010), the lobate scarps are interpreted as representing thrusts. The kinematics of northeast-trending fractures are not well defined. They are generally short and discontinuous (2–4 km) and do not offset any preexisting features laterally. Because of this, they are tentatively interpreted as normal faults or extensional fractures. This interpretation is consistent with their trend being perpendicular to the northwest-trending contractional lobate scarps.

East- and east-northeast–striking fractures are also present. They act either as linking structures between northwest-trending lobate scarps or small pull-apart extensional structures (Fig. 16). It appears that thrusting and folding along lobate scarps have caused exposure of older and more weathering-resistant trough-fill deposits, which are expressed as small mesas against the interpreted thrusts or inside the interpreted folds (Fig. 16).

A nearly continuous lobate scarp zone trending northwest is present along the southern margin of the subtrough zone. South of the scarp-defined thrust, there is a west-northwest–striking, left-slip fault that offsets a resistant marker bed for ~2–3 km. This same fault also defines a linear scarp that bounds the southern edge of the subtrough zone. This structural association (northwest-trending contractional structures and northeast-trending normal faults) indicates distributed left-slip shear parallel to the trough. From the regional geologic map (Fig. 1), it can be seen that the central segment of Coprates Chasma trends northwest, departing from the regional west-northwest trend of the trough. The localized contractional structures trending northwest may thus be induced by the development of a restraining bend in a broad trough-parallel left-slip shear zone.

Eastern Area

A detailed geologic map was constructed based on a CTX image covering a part of the eastern Coprates Chasma trough (B03_010712_1656_XN_14S053W) (Fig. 17). The following units, from oldest to youngest, were recognized: (1) slide complexes on the trough wall that are truncated by fault scarps (unit ls), (2) young surface deposits displaying smooth surfaces (unit sd_y), (3) deposits of a sand dune field (unit Asd),

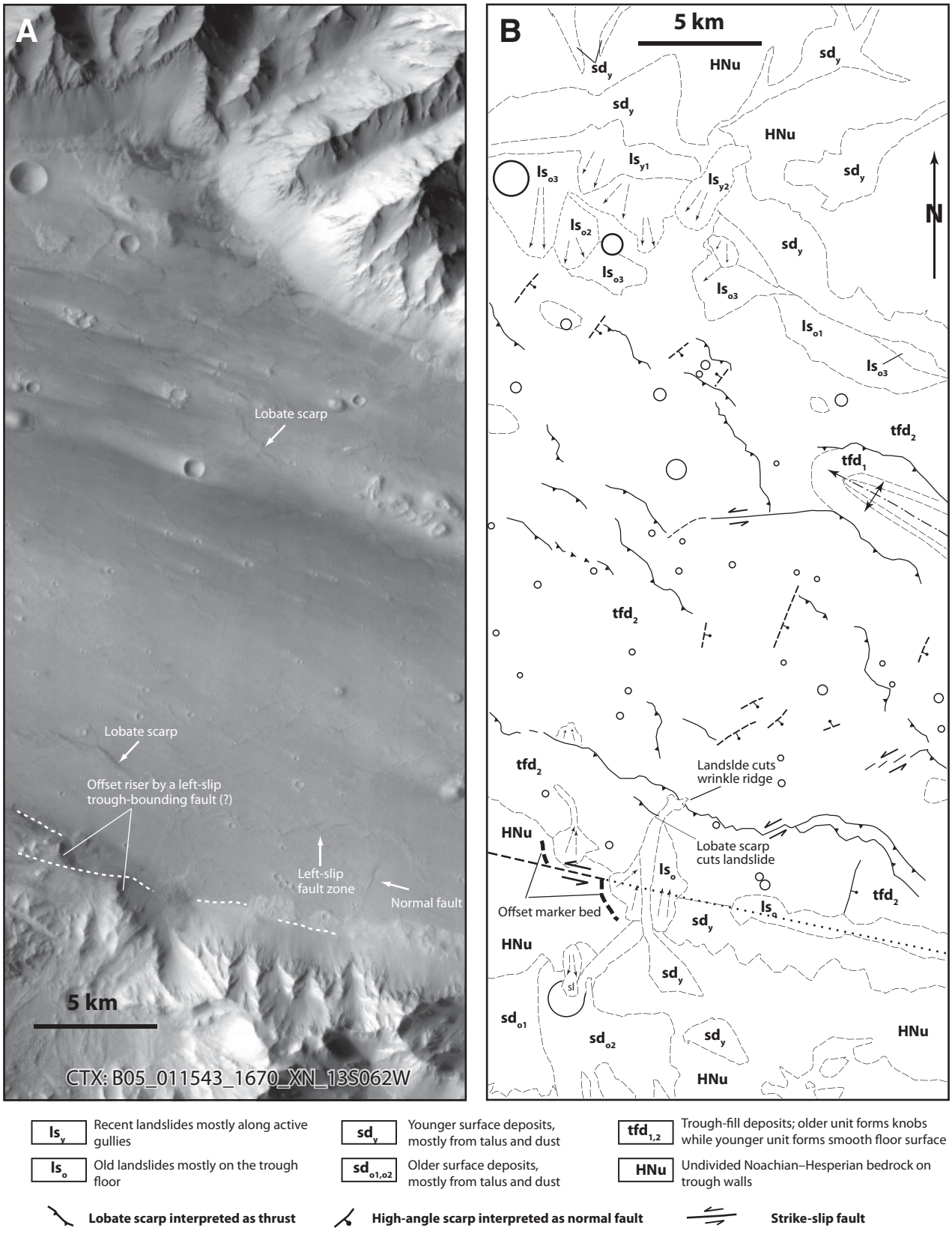

Figure 16. (A) Uninterpreted Context Camera (CTX) image B05_011543_1670_XN_13S062W displaying structures on the floor of Coprates Chasma. See Figure 1C for location. White triangles point to the trace of an interpreted left-slip fault bounding the southern edge of the trough zone. Possible offset of a riser and/or cliff-forming marker is also shown. (B) Interpreted geologic map based on image shown in A.

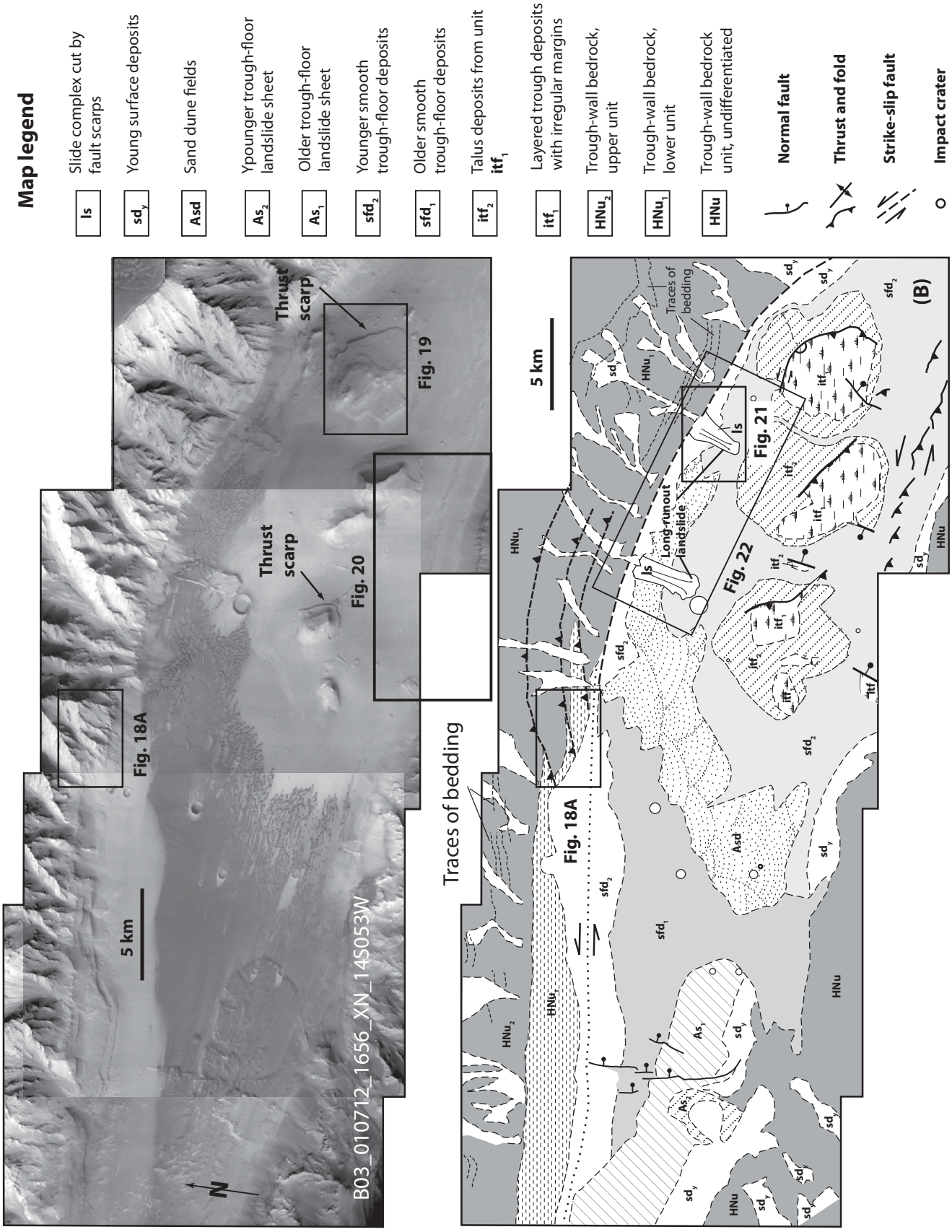

Figure 17. (A) Uninterpreted Context Camera (CTX) image (B03_010712_1656_XN_14S053W) of Coprates Chasma. See Figure 1C for location. (B) Interpreted geologic map of the northern trough zone of easternmost Coprates Chasma based on image shown in A.

(4) a younger trough-floor landslide sheet (unit As_2), (5) an old trough-floor landslide sheet (unit As_1), (6) younger smooth trough-floor deposits (unit sfd_2) along the base on the north trough wall, (7) older smooth trough-floor deposits (unit sfd_1), (8) mass-wasting deposits derived from the cliff-forming unit itf_2, (9) layered trough-floor deposits with irregular margins (unit itf_1), (10) the upper unit of the trough-wall bedrock (unit HNu_2), and (11) the lower unit of the trough-wall bedrock (unit HNu_1).

Structures on the North Trough Wall

The trend of the trough zone of Coprates Chasma in the study area generally makes a right-step bend (Fig. 17). Associated with the sharp bend, there are complex structures on the trough wall (Fig. 17). First, at the western end of the bend, discordant beds can be seen on the curved cliff face of the trough wall (Figs. 18A and 18B). A thick and weathering-resistant layer can be traced on the lower-right corner of the image in Figure 18. Given its resistant appearance, it is expected that the same bed is continuous along the cliff face, barring any abrupt facies changes in the layered wall rocks. On the right side of the image, above this nearly flat-lying bed on the cliff face, there are layers that have different orientations with markedly more steep dips. The projected contact between the two discordant packages of beds also terminates the western end of the thickly bedded subhorizontal unit (Fig. 18). This relationship may be explained by the presence of a thrust ramp that cuts up section. This interpretation is shown in Figure 18C, which requires that the tilting of beds above the faults was induced by upward motion on the thrust ramp. The interpreted thrust trace coincides with a region where beds appear to be fractured as expressed by discontinuous bedding (see white arrows in Fig. 18A).

Farther west, a thin weathering-resistant bed appears to be locally repeated and terminates laterally away from the repeated section (Fig. 18A). This relationship may be explained by the presence of a minor thrust (Figs. 18A and 18C). As no fault scarps at the base of the trough wall are exposed, it is inferred that the trough-bounding fault is buried by talus deposits originating from the trough wall (Fig. 18A). The kinematic nature of this inferred and now-buried fault is unknown.

Structures on the Trough Floor

Contractional structures can also be recognized on the trough floor at the right-step bend of the northern Coprates trough (Fig. 19). Bedded outcrops of isolated mesas display northwest-trending folds; their shapes can be deduced from bedding attitudes estimated according to the "rule of V's" (Fig. 19). Lobate scarps on the trough floor are concentrated along the southern margin of the trough zone (Fig. 20). Some of the short scarps display an en echelon pattern indicating left-slip shear (Fig. 20).

Trough-Bounding Structures along the Central Segment of a Right-Step Bend

The trough-bounding fault at the base of the north wall is best expressed in the central segment of the right-step bend (Figs. 17 and 21). This fault is marked by a continuous and abrupt escarpment separating the bedrock of the north wall from trough-fill deposits (Fig. 21). The escarpment cuts spurs and truncates hanging gullies at its upper edge (Fig. 21). The lower edge of the escarpment is covered by recent surficial deposits (talus and dust). The young deposits themselves are also cut by linear scarps that dip both to the north and south (Fig. 21). In addition to scarps parallel to the main escarpment, several northeast-trending high-angle scarps and one northwest-trending curvilinear scarp are also exposed against the north trough wall. The curvilinear scarp is interpreted to have originated from thrusting, while the high-angle scarps trending northeast are interpreted to have resulted from normal faulting.

A detailed geologic map was constructed in this area (Fig. 21). Major lithologic and morphologic units, from youngest to oldest, recognized by this study include: (1) young surface deposits comprising mostly talus and gully-fill deposits with smooth surfaces (unit sd_y), (2) slide deposits including both landslides and debris flows mostly concentrated at the base of the north wall (unit sl), (3) sand dune deposits (unit Asd), (4) long-runout landslides or debris flows (unit sl_{lr}), (5) recent trough-fill deposits with smooth surfaces (unit sfd_2), (6) trough-floor deposits with irregular margins (unit ifd_1), (7) the upper unit of the undivided Hesperian–Noachian strata characterized by dark-toned, gentler slope-forming and flat-lying beds (unit HNu_2), and (8) the lower unit of the undivided Hesperian–Noachian strata characterized by light-toned and cliff-forming strata (unit HNu_1).

The most interesting relationship in the map area is that the landslide scarps on the trough wall and the long-runout landslides on trough floors are both truncated by the trough-bounding escarpment without clear matching counterparts across the fault (Fig. 21). For example, a large bowl-shaped landslide scarp is present in the north-central part of the image; their two edges both terminate at the fault scarp, and there is no obvious landslide of the same width and volume directly south of the fault (Fig. 21). Similarly, a long-runout landslide that is ~7 km long and less than 2 km wide is truncated at its northern end by the escarpment. These relationships are perhaps some of the best lines of evidence for the tectonic origin of the trough-bounding escarpment.

The lack of a breakaway zone for the long-runout landslide on the trough floor is puzzling. One possibility is that the source region of this landslide has been completely eroded away above the escarpment. Given the youthfulness of the landslide, which has hardly any impact craters and displays pristine landforms of a typical landslide, this interpretation would require unusually high erosion rates in recent Martian history. This interpretation, however, does not explain why the source region of the landslide was eroded away while the nearby landslide itself is not eroded at all (Fig. 21). The same argument can also be applied to the preserved landslide scarps on the trough wall that do not have a matching counterpart in the trough floor. Because of this difficulty, a tectonic origin of the mismatch of landslides on the trough wall and trough floor is proposed here. A possible, though nonunique, explanation is that the headless and toeless landslides were offset by strike-slip motion on the trough-bounding fault. Assuming that the long-runout landslides were derived from debris flows out of trough-wall canyons, a good match can be achieved by shifting the landslides on the trough floor eastward for 4.8 km, with the approximation that the trough-bounding fault is straight (Fig. 22). Although this reconstruction allows two long-runout landslides to match two different trough-wall canyons simultaneously, the solution does not preclude other possible matches of the truncated landslides with different canyon walls. That is, the matching could lie outside the satellite image. For this possibility, it is important to point out that the structures on the trough wall along the right-step bend of the northern Coprates trough zone are dominated by thrusts and folds. Only left-slip faulting across a right-step bend can produce contractional deformation (e.g., Sylvester, 1988). For this reason, left-slip motion on the trough-bounding fault is favored. One should also note that the estimated slip based on matching truncated the landslides and their sources has been accumulated only since the emplacement of the landslides, thus the total slip of the trough-bounding fault could be much larger than the 4.8-km left-slip motion based on the estimated offset of the landslides.

STRUCTURES ON THE PLATEAU MARGINS

Consistent with terrestrial field-based and photogeologic mapping investigations, unfolding the evolutional history of Valles Marineris also requires mapping and characterizing the geology surrounding the canyon system. One of the problems with mapping structures only

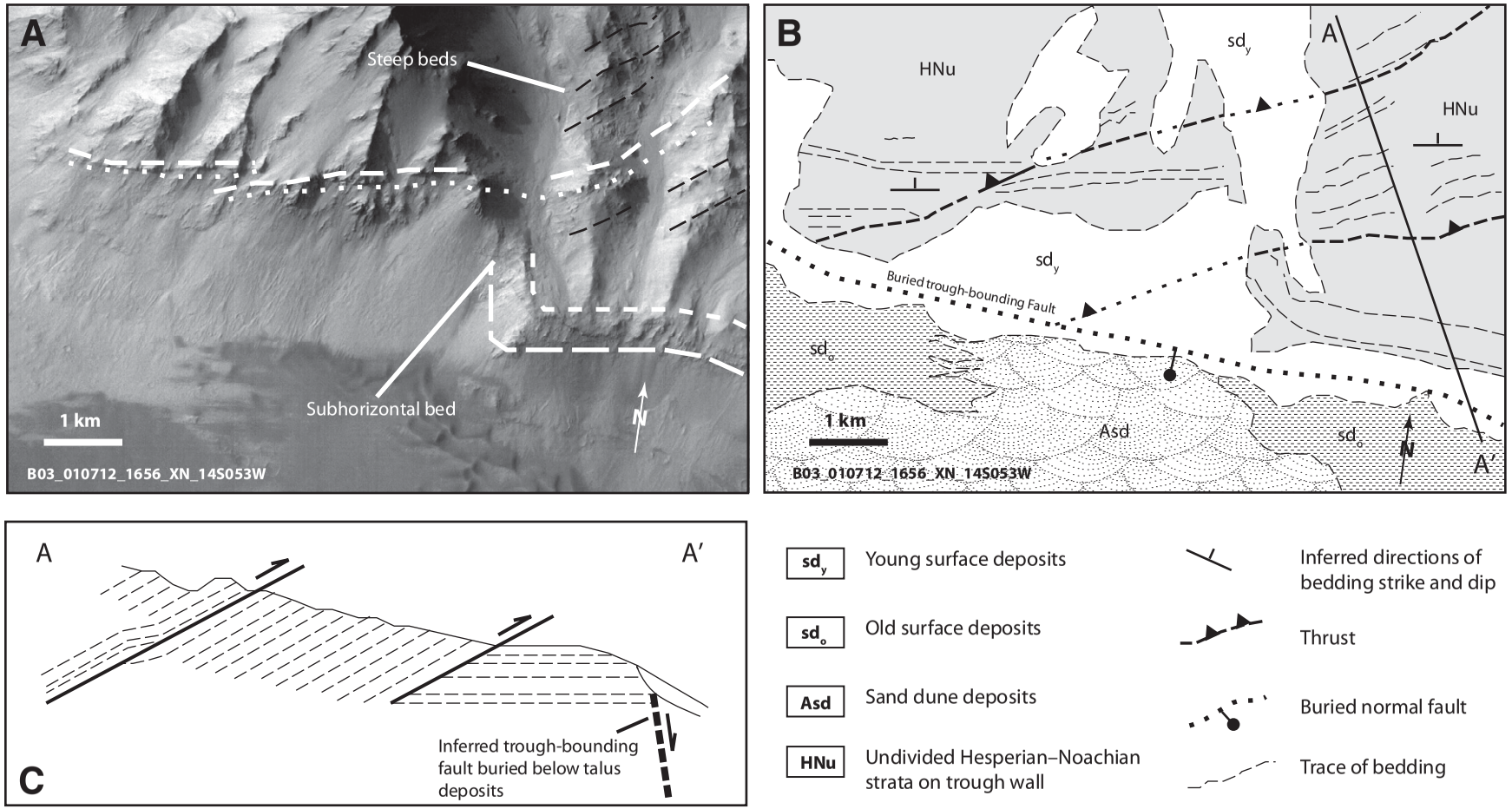

Figure 18. (A) Uninterpreted Context Camera (CTX) image B03_010712_1656_XN_14S053W with location shown in Figure 17. (B) A geologic map based on interpretation of the CTX image shown in A. (C) A schematic cross section showing possible relationship between bedding and interpreted thrusts.

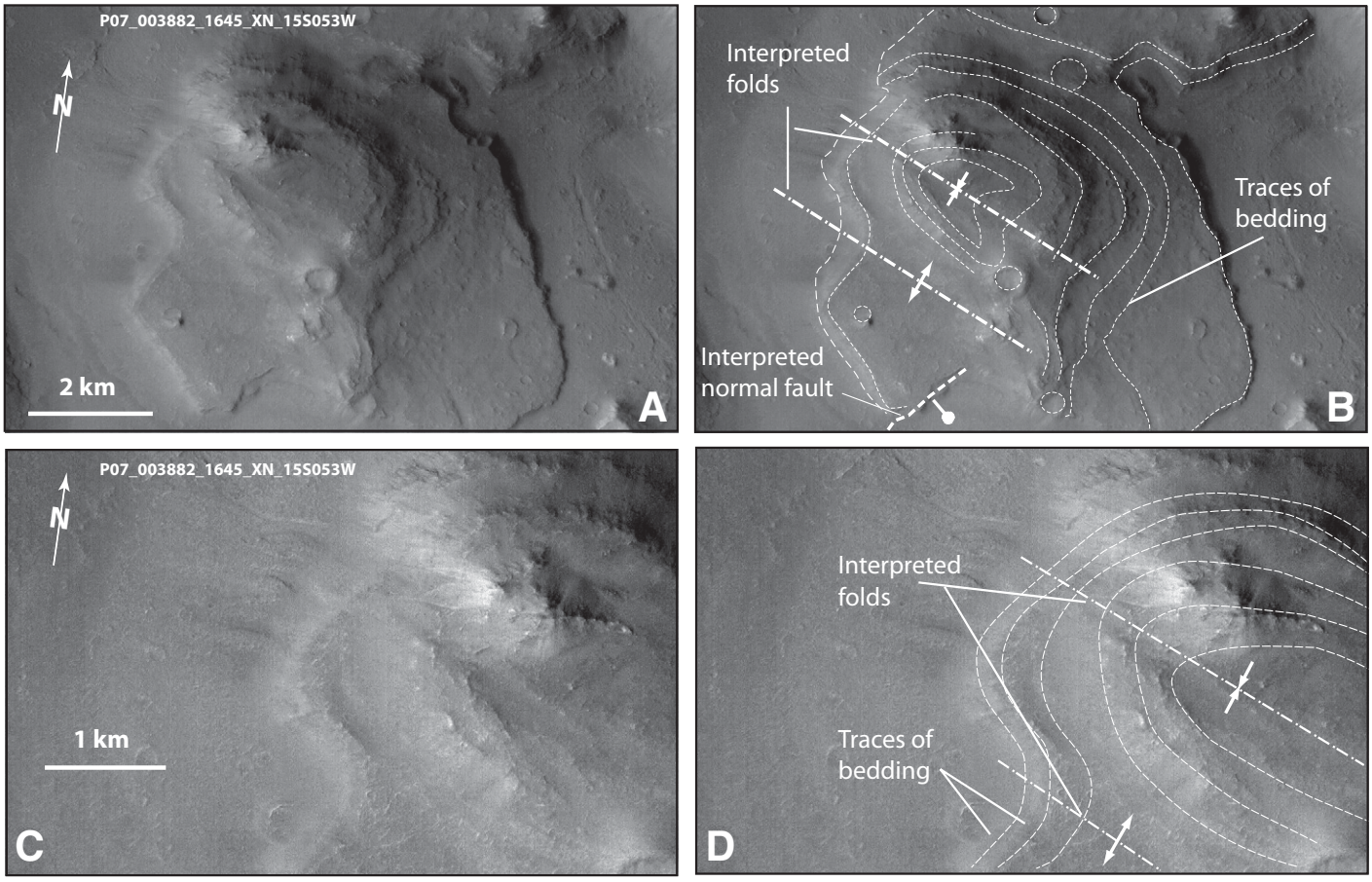

Figure 19. (A) Uninterpreted Context Camera (CTX) image P07_003882_1645_XN_15S053W, with location shown in Figure 17. (B) A geologic map based on interpretation of the CTX image shown in A. (C) Uninterpreted close-up view of CTX image P07_003882_1645_XN_15S053W shown in A. (D) Interpreted geology based on image shown in C.

within the trough zones of Valles Marineris, for example, is that it is difficult to ascertain whether the structures are uniquely associated with the development of the trough floors via tectonics, surface processes, or a combination of both. To address this issue, structures on the northern plateau margin of Coprates Chasma were also investigated in this study. A major finding of this investigation is that normal, left-slip, and thrust faults may all be present in the region within a distributed left-slip shear zone parallel to Valles Marineris.

The existence of left-slip faults on the plateau margin is evident in a THEMIS image (THEMIS V09827002) shown in Figure 23. In this image, left-lateral offsets of a ridge coming out of a crater in the south vary from 600 to 2000 m across several northwest-trending faults. The trend of the left-slip faults is slightly oblique at an angle of 10°–15° to the west-northwest–trending Coprates trough zone (Fig. 1). All the left-slip faults have north-facing scarps, indicating a component of down-to-the-north normal-slip motion. Grabens subparallel or at a small angle to the observed left-slip faults are also present in the area. They are geometrically linked with the left-slip faults, suggesting that the normal and left-slip faulting occurred at the same time. Together, these observations suggest the occurrence of left-slip transtensional tectonics across this segment of the plateau margin.

The presence of left-slip faults on the northern plateau margin of Coprates Chasma is also evident from THEMIS image V06856002 (Fig. 24). In this image, a fault is defined by north-facing scarps across which channels are systematically deflected in a left-lateral sense (Fig. 24). Such a stream deflection pattern is typically related to strike-slip motion on Earth (e.g., Yeats et al., 1997), with the best example in the Wallace Creek area of central California along the San Andreas fault (Figs. 24F and 24G) (Sieh and Jahns, 1984). In Figure 24A, at least eight deflected channels can be recognized. The morphology of channel margins becomes less and less well defined westward, consistent with the westernmost channel being the oldest as well as the first to have been offset by the inferred left-slip fault. The deflection pattern implies at least 11 km of left-slip motion after the initiation of the deflected drainage system (Fig. 24B). Notice also that the latest drainage activity on the Valles Marineris plateau dates from the Late Hesperian (Mangold et al., 2004, 2008). Thus, these observations indicate that left-slip faulting was active around that period. As the fault cuts the drainages, its offset could have postdated the Late Hesperian.

Another feature shown in Figure 24A is a northwest-trending narrow linear topographic high present north of the interpreted fault. The shape of the linear ridge resembles that of a wrinkle ridge, which may lie above a blind thrust system below or thrusts along the edges of the fold (Fig. 24B). South of the interpreted left-slip fault, series of north-northeast–striking and south-southeast–facing linear scarps are present. A prominent basin is present against one of the major scarps, which may resemble a half-graben bounded by a normal fault on the northwest side of the basin. The interpreted orientations of the normal faults and the wrinkle ridge are all

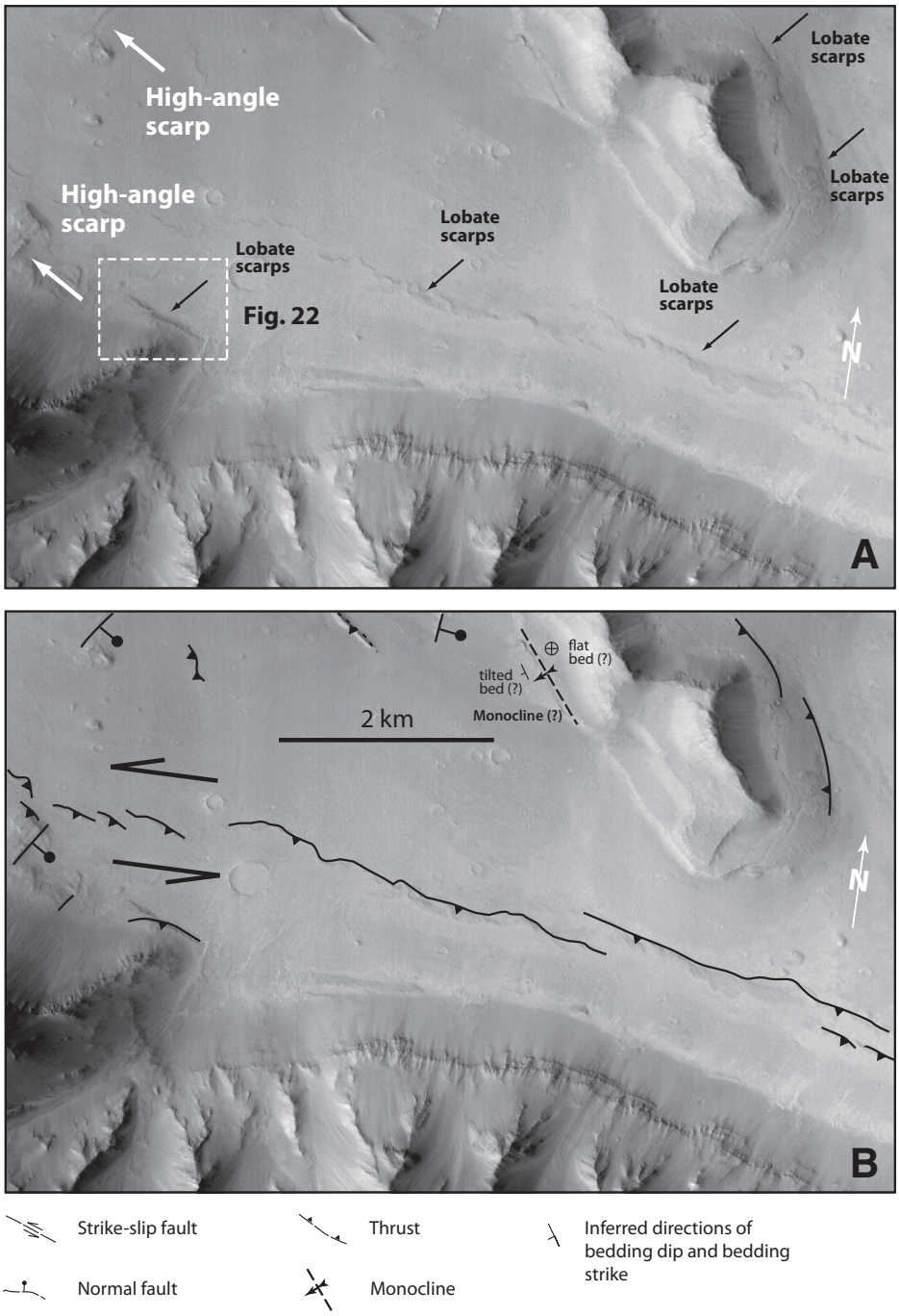

Figure 20. (B) Uninterpreted Context Camera (CTX) image P07_003882_1645_XN_15S053W, with location shown in Figure 17. Black arrows point to lobate scarps interpreted as surface traces of thrusts, and white arrows point to interpreted normal fault scarps. (B) Interpreted geology based on image shown in A.

consistent with left-slip shear. Assuming that the main trunks of the drainage system were straight, restoring the drainage network yields total left-slip motion of 13 km and ~30° of counterclockwise rotation (Figs. 24C, 24D, and 24E).

Distributed left-slip deformation is also observed in the plateau region between eastern Candor and western Coprates Chasmata. As shown in THEMIS image I09802001, this deformation is expressed by the development of major and widely spaced (~15 km) north-northeast–striking normal faults (Fig. 25). These structures are expressed by linear scarps and were mapped earlier by Witbeck et al. (1991) as normal faults. A graben structure is bounded by a southeast-dipping normal fault on the northwest side and three northwest-dipping normal faults on the southeast side (Fig. 25). The surfaces of the footwall blocks are all tilted in the opposite directions of the fault dips, which are expressed by gentle back slopes. This observation is consistent with the classic isostatic rebound pattern of normal-fault footwalls (e.g., Masek et al., 1994). The range-bounding normal faults in the northern part of the image terminate at a zone of closely spaced (<1 km) fractures (Fig. 25). At a first glance, they appear to represent a series of narrow grabens, but a closer examination suggests a mixed mode of fracture formations, with some displaying left-slip motion and others displaying normal slip (shown by white lines in Fig. 25). This is evidenced by a groove feature that is offset by both left-slip and normal faults across the same northwest-striking fault zone. This indicates that the northwest-trending closely spaced fracture zone may be a left-slip transtensional system. Mutual crosscutting relationships can be detected between northwest-striking faults and the southeasternmost range-bounding normal fault. The southernmost scarp of this northeast-striking fault is offset by a left-slip fault. However, the same northeast-striking normal fault also terminates northwest-trending fractures that display the same morphological features (i.e., grabens next to the faults) as those to the south. Because of this relationship, the northwest-striking left-slip transtensional system and northeast-striking range-bounding normal faults must have been developed synchronously with the northwest-trending fracture zone at their southern terminations. Their orientations are consistent with deformation in a broad left-slip shear zone.

Although the northwest-trending fracture zone and northeast-trending graben-bounding structures may be coeval, closely spaced northwest-trending graben structures are also present in the uplifted blocks of the normal-fault footwalls (Fig. 25). This relationship suggests that an event of northeast-southwest extension predates the inferred distributed left-slip transtensional faulting expressed by the widely spaced, northeast-trending normal faults.

DISCUSSION

Ius-Melas-Coprates Left-Slip Transtensional Fault Zone

The new observations obtained by this study are consistent with the original interpretation of Blasius et al. (1977), in which trough zones of the Valles Mariners are bounded by major scarp-forming faults with significant normal-slip

components. However, the detailed mapping conducted here also reveals several unexpected results. First, some trough-bounding faults display clear evidence for left-slip motion in addition to trough-side-down normal faulting. Second, structures in the trough zones of Ius Chasma are dominated by northwest-trending folds. Third, east-striking left-slip faults and northeast-trending extensional structures (joints) also occur in the trough zone of Ius Chasma. These structures consistently cut all trough-fill units and are thus interpreted to have tectonic origins rather than being induced by surface processes such as emplacement of landslides. Locally, northeast-striking left-slip faults and north-northwest–striking right-slip faults are also present. The mutual crosscutting relationships suggest that these structures were developed synchronously under the same simple-shear regime. The geometric relationships among these structures are consistent with left-slip shear parallel to the Valles Marineris troughs.

The occurrence of folded intraformational soft-sediment structures with broken beds displaying folds in southern Ius Chasma suggests coeval development of basin fills, slump structures, and northwest-trending folds. Rocks involving soft-sediment deformation are thinly bedded and light-toned and do not match rocks on trough walls, which are typically dark-toned, thickly bedded, and resistant to folding along Ius Chasma (Fig. 12). For these reasons, broken beds via soft-sediment deformation were most likely derived from margins of the basins or transported from elsewhere. The high intensity of deformation expressed by the formation of <15 m angular breccias (see Figs. 12C–12F) and the lack of large topographic relief from basin margins to basin centers suggest that the fragmentation and transport of the broken bed unit were induced by seismic activity during strong ground shaking (also see Metz et al., 2010).

Although folding in Ius Chasma, particularly in its southern trough where soft-sediment structures are present, may intuitively be related to emplacement of large landslides, the timing is incompatible, as landslide emplacement clearly postdates folding (Fig. 9). The hypothesis of landslides as the driving mechanism for fold development also faces the difficulty of explaining the uniform northwest trend of first-order folds wherever they are observed, as the directions of landslide emplacement are highly variable in Valles Marineris (Lucchitta, 1979).

Observations from Coprates Chasma also support the hypothesis of its formation being controlled by left-slip faulting, such as the presence of a left-slip trough-bounding fault associated with prominent drag folds (Fig. 15). Developmentofnorthwest-trendingcontractional

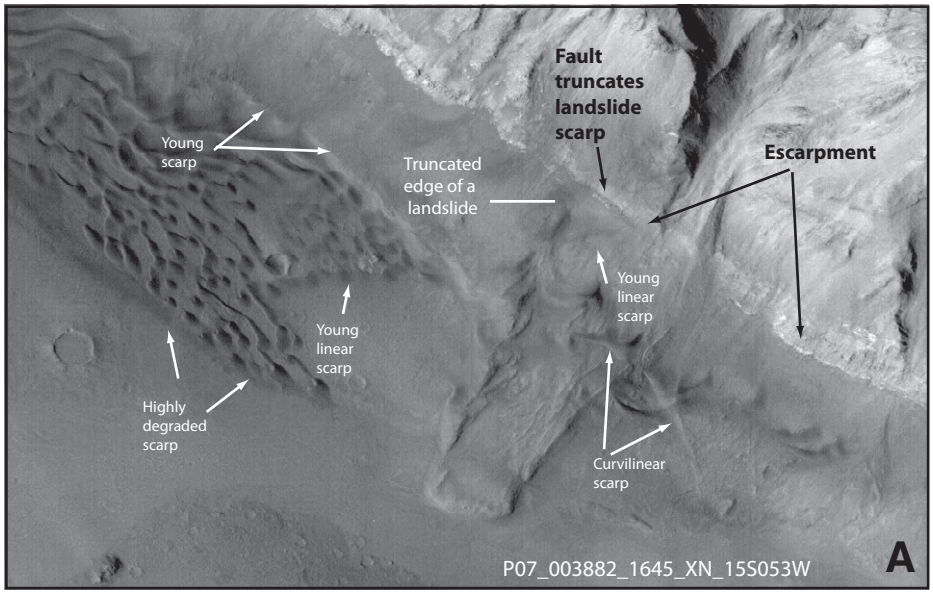

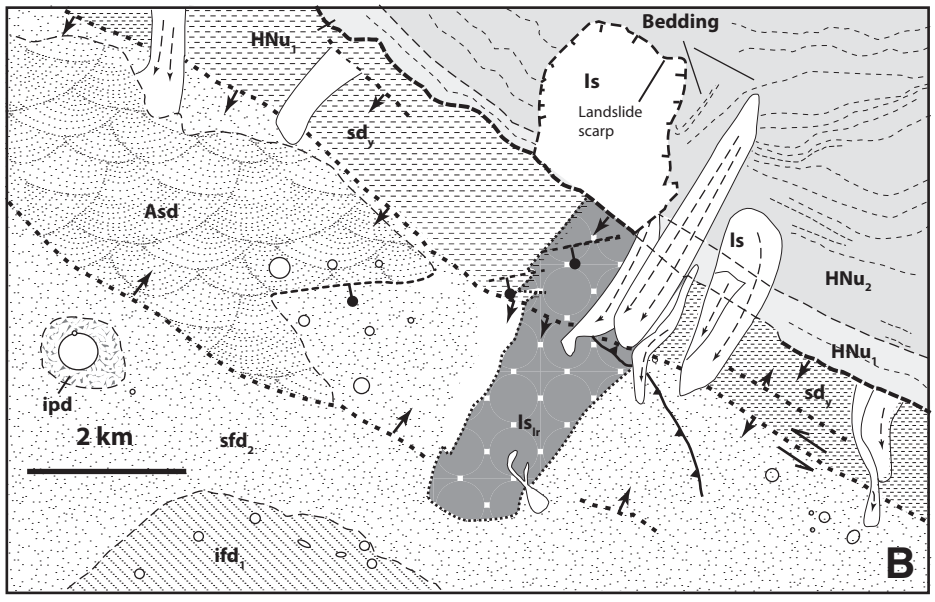

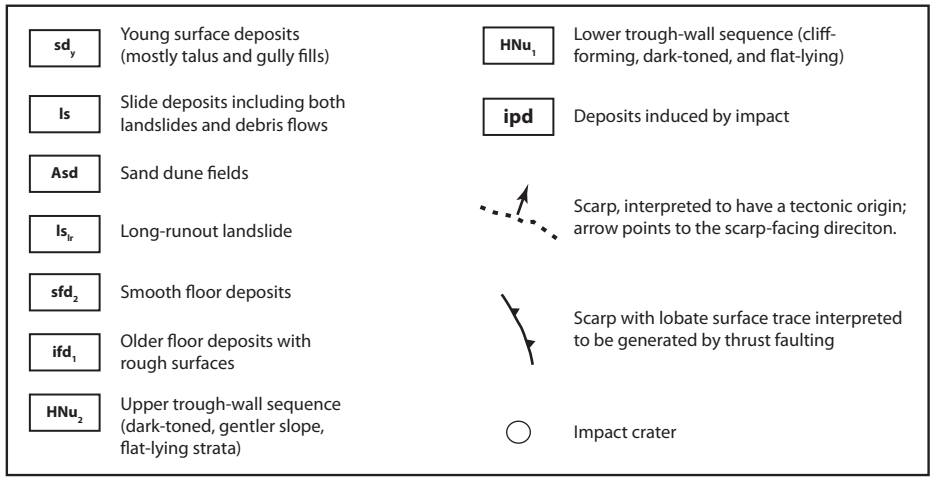

Figure 21. (A) Uninterpreted Context Camera (CTX) image P07_003882_1645_XN_15S053W, with location shown in Figure 17. (A) Detailed geologic map based on interpretation of image shown in A.

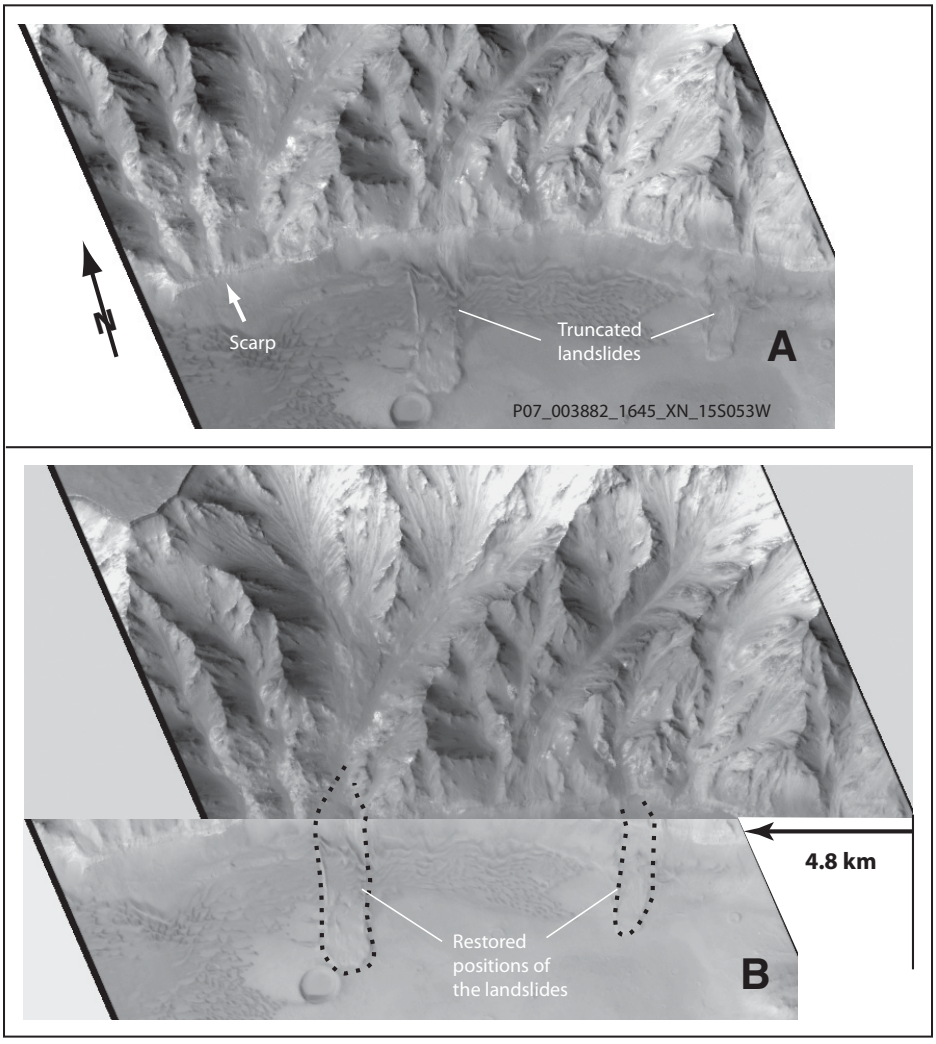

Figure 22. (A) Context Camera (CTX) image P07_003882_1645_XN_15S053W showing truncation of two landslides by a sharp fault scarp at the base of the north wall of the northern Coprates trough zone. See Figure 17 for location. (B) Restored landslide positions after matching their truncated upper edges against compatible channel outlets at the northern trough walls.

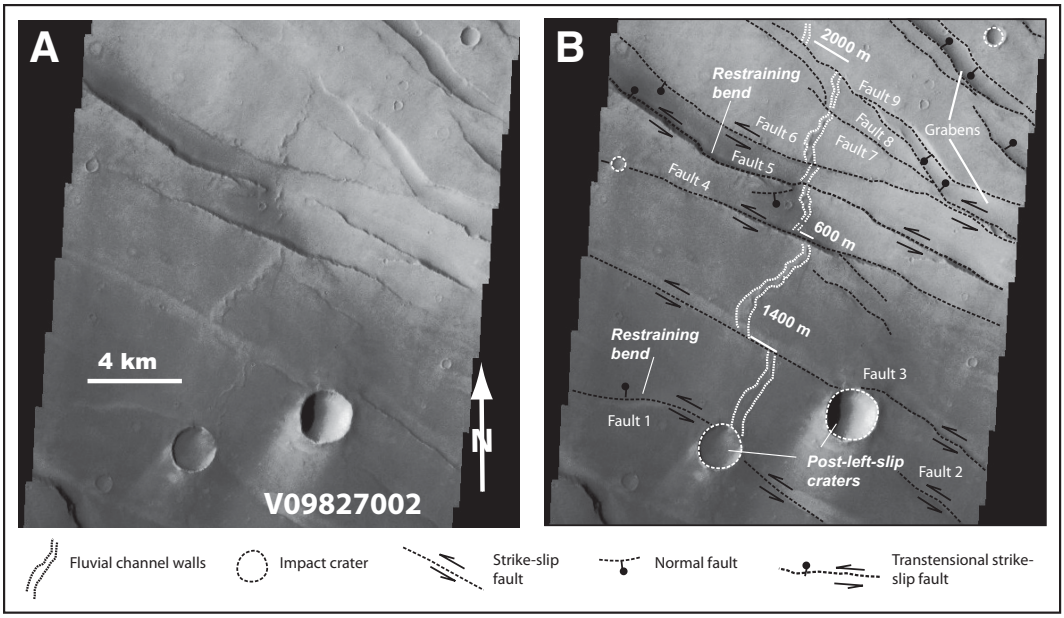

Figure 23. (A) Uninterpreted THEMIS (Thermal Emission Imaging System) image V09827002, with location shown in Figure 1C on the plateau region north of Coprates Chasma. (B) Interpreted geologic map based on image shown in A. Note presence of a series of left-slip faults trending parallel to Valles Marineris on the plateau margin north of Coprates Chasma.

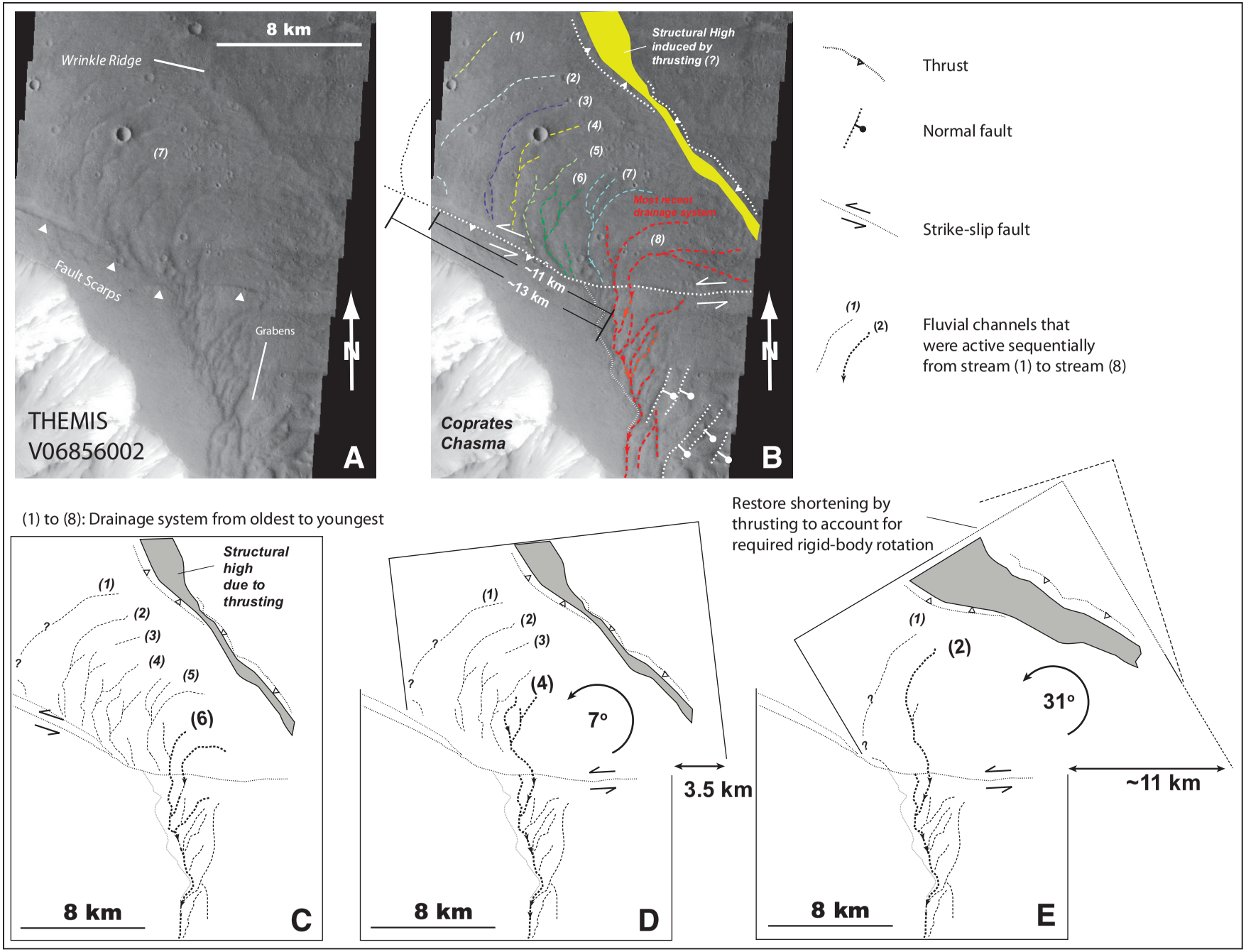

Figure 24. (Continued on following page).

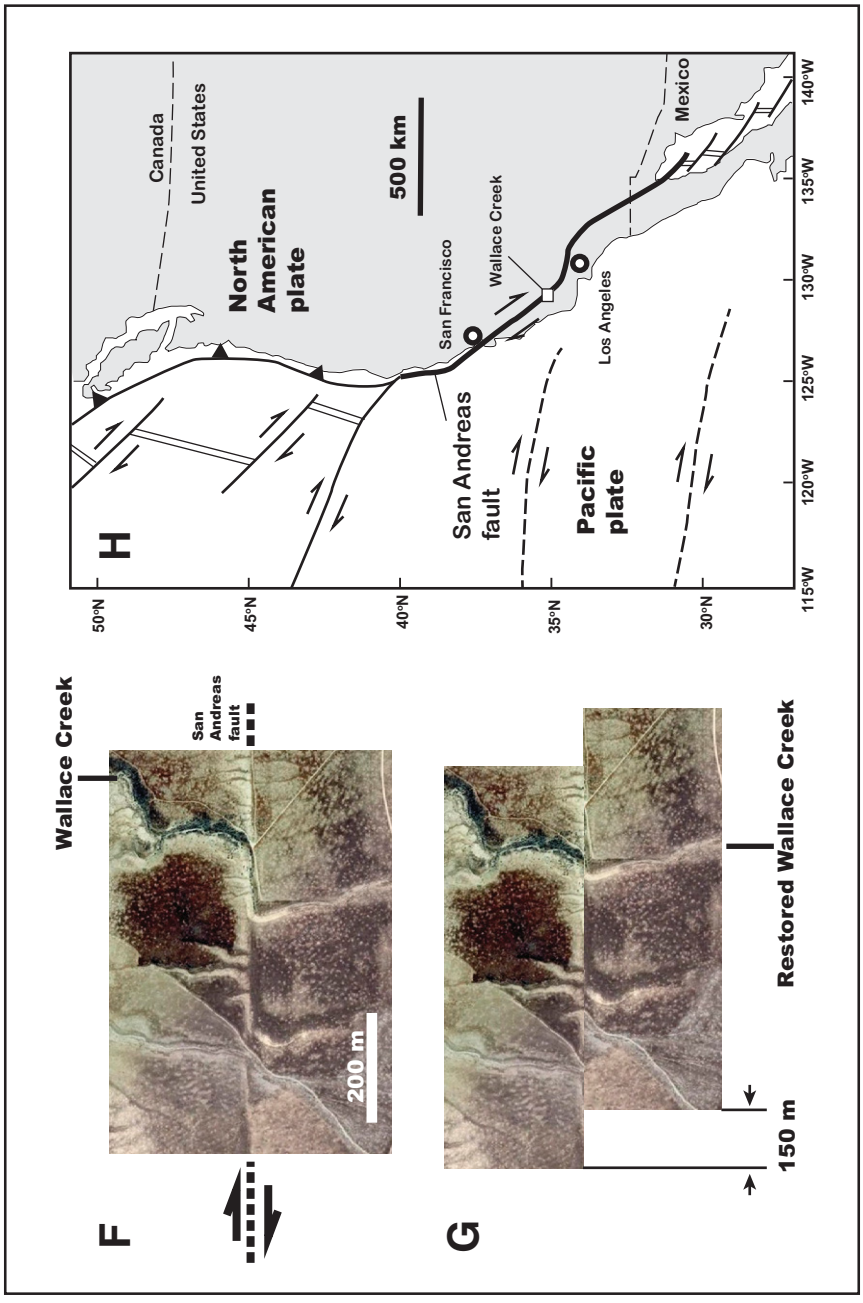

Figure 24. (A) Uninterpreted THEMIS (Thermal Emission Imaging System) image V06856002 on plateau margin north of Coprates Chasma, with location shown in Figure 1C. Note that the interpreted fault is expressed by linear scarps. (B) Interpreted geologic map based on image shown in A. Note left-lateral deflection of a south-flowing drainage system across a left-slip fault on plateau margin. (C–E) Step-by-step kinematic restoration of the drainage system by removing left-slip motion on the interpreted fault. (F–G) Present and restored stream channels along the right-slip San Andreas fault in central California. Image was taken from Google Earth. (H) Location of the image.

structures (folds, lobate scarps, and thrusts), northeast-trending normal faults, and west-northwest–trending left-slip shear zones in the trough zones is also compatible with trough-parallel left-slip shear (Figs. 16, 17, and 20).

The strongest evidence for left-slip faulting across Coprates Chasma is the presence of left-slip faults on the plateau margin north of Coprates Chasma (Figs. 23, 24, and 25). Similar to the observed structures within the trough zones, left-slip transtensional deformation also occurred on the plateau margin, which is indicated by the formation of closely spaced trough-parallel, left-slip faults, northeast-striking normal faults, and northwest-trending contractional structures (Fig. 25). The fresh fault scarps and left-lateral deflection of recent drainages all indicate that left-slip faulting on plateau margins occurred recently, similar to the age of faulting within the trough zones in the Late Amazonian (i.e., younger than 0.7 Ga) (Witbeck et al., 1991).

Due to extensive cover of sand dunes and recent landslides (unit Avm of Witbeck et al., 1991; Peulvast and Masson, 1993), Melas Chasma does not display long linear traces of scarps as those seen along Ius and Coprates Chasmata. For this reason, this study did not examine the margin and interior structures of this trough. However, my reconnaissance work indicates that the trough floors of Melas Chasma also expose northwest-trending folds (e.g., see CTX image P01_001575_1702_XN_09S075W), compatible with trough-parallel left-slip shear as seen in Ius and Coprates Chasmata. The details of this work will be presented elsewhere. In any case, it appears that the trough-bounding fault zone in Melas Chasma linking the North Ius fault in the west and the North Coprates fault in the east may have been largely buried below thick trough-fill deposits, some of which are folded due to deep-seated, left-slip faulting.

Testing Models for the Origin of Valles Marineris

Observations from this study have important implications for testing the competing models for the origin of the Valles Marineris trough system. First, the occurrence of continuous linear scarps over tens of kilometers to >100 km along the bases of the steep trough walls of Ius and Coprates Chasmata is best explained by the formation of fault scarps as originally suggested by Blasius et al. (1977). This argument is supported by the observation that trough-bounding scarps can be related to left-slip faults at several places examined by this study (Figs. 7, 15, 16, and 17). Thus, the results from this study strongly favor

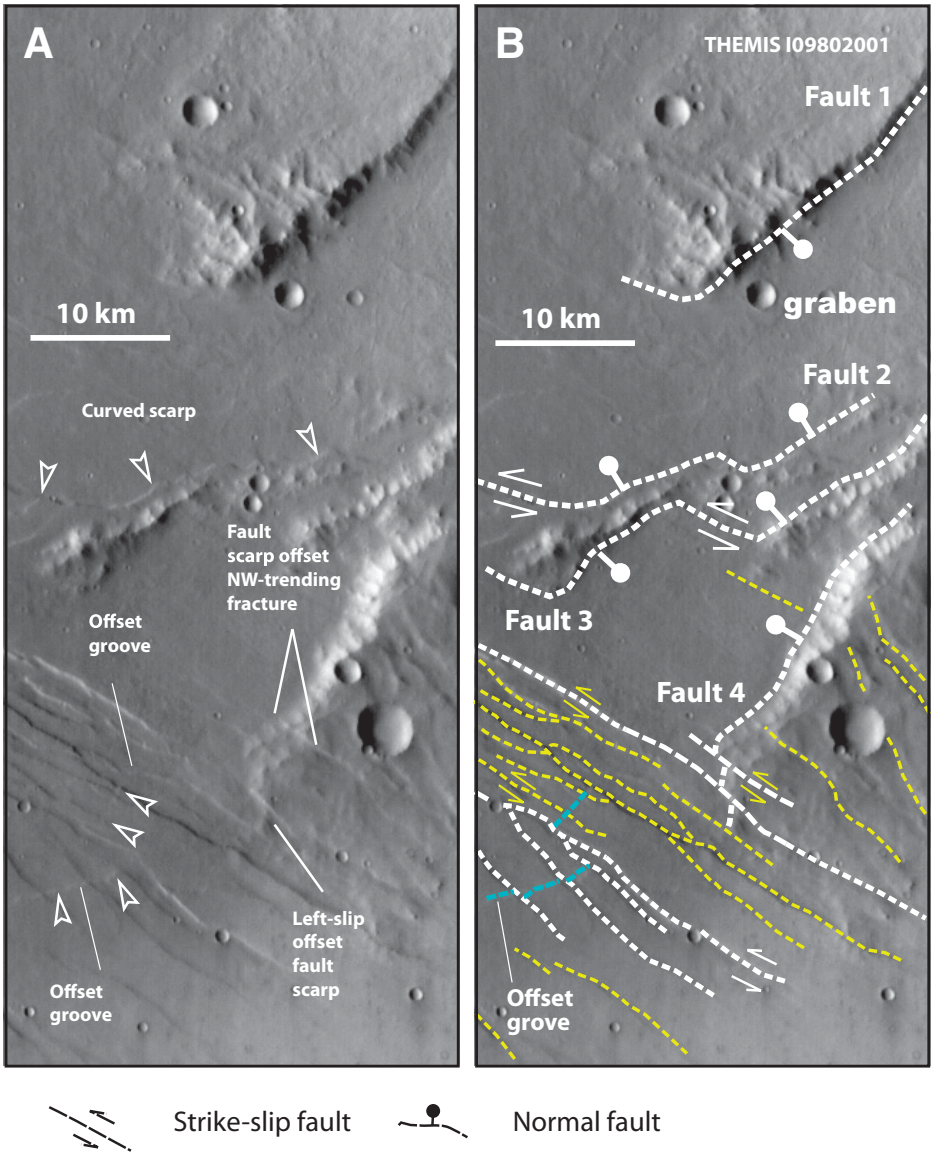

Figure 25. (A) Uninterpreted THEMIS (Thermal Emission Imaging System) image I09802001, with location shown in Figure 1C. (B) Interpreted fault map based on image shown in A. Note that interpreted northeast-striking normal faults either terminate into or are cut by the west-northwest–striking left-slip faults. Also note that west-northwest–trending narrow grabens are present in the uplifted footwalls of northeast-striking normal faults.

a tectonic origin for the development of Ius and Coprates Chasma and likely for the entire Valles Marineris system (see following discussion on closed basins). Second, wide occurrence of left-slip faults parallel to trough walls, as well as northwest-trending folds and thrusts oblique to trough walls, does not support either the right-slip or pure-rift models (Fig. 3). Third, the Coprates fault zone extends at least several hundreds of kilometers east of the northern termination of the Thaumasia thrust belt, which rules out the suggestion that the left-slip Valles Marineris fault zone terminates at the thrust belt as required by the megalandslide model of Montgomery et al. (2009) and the gravitational-spreading or extrusion model of Webb and Head (2002) and Anguita et al. (2006) (Table 1).

Magnitude of Left-Slip Motion, Fault Termination, and Palinspastic Reconstruction

The overwhelming evidence for a left-slip origin of Ius and Coprates Chasmata begs two important questions: (1) What is the total magnitude of left-slip motion along the trough-bounding fault zone? (2) How does the Ius-Melas-Coprates fault system terminate at the western and eastern ends? The two issues are discussed next.

Magnitude of Left-Slip Motion

Offset of the Thaumasia thrust. A potential candidate for measuring left-slip offset of the Ius-Melas-Coprates fault zone is the truncated Thaumasia mountain belt consisting of the Coprates Rise directly south of Coprates Chasma. The origin of the Thaumasia mountain belt has been attributed to two mechanisms. First, Schultz and Tanaka (1994), Dohm and Tanaka (1999), Anguita et al. (2006), Dohm et al. (2001a, 2001b, 2007, 2009), and Nahm and Schultz (2010) all suggested that the base of the eastern topographic front of the mountain range is marked by a major thrust they termed the Thaumasia thrust (Fig. 1). This inference is consistent with terrestrial analogues for a mountain belt such as the Himalayan orogen. There, the leading edge thrust is the Main Frontal thrust, marking the base of the Himalayan orogen against the Indus-Ganges plains (Yin, 2006). This interpretation yields ~160 km of left-slip displacement across the Coprates fault zone (Fig. 1C). Alternatively, the Thaumasia mountain belt is interpreted to have been created by the construction of a large volcanic pile (Williams et al., 2008). Both models explain the presence of a negative gravity anomaly rimming the eastern margin of the range and its topography. Regardless of the mountain-building mechanism, the location of the topographic front correlates closely to the geologic contact between the Early Hesperian volcanic unit of Hr and the Late Noachian plain units of Npl2 and Npl3 in Witbeck et al. (1991) (Fig. 1C). The contact between the Hesperian wrinkle-ridge terrane in the east and the Noachian plain deposits in the west in the map by Witbeck et al. (1991) is offset by ~160 km. This same contact corresponds to the topographic front.

Offset of a pluton. As shown in Figure 17, the north wall of easternmost Coprates Chasma is dominated by layered rocks that are locally disrupted by thrusts and folds (also see Williams et al., 2003). The layered unit terminates at the very eastern end of the north trough wall where a southward-pointing promontory occurs at the intersection between Coprates and Capri Chasmata (Fig. 1B). Williams et al. (2003) suggested that this feature is related to the presence of a mafic pluton covered by younger Early Hesperian volcanic flows. An examination of a CTX image indicates the presence of a massive unit overlain by layered rocks at this promontory. The homogeneous appearance of this massive unit is best interpreted as a pluton and thus supports the interpretation by Williams et al. (2003) (Figs. 26A and 26B).

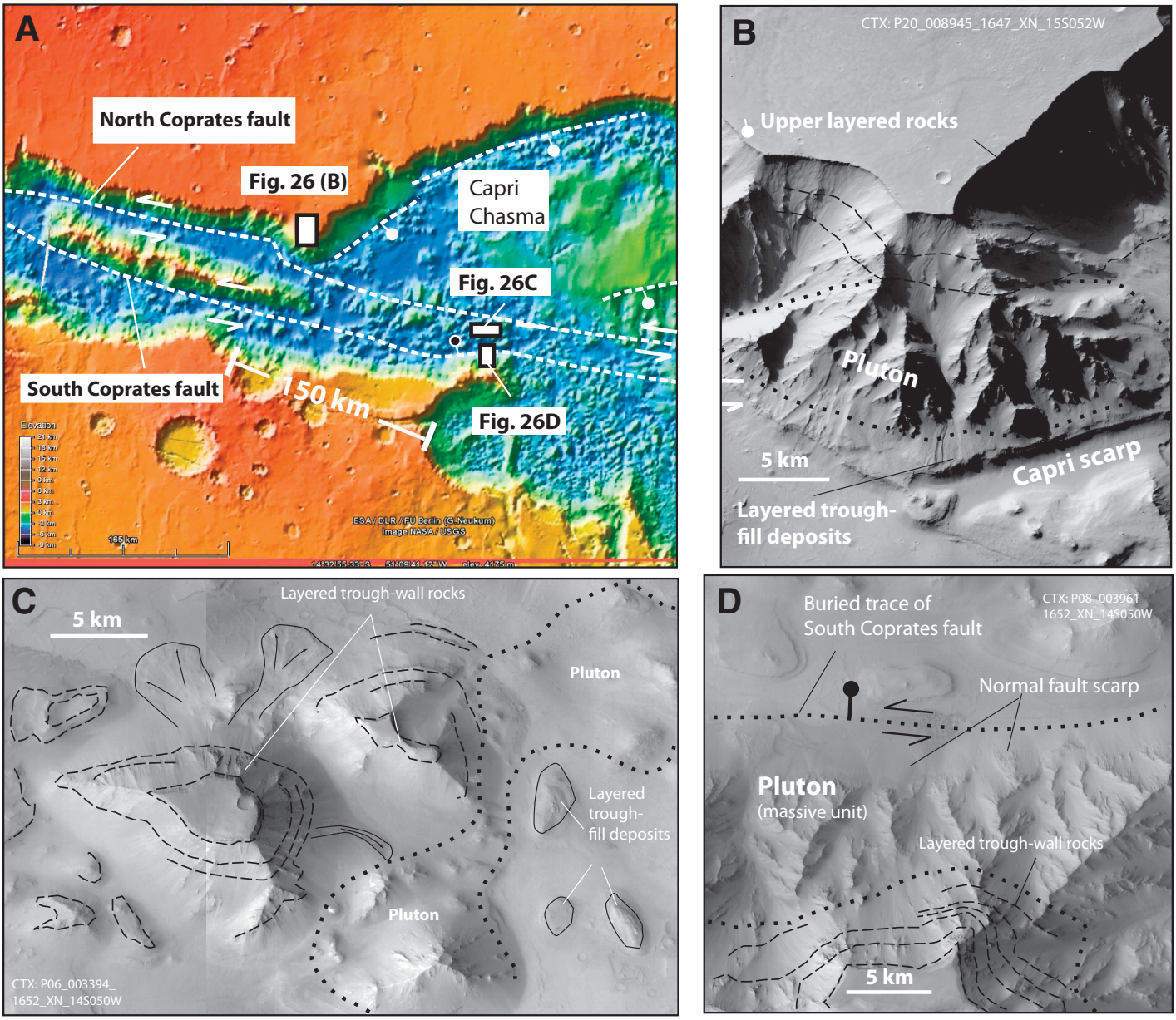

Figure 26. (A) MOLA (Mars Orbiter Laser Altimeter) topographic map of eastern Coprates and Capri Chasmata area viewed from Google Mars. Traces of the North and South Coprates faults across Capri Chasma are interpreted based on their linear morphologic expression. Locations of B, C, and D are also shown. (B) A massive unit at the easternmost end of Coprates Chasma interpreted as a pluton. Background is Context Camera (CTX) image P20_008945_1647_XN_15S052W. (C) A massive unit inside Capri Chasma interpreted as a pluton against layered Noachian–Hesperian strata to the west. Background is CTX image P06_003394_1652_XN_14S050. (D) Normal-fault scarps along a releasing bend of the South Coprates fault in Capri Chasma. The fault trace is buried below young surficial deposits. Background is CTX image P08_003961_1652_XN_14S050W.

The traces of the North Coprates fault can be followed farther eastward across Capri Chasma along a linear morphologic depression (Fig. 26A). A reconnaissance examination of the fault trace using CTX and HiRISE images indicates that the fault trace is mostly covered by unconsolidated young deposits that do not display observable deformation. As morphological expression of a terrestrial active fault is a result of competition between the rates of deformation and sedimentation/erosion, a high sedimentation/erosion rate can completely cover or remove the morphologic expression of the active structures. Thus, the buried fault and its related structures might have been covered by young sediments.

If the interpreted pluton at the mouth of Coprates Chasma is cut by the North Coprates fault, its offset counterpart should be exposed south of the fault, exhibiting similar weathering-resistant morphology. A small mesa with relics of the old plateau surface is preserved south of the projected North Coprates fault in central Capri Chasma at the eastern end of the central ridge separating the northern and southern subtrough zones of Coprates Chasma (Fig. 26C). The mesa is composed entirely of layered rocks, which are bounded to the east by an irregularly shaped, massive, and homogeneous unit that is interpreted in this study as a pluton. Correlating this pluton with the one at the eastern mount of Coprates Chasma yields ~150 km of left-slip motion along the North Coprates fault. A possible test is to use Compact Reconnaissance Imaging Spectrometer Data for Mars (CRISM) aboard the *Mars Reconnaissance Orbiter* (MRO) (Pelkey et al., 2007). Its hyperspectral imager, covering visible to near-infrared wavelengths (0.37–3.92 μm at 6.55 nm/channel), allows characterization of possible mineralogical composition of surface rock. To make this technique effective in detecting the composition of bedrock, its exposure must be pristine and free of dust cover (e.g., Flahaut et al., 2011). From the images shown in Figure 26, dust cover is clearly a problem, and a CRISM test would yield an ambiguous result.

The trace of the South Coprates fault can also be followed along a sharp linear depression in the MOLA (Mars Orbiter Laser Altimeter) topographic map into Capri Chasma (Fig. 26A). The fault makes a sharp left-step bend, along which a well-developed linear normal-fault scarp occurs at a northward-pointing promontory (Fig. 26D). This promontory, extending far into the lowlands of Capri Chasma from the plateau margin, also appears to be controlled by the presence of a pluton (Fig. 26D). The presence of normal faulting at this left-step bend is consistent with the South Coprates fault being a left-slip structure with a significant normal-slip component.

Offset of a caldera complex or an impact basin. Melas Chasma is unusual in the Valles Marineris trough system in that its trough zone is much wider and its trough margins are curvilinear rather than linear, as in all other troughs of Valles Marineris (Fig. 1). The southern trough margin is dominated by two semicircular, spoon-shaped scarps. The smaller western scarp has a radius of ~50 km and does not display scarp-parallel fractures. In contrast, the larger and eastern scarp has a radius of ~150 km and displays margin-parallel concentric-ring fractures that extend more than 100 km southward into the interior of the plateau region (Fig. 27). Note the smaller western scarp truncates the concentric-ring fractures parallel to the eastern and larger scarp (Fig. 27B) indicating that the smaller western scarp postdates the eastern scarp.

Despite its unusual geometry, the origin of Melas Chasma has not been discussed systematically in the literature. Borraccini et al. (2007) attributed the formation of concentric-ring structures to collapse of the trough walls via landsliding. However, this would require the presence of a large volume of landslide materials at the base of the scarp, an inference that is inconsistent with the mapping by Witbeck et al. (1991). Witbeck et al. (1991) showed that the area is dominated by Hesperian trough-fill layered deposits covering isolated Noachian and early Hesperian basement rocks sticking out as isolated knobs inside the Melas basin (Fig. 1). For a landslide origin, one would expect the base of the scarp to be dominated by chaotically deformed rocks from the Noachian and Early Hesperian wall rocks. Furthermore, it is also difficult to conceive how a landslide scarp can generate concentric-ring fractures that are located more than 100 km away.

It is also possible that the Melas basin originated from magmatic-driven tectonic activity, which includes uplift (Dohm et al., 2001a, 2001b, 2009). This hypothesis is consistent with the fact that the region associated with ring fractures is a broad uplift, although the uplift appears to be a broad linear ridge trending in the northwest direction. Thus, it is possible that the large circular basin originated from a highly modified volcanic center.

The semicircular Melas basin and the associated concentric-ring structures could also have been generated by impact. A pristine complex impact crater should have well-defined rims, a central peak, well-developed ejecta surrounding the impact basin, and concentric ring fractures commonly exposed by step terraces (Melosh, 1989). However, if crater basins had experienced significant erosion, their morphologic and sedimentologic expressions such as crater rims, central peaks, and ejecta could all be removed. In this case, only the concentric-ring fractures rooting deep into the crust may be preserved. This scenario implies that if the Melas basin originated from an impact, its central peak may have been eroded away by catastrophic floods traveling through Valles Marineris (e.g., Burr et al., 2009). Abundant dendritic networks of drainage channels, which dissect the southern margin of Ius Chasma, for example, display evidence of regional fluvial modification of landscape (e.g., Sharp, 1973). Such a process may have removed the inferred crater rims and the related ejecta deposits.

Admittedly, the impact-basin interpretation for the origin of Melas Chasma is tenuous. However, if the Melas basin had original circular geometry regardless of its origin, the northern rim of the circular basin is missing; the inferred circular depression may have been offset ~150 km in a left-slip sense along the North Ius–Coprates fault zone (Fig. 27). This inference is consistent with the estimates from offsets of the pluton and a thrust belt discussed earlier. The "circular-basin" hypothesis may be testable using detailed gravity modeling in the future, expanding from the work of Dohm et al. (2009).

Note that the 160 km left-slip estimate from the offset of the Thaumasia topographic front measures the total offset across the whole Coprates fault zone, while the 150 km estimate from inferred offsets of the pluton and the inferred impact or volcanic basin only measures the slip on the North Ius–Coprates fault. The difference, at a face value, between the two estimates implies that the total left-slip motion on the South Coprates fault is much less than that on the North Coprates fault (i.e., only ~10 km). The inference is clearly crude with a large uncertainty. First, the exact cutoff point of the Thaumasia topographic front at the Coprates fault zone is uncertain, because the thrust may have variable trend across the 100-km-wide trough zone that has erased or buried the thrust trace. Uncertainty with this estimate ranges 60 km to 100 km, depending on how the trend of the thrust is projected from north to south. Second, the three-dimensional shape of the offset pluton could vary considerably, leaving a large range of possibilities for the cutoff location of the pluton against the fault (e.g., the truncation points in the west and east are exposed at the same structural levels). The exposed size of the pluton of 20–30 km across may be used as a bound for this uncertainty. Third, the margins of the inferred impact basin across Melas Chasma may have been modified by later erosion; its original radius may be much smaller than its present size, which would affect the previous estimate.

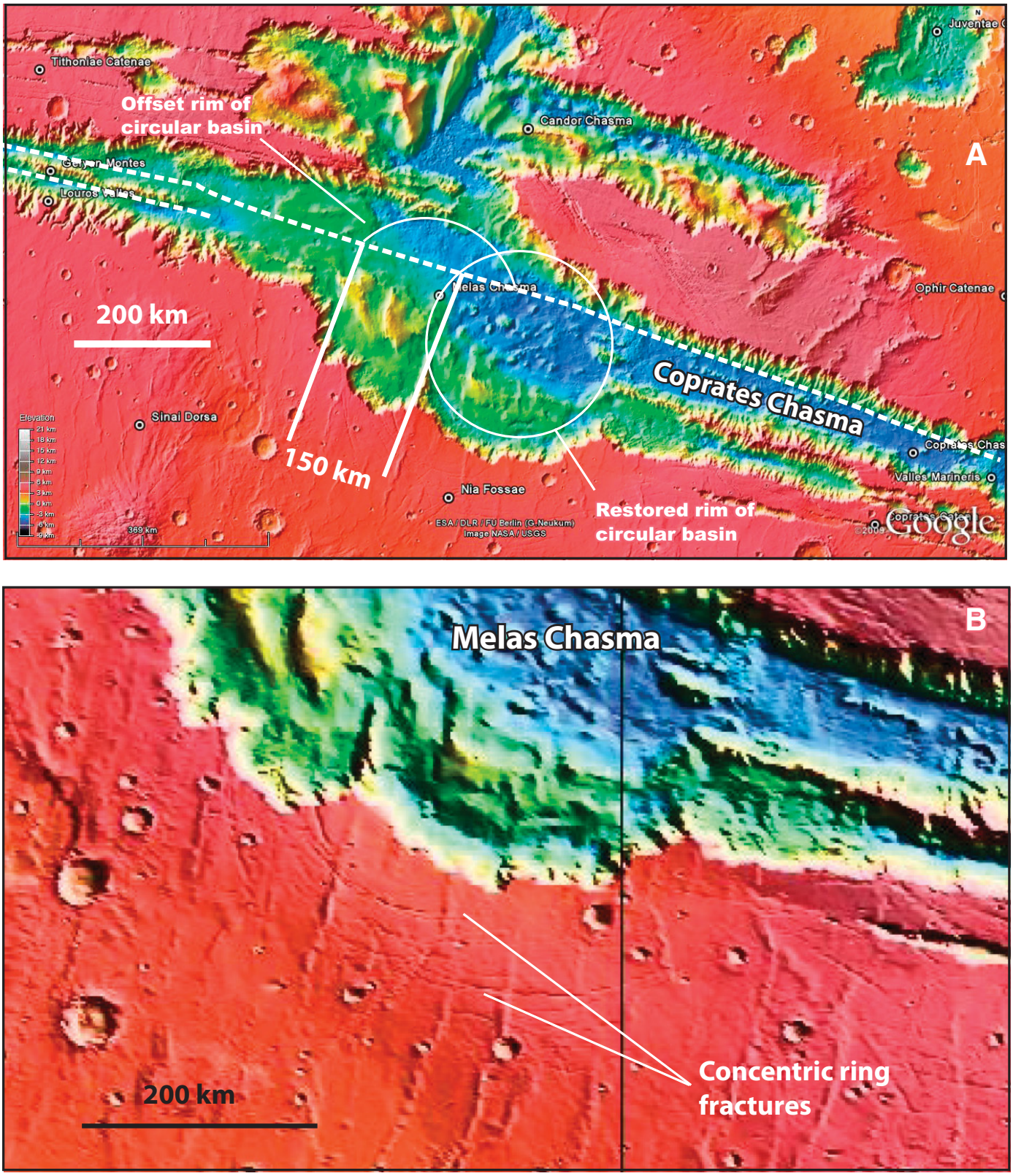

Figure 27. (A) MOLA (Mars Orbiter Laser Altimeter) topographic map of Melas Chasma viewed from Google Mars. The origin of the semicircular basin in southern Melas Chasma may have been related to deep magmatic-driven tectonic activity as proposed by Dohm et al. (2009), forming a caldera-like feature that was later offset by the Valles Marineris fault zone left laterally. (B) Close-up view of concentric ring fractures parallel to the circular scarp directly south of Melas Chasma. The ring fractures may have been related to deep magmatic processes causing local uplift, development of a landslide complex, and possibly formation of an impact basin (see text for details).

Most importantly, there is a range of possible fits up to 40–80 km for the postulated location of the northern offset impact basin. Considering these uncertainties, the estimated total slip across the Coprates fault zone is probably on the order of 160 ± 50 km. It is interesting to note that the north-trending boundary between regions with and without crustal magnetic anomalies across the Coprates fault zone is ~150 km (Purucker et al., 2000; also see fig. 1 *in* Lillis et al., 2009) which is broadly consistent with the estimate slip obtained from this study.

Termination Mechanism of Ius-Melas-Coprates Fault Zone

It has long been known that northeast-trending troughs north of and at the eastern end of the Valles Marineris trough system are controlled by normal faults (Witbeck et al., 1991; Flahaut et al., 2010). These troughs either terminate at the Valles Marineris system or are linked at its two ends (Fig. 1). A kinematic linkage between possible left-slip faulting and extension across this area and at the western end of the Valles Marineris in the Noctis Labyrinthus and Syria Planum area has been inferred by Webb and Head (2002) and Montgomery et al. (2009). However, the way in which the fault zone terminates east of the inferred Thaumasia thrust has never been discussed explicitly. Mapping by Witbeck et al. (1991) indicated that the fault bounding the northern Coprates trough links the northeast-striking trough-bounding fault of Capri Chasma (Fig. 1). As the North Coprates fault is a left-slip structure, it requires the Capri fault to be a normal fault. Indeed, the Capri fault shows prominent down-to-the-east scarps (Witbeck et al., 1991). The North and South Coprates faults also extend into Eos Chasma (Fig. 26). This interpretation requires that Eos Chasma also be bounded by normal faults. A preliminary analysis of a HiRISE image indicates this is indeed the case. As shown in Figure 28, small gullies cut by the scarp-forming faults are not offset laterally, supporting the interpretation that the structures are normal faults. Note that there are two phases of fan constructions. The first phase predates most scarp-forming faults and exhibits rough surfaces with numerous craters. The second phase is spatially restricted and displays smooth- and fine-textured surfaces along younger narrow channels. The young channel deposits drape over fault scarps, suggesting its occurrence to have postdated scarp-forming normal faulting. The spatial correlation of the channels originated from deep valleys on the north trough wall of Capri Chasma and fine-textured channel fills suggests that the fluvial sediments were delivered by surface water.

Extensional structures across the Noctis Labyrinthus and Syria Planum areas have been documented by Masson (1977), Tanaka and Davis (1988), Anderson et al. (2004), and Bistacchi et al. (2004). The area has been complexly deformed, and its northern part is marked by two sets of orthogonal fractures. Their relations to faults in Valles Marineris are all not well constrained. Additionally, there has been no systematic evaluation of the magnitude of deformation in this area. For these reasons, the way in which the Ius left-slip fault zone terminates at its western end remains unknown.

The estimated left-slip motion on the Coprates fault zone implies >100 km of east-west extension across Capri and Eos Chasmata. At this point, it is difficult to test this prediction because the older normal faults in Capri and Eos Chasma may have been buried in the rift basins, preserving only the younger and most outward trough-bounding normal faults. Perhaps detailed gravity modeling in the future could shed some light on this issue.

Regardless of the uncertainties on the magnitude of extension along northeast-striking normal faults adjacent to the Valles Marineris system, it appears that the left-slip fault zones across Valles Marineris act as a large accommodation system, which separates the more extended northern domain (Lunae Planum to Xanthe Terra) from the less extended southern domain (i.e., across the Thaumasia plateau bounded by Syria Planum to the west, Claritas Fossae to the south, and Valles Marineris to the north). The dynamic cause for the formation of this accommodation zone is currently unknown.

Palinspastic Reconstruction

Based on the estimated magnitude of slip on the Ius-Melas-Coprates fault zone, a palinspastic reconstruction of the southern Valles Marineris trough system was performed (Figs. 29A and 29B). In this reconstruction, the Ius-Melas-Coprates fault zone is treated as a left-slip transtensional structure, and the Capri and Eos faults are trough-bounding normal faults without any strike-slip motion. The latter assumption, supported by the observation made in this study, implies that the relative motion of the blocks north and south of the Ius-Melas-Coprates fault zone (i.e., the Valles Marineris–North and Valles Marineris–South blocks in Figs. 29A and 29B) is not parallel to the strike of the Ius-Melas-Coprates fault zone. The oblique angle at 136° rather than 90° requires transtensional tectonics across southern Valles Marineris. A leaky transform-fault model is proposed here for the origin of the Ius-Melas-Coprates fault zone. The fault zone separating the Valles Marineris–North and Valles Marineris–South blocks terminates at an expanding zone filled by intrusive and extrusive igneous rocks that had accommodated east-west extension in the west. In the east, the fault zone ends at the Capri-Eos rift zone, which had accommodated northwest-southeast extension. The transtensional motion and the oblique relationship between the Ius-Melas-Coprates and Capri-Eos rift fault zones is similar to the Dead Sea transform rift zone on Earth (Garfunkel, 1981).

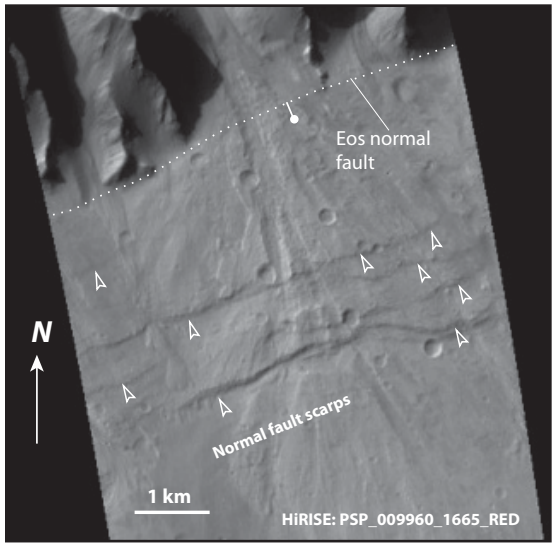

Figure 28. Normal fault scarps cutting young sediments derived from trough-wall channels along the Eos normal fault. Background is HiRISE image PSP_009960_1665_RED. See Figure 1B for location. Note that there are two phases of fan construction. The first phase predated most scarp-forming faults and exhibits rough surfaces with numerous craters. The second phase is spatially restricted and displays smooth and fine-textured surfaces along younger narrow channels. The young channel deposits drape over fault scarps, suggesting its occurrence to have postdated scarp-forming normal faulting. The spatial correlation of the channels originated from deep valleys in the mountains, and fine-textured channel fills suggest that the sediments were delivered by surface water.

Implications for the Formation Mechanism of the Closed Basin in Northern Valles Marineris

The presence of folds or tilted beds in Candor Chasma has been long known (Lucchitta et al., 1992; Lucchitta, 1999; Fueten et al., 2005,

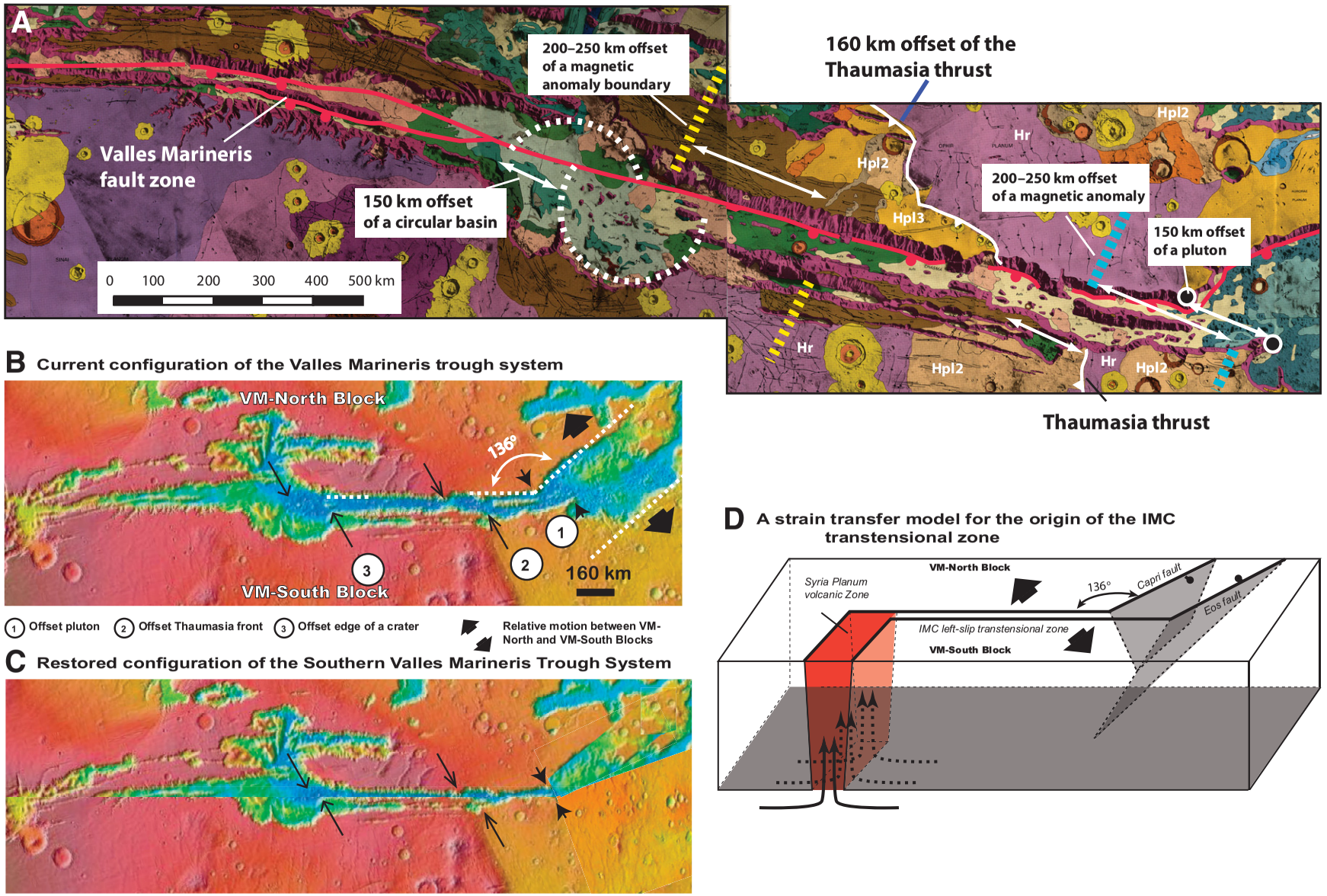

Figure 29. (A) Geologic map of Valles Marineris from Witbeck et al. (1991). Major offset geological and geophysical markers are also indicated. See text for details. (B) Current configuration of the southern Valles Marineris trough zone. (C) Restored configuration of the southern Valles Marineris trough zone after removing 150 km of left-slip motion on the Ius-Melas-Coprates fault. (D) A strain transfer model for the origin of the Ius-Melas-Coprates (IMC) fault zone in southern Valles Marineris. The fault zone separates the Valles Marineris–North block from the Valles Marineris–South block and terminates at an expanding zone filled by intrusive and extrusive igneous rocks at Syria Planum that had accommodated east-west extension in the west. In the east, motion on the fault zone is absorbed by northwest-southeast extension across the Capri-Eos rift (CER) zone. Note that the Capri normal fault is oriented at 136° rather than 90°, as would be expected for a typical transform-spreading center relationship on Earth. The transtensional motion and the oblique relationship between the Ius-Melas-Coprates and Capri-Eos rift fault zones suggest a leaky transform fault origin for the formation of the southern Valles Marineris (VM) fault zone (Garfunkel, 1981).

2006, 2008). The work by Fueten et al. (2008) regarding western Candor Chasma indicates that (1) most faults are trough-parallel and show left-slip motion when examined closely (see their fig. 8d) and (2) most folds trend northwest or west-northwest oblique to the main trend of the trough walls (see their fig. 3). These observations are similar to those made in this study and suggest that Candor Chasma may have also been induced by trough-parallel left-slip shear. Note that the most recent work by Fueten et al. (2010) also showed the presence of northwest-trending folds of interior layered sediments, which were deposited on top of bedrock of the north wall of Coprates Chasma, and thus the bedrock must have also been folded together (see fig. 10b *in* Fueten et al., 2010). This is consistent with the observed northwest-trending contractional structures from this study. A north-trending anticline was also observed nearby by Fueten et al. (2010). As this fold is located in the center of a large landslide scarp and its relation to the bedrock of the trough wall is not exposed, it is not clear if the fold was induced by landslide emplacement or was generated first by tectonic stress and was later rotated during landsliding.

Okubo et al. (2008) and Okubo (2010) also mapped part of western Candor Chasma ~80 km west of Fueten et al.'s (2008) study area. Okubo (2010) mapped a disharmonic fold complex and interpreted it to have been generated by landslide emplacement. This landslide is cut by later northwest-striking thrusts and northeast-striking normal faults oblique to the trough walls. The observations are consistent with left-slip deformation as seen in Ius and Coprates Chasmata.

Interpreting deformation across Candor Chasma to be related to left-slip shear offers a new mechanism for the formation of closed basins in Valles Marineris. Wilkins and Schultz (2003) documented the presence of normal faults bounding the north-northeast–trending blunt edges of Candor Chasma. They suggested that these blunt and short trough edges were developed by orthogonal extension, assuming the main trough-bounding faults are also normal-slip structures. However, the presence of left-slip, trough-bounding faults together with the occurrence of normal faults at the short and blunt edges of the closed basins in the Valles Marineris requires an alternative mechanism for the formation of the closed basins. In the context of left-slip tectonics, the closed basins may have developed first via formation of two parallel left-slip faults. The faults were later linked by cross faults that are normal-slip and oriented perpendicularly to the early long strike-slip faults (Fig. 3). Further development of left-slip faults with the short linking extensional structures led to the formation of pull-apart basins, which created accommodation space for trough fills. The trough-fill strata were in turn folded and faulted by broad and continued left-slip shear deformation parallel to the regional trend of the trough zones (Fig. 3).

Timing of Deformation in Valles Marineris

Left-slip structures, as examined in this study, all involve latest Amazonian (i.e., younger than 200 Ma) units of Witbeck et al. (1991) or have fresh morphologic expressions such as those exposed on plateau margins. This suggests that left-slip deformation occurred recently across the Valles Marineris. Displacement of recently emplaced landslides and fault scarps cutting into unconsolidated young talus deposits (Fig. 19) all indicate that segments of the trough-bounding faults are still active, supporting the early proposal by Blasius et al. (1977). The synchronous development of soft-sediment deformation in Amazonian strata and left-slip deformation (mostly folding) requires, at least locally, that tectonically controlled basins were saturated with water, allowing load structures and fluidized slump structures to develop (Fig. 8). This inference is consistent with the coeval development of left-slip faulting and left-lateral drainage deflection along minor left-slip faults on plateau margins north of Coprates Chasma (Fig. 24). Since the Ius-Melas-Coprates fault zone cuts the Late Hesperian upper Syria Planum Formation (unit Hsu of Witbeck et al., 1991) (Fig. 1), its initiation must be younger than the emplacement of this unit. This conclusion is consistent with the timing of faulting in the Valles Marineris established long ago by Schultz (1998). Also, since the Ius-Melas-Coprates fault zone links northeast-trending normal faults at its two ends, it appears that the eastern Tharsis Rise experienced two drastically different tectonic events: the Late Hesperian east-west contraction as expressed by the development of the Thaumasia topographic front and Late Amazonian (younger than 0.7 Ga) northwest-southeast extension linked by large-scale left-slip faulting. The Thaumasia topographic front and Coprates Rise south of Valles Marineris may have formed in the Noachian (Dohm and Tanaka, 1999) and were later offset by the Valles Marineris fault zone.

TERRESTRIAL ANALOGUE AND TECTONIC IMPLICATIONS OF LARGE-SCALE STRIKE-SLIP FAULTING

Andrews-Hanna et al. (2008) discovered Late Noachian–Early Hesperian conjugate strike-slip faults subject to east-west contraction near Sirenum Fossae west-southwest of the Tharsis Rise. These authors attributed strike-slip faulting to Tharsis loading. More recently, Anderson et al. (2012) and Karasozen et al. (2012) showed that structures controlling the Basin-and-Range–like topography across Terra Sirenum formed both prior to and during the formation of Tharsis Rise. Amazonian-aged north- and northwest-striking left-slip faults were also described in the northwestern Tharsis Rise by Forsythe and Zimbelman (1988) and Anguita et al. (2001). In the northern lowland region directly northwest of the Tharsis Rise, Okubo and Schultz (2006) documented Amazonian conjugate strike-slip faults associated with north-trending thrusts accommodating east-west contraction. Right-slip and left-slip strike-slip faults parallel to the Valles Marineris were also described by Anguita et al. (2001) and Borraccini et al. (2007) within the Thaumasia Highlands south of the Valles Marineris. Because these structures terminate or link with wrinkle ridges, they were most likely developed during the formation of the contractional wrinkle ridges as transfer faults (e.g., Borraccini et al., 2007; Golombek and Phillips, 2010) rather than related to the Late Amazonian (younger than 0.7 Ga) left-slip faulting across the southern Valles Marineris. Most interestingly, the work by Schultz (1989) directly south of the eastern end of the Coprates fault zone in Capri Chasma showed the occurrence of east-striking left-slip shear zones linking small pull-apart basins. These faults cut wrinkle ridges in the Early Hesperian volcanic flow unit (i.e., unit Hr of Witbeck et al., 1991) and are subparallel to those described in this study along the southern Valles Marineris trough system. For these reasons, the left-slip faults documented by Schultz (1989) could have been genetically related to the formation of Valles Marineris during broadly distributed left-slip shear deformation.

It appears difficult to generate a left-slip fault system with >100 km of displacement purely by flexural loading of the Tharsis Rise (Sleep and Phillips, 1985), not to mention that Valles Marineris itself is located within this supposed load. It is also unclear how such large-scale faulting, which developed so late in the Tharsis history, was induced by a plume from below (e.g., Golombek and Phillips, 2010).

A possible terrestrial analogue for the development of the Ius-Melas-Coprates fault zone may be the 1000-km-long, left-slip transtensional Dead Sea fault system on Earth (Fig. 30) (Garfunkel and Zvi Ben-Avraham, 1996). This structure bounds the western edge of the Arabian plate and forms a prominent rift zone. It links with the Red Sea spreading center in the south and the Zagros suture zone in the north (Ben-Avraham et al., 2008; Yin, 2010a). Although the main motion across the fault zone

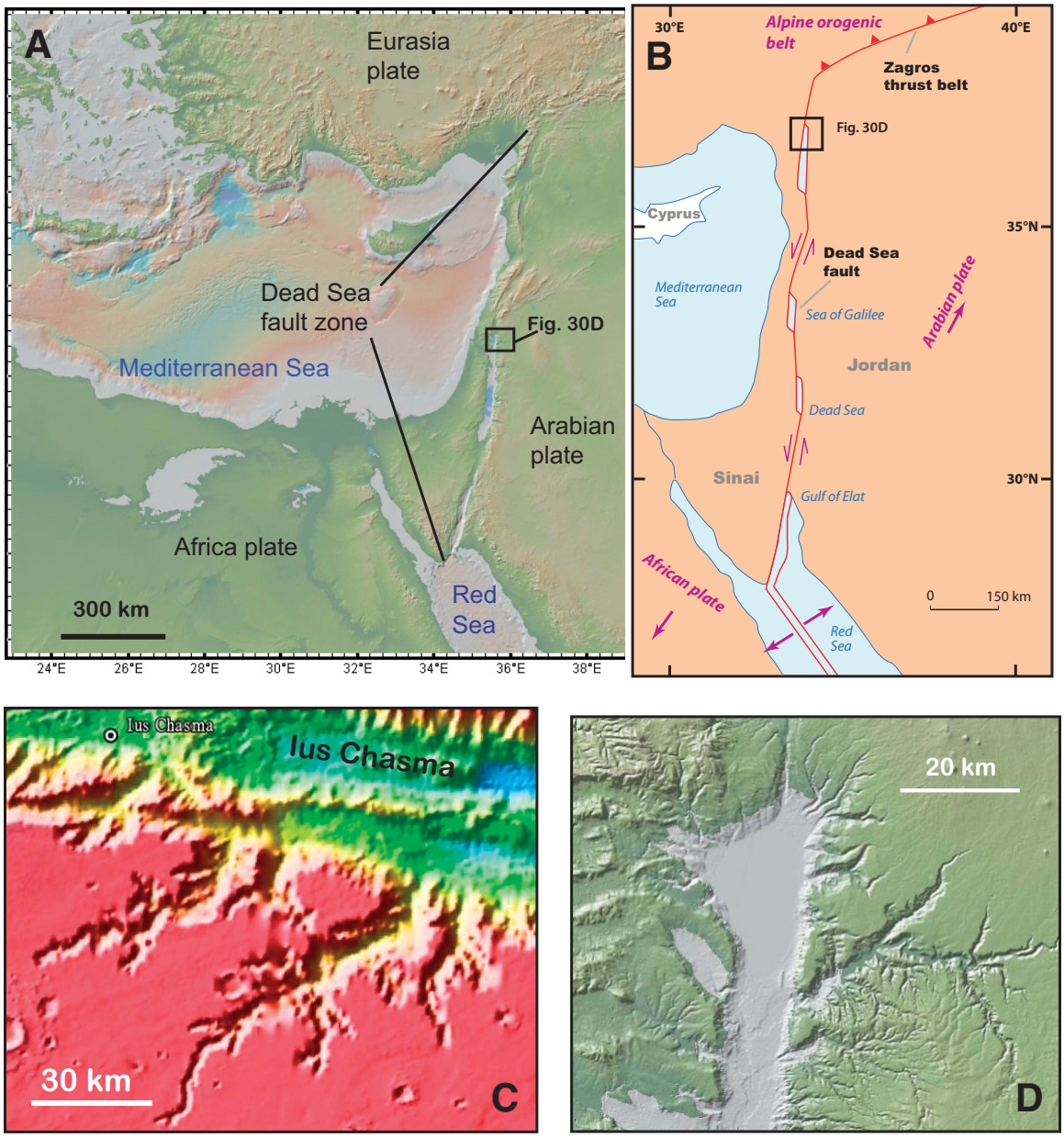

Figure 30. (A) Topographic expression of the Dead Sea fault zone separating the African plate from Arabian plate. (B) Tectonic map of the Dead Sea fault zone adopted from Ben-Avraham et al. (2008). (C) Drainage pattern on the southern margin of western Ius Chasma. (D) Drainage pattern across the central segment of the Dead Sea rift zone.

has a left-slip motion of ~100 km (Garfunkel and Zvi Ben-Avraham, 1996), faults in this left-slip zone also have significant normal-slip components (Ben-Avraham et al., 2008). This led to the development of the prominent trough zone along the Dead Sea fault system (Fig. 30). It is interesting to note that the nearby drainage patterns next to the Dead Sea transtensional zone are remarkably similar to those observed near Ius Chasma (Fig. 30).

Inspired by the work of Garfunkel and Zvi Ben-Avraham (1996), a three-dimensional structural model is proposed for the current deformation of the Ius-Melas-Coprates trough zone (Fig. 31). In this model, the trough-bounding faults could either be pure normal-slip faults or oblique left-slip transtensional faults. It is likely that the axis of the trough zone is dominated by a distributed left-slip fault zone. Motion on this fault produced the observed en echelon folds and thrusts, and locally extensional structures such as joints and normal faults. This model provides a new structural framework that accounts for the early observations of rift deformation across Valles Mariners and at same time is capable of explaining diverse structures that have been observed in the trough zones and on the plateau margins in this study.

As the Dead Sea fault zone is an undisputed plate boundary, the similarity between this fault system and the Ius-Melas-Coprates fault zone raises the question about the tectonic nature of large-scale strike-slip faulting on Mars. As the radius of Mars (3397 km) is about one half of the radius of Earth (6378 km), the obtained slip of the Ius-Melas-Coprates fault zone may be

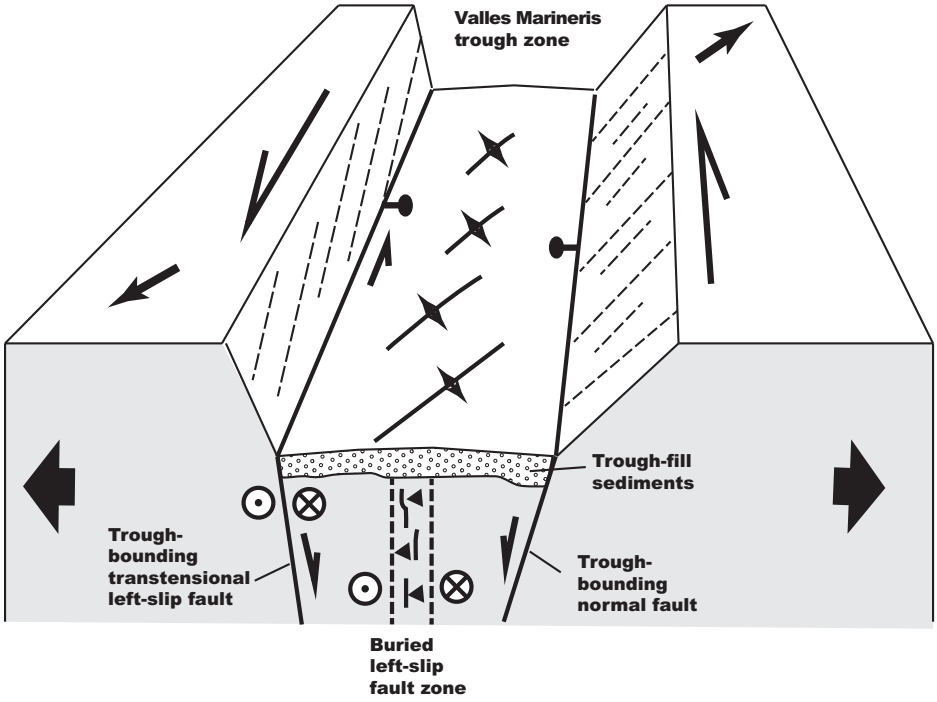

Figure 31. A three-dimensional structural model for the Ius-Melas-Coprates fault zone. Notice that the fault zone consists of multiple faults, and a trough zone that may be bounded on one side by a normal fault and another side by a strike-slip fault due to strain partitioning of transtensional tectonics. A strike-slip shear zone may also lie below a thick section of trough-fill sediments.

normalized to the surface area of the planet in order to compare to slip magnitudes on major transform faults on Earth. The ratio of fault slip versus planet area is 3.5 m/km^2 for the Ius-Melas-Coprates fault zone, assuming its total slip is 150 km. This value is significantly greater than 1.3 m/km^2 for the Dead Sea fault (~105 km total slip; see Garfunkel and Zvi Ben-Avraham, 1996) and slightly greater than 3.2 m/km^2 for the southern San Andreas fault (~255 km of total slip; see Oskin et al., 2001). This simple comparison suggests that the magnitude of horizontal motion on the Ius-Melas-Coprates fault zone is significant. The consistent displacement of 150–160 km across the Ius-Melas-Coprates fault zone over a distance of 500 km indicates that the regions bounded by the fault behave as rigid blocks, and their kinematics can be quantified in a similar way to the classic description of plate kinematics on Earth (McKenzie and Morgan, 1969). As Mars is considered to be a planet without plate tectonics in the past 4 billion years (e.g., Golombek and Phillips, 2010), Late Amazonian (i.e., younger than 700 Ma) large-scale (>100 km) strike-slip faulting as inferred from this study begs the question of why such a process would have occurred at all on the planet. This issue may be addressed by systematic examination of the tectonic origin of the Tharsis Rise, within which the Ius-Melas-Coprates fault investigated here has developed (Yin, 2010b, 2011).

CONCLUSIONS

This study focuses on the structural geology of Ius and Coprates Chasmata and the nearby plateau margins in the southern Valles Marineris trough system. Its main result is that the trough zones and trough margins of the two chasmata have experienced trough-parallel left-slip deformation and trough-perpendicular extension. This style of deformation is expressed by the presence of trough-bounding left-slip and normal faults, formation of northeast-trending extensional structures (joints), northwest-trending contractional structures (thrusts and folds), and locally developed minor northwest-trending left-slip structures either across the plateau margins or within trough zones. Crosscutting relationships of the left-slip structures indicate their development in the Late Amazonian (younger than 0.7 Ga), though perhaps complex tectonic fabrics may have existed in the region dating back to the Noachian Period. Locally, trough-bounding faults may still be active, as they cut young surface deposits and offset recently emplaced landslides with smooth surfaces that have nearly no impact craters. The presence of syntectonic and intraformational soft-sediment structures in Upper Amazonian strata and the coeval development of left-slip transtensional faulting and drainage deflections all suggest that surface water was present during the tectonic formation of the southern Valles Marineris trough system. Displacement on individual left-slip faults varies from a few meters to ~13 km. The total estimated left-slip motion across the Ius-Melas-Coprates fault zone is 160 ± 50 km, 150 ± 30 km, and 150 ± 30 km based on the offsets of (1) the Thaumasia thrust, (2) an inferred circular basin, and (3) a pluton. The 150–160 km of left-slip motion on the Ius-Melas-Coprates fault zone may have been accommodated by NW-SE extension across Noctis Labyrinthus and Syria Planum in the west and extension across Capri and Eos Chasmata in the east. This interpretation, together with the known regional tectonic history, suggests that the eastern Tharsis Rise experienced two major episodes of tectonism: (1) Late Hesperian east-west contraction forming widespread wrinkle ridges in the northern and eastern Tharsis Rise and (2) Late Amazonian left-slip faulting linking extension across the central and northeastern parts of the Tharsis Rise. The discovery of a large-scale (>2000 km in length and >100 km in total slip) and rather narrow (<50 km in width) strike-slip fault zone begs the question of why such a structure, typically associated with plate tectonics on Earth, was developed on Mars.

ACKNOWLEDGMENTS

This study was partially supported by a grant from the Tectonics Program of the U.S. National Science Foundation on the mechanics of V-shaped conjugate strike-slip systems. I thank Robert Lovdahl, who critically read early drafts of the manuscript and made many useful suggestions. I am especially grateful for the critical and constructive comments made by James Dohm. I also thank Ernst Hauber, Frank Fueten, Nicolas Mangold, Donna Jurdy, and an anonymous reviewer of the journal. Their comments helped to improve the scientific content and clarity of the paper.

REFERENCES CITED

Adams, J.B., Gillespie, A.R., Jackson, M.P.A., Montgomery, D.R., Dooley, T.P., Combe, J.-P., and Schreiber, B.C., 2009, Salt tectonics and collapse of Hebes Chasma, Valles Marineris, Mars: Geology, v. 37, p. 691–694, doi:10.1130/G30024A.1.

Anderson, R.C., Dohm, J.M., Golombek, M.P., Haldemann, A.F.C., and Franklin, B.J., 2001, Primary centers and secondary concentrations of tectonic activity through time in the western hemisphere of Mars: Journal of Geophysical Research, v. 106, p. 20,563–20,585, doi:10.1029/2000JE001278.

Anderson, R.C., Dohm, J.M., Haldemann, A.F.C., Hare, T.M., and Baker, V.R., 2004, Tectonic histories between Alba Patera and Syria Planum, Mars: Icarus, v. 171, p. 31–38, doi:10.1016/j.icarus.2004.04.018.

Anderson, R.C., Dohm, J.M., Robbins, S., Hynek, B., and Andrews-Hanna, J., 2012, Terra Sirenum: Window into pre-Tharsis and Tharsis phases of Mars evolution: Houston, Texas, Lunar and Planetary Institute, Lunar Planetary Science Conference XXXXIII, abstract 2803 (CD-ROM).

Andrews-Hanna, J.C., Zuber, M.T., and Hauck, S.A., II, 2008, Strike-slip faults on Mars: Observations and implications for global tectonics and geodynamics: Journal of Geophysical Research, v. 113, E08002, doi:10.1029/2007JE002980.

Anguita, F., Farelo, A.-F., Lopez, V., Mas, C., Munoz-Espadas, M.-J., Marquez, A., and Ruiz, J., 2001, Tharsis dome, Mars: New evidence for Noachian–Hesperian thick-skin and Amazonian thin-skin tectonics: Journal of Geophysical Research, v. 106, p. 7577–7589.

Anguita, F., Fernandez, C., Cordero, G., Carrasquilla, S., Anguita, J., Nunez, A., Rodriguez, S., and Garcia, J., 2006, Evidences for a Noachian–Hesperian orogeny in Mars: Icarus, v. 185, p. 331–357, doi:10.1016/j.icarus.2006.07.026.

Banerdt, W.B., Golombek, M.P., and Tanaka, K.L., 1992, Stress and tectonics on Mars, *in* Keiffer, H.H., et al., eds., Mars: Tucson, University of Arizona Press, p. 249–297.

Barnouin-Jha, O.S., Baloga, S., and Glaze, L., 2005, Comparing landslides to fluidized crater ejecta on Mars: Journal of Geophysical Research, v. 110, E04010, doi:10.1029/2003JE002214.

Ben-Avraham, Z., Garfunkel, Z., and Lazar, M., 2008, Geology and evolution of the Southern Dead Sea fault with emphasis on subsurface structure: Annual Review of Earth and Planetary Sciences, v. 36, p. 357–387, doi:10.1146/annurev.earth.36.031207.124201.

Bistacchi, N., Massironi, M., and Baggio, P., 2004, Large-scale fault kinematic analysis in Noctis Labyrinthus (Mars): Planetary and Space Science, v. 52, p. 215–222, doi:10.1016/j.pss.2003.08.015.

Blasius, K.R., Cutts, J.A., Guest, J.E., and Masursky, H., 1977, Geology of Valles Marineris: First analysis of imaging from the *Viking 1 Orbiter* primary mission: Journal of Geophysical Research, v. 82, p. 4067–4091, doi:10.1029/JS082i028p04067.

Borraccini, F., Di Achille, G., Ori, G.G., and Wezel, F.G., 2007, Tectonic evolution of the eastern margin of the Thaumasia Plateau (Mars) as inferred from detailed structural mapping and analysis: Journal of Geophysical Research, v. 112, E05005, doi:10.1029/2006JE002866.

Burbank, D.W., and Anderson, R.S., 2001, Tectonic Geomorphology: Oxford, UK, Blackwell, 274 p.

Burr, D.M., Carling, P.A., and Baker, V.R., 2009, Megaflooding on Earth and Mars: Cambridge, UK, Cambridge University Press, 330 p.

Carr, M.H., 1974, Tectonism and volcanism of the Tharsis region of Mars: Journal of Geophysical Research, v. 79, p. 3943–3949.

Christensen, P.R., Bandfield, J.L., Hamilton, V.E., Ruff, S.W., Kieffer, H.H., Titus, T.N., Malin, M.C., Morris, R.V., Lane, M.D., Clark, R.L., Jakosky, B.M., Mellon, M.T., Pearl, J.C., Conrath, B.J., Smith, M.D., Clancy, R.T., Kuzmin, R.O., Roush, T., Mehall, G.L., Gorelick, N., Bender, K., Murray, K., Dason, S., Greene, E., Silverman, S., and Greenfield, M., 2000, *Mars Global Surveyor* Thermal Emission Spectrometer Experiment: Investigation description and surface science results: Journal of Geophysical Research–Planets, v. 106, p. 23,823–23,872.

Courtillot, V.E., Allegre, C.J., and Mattauer, M., 1975, On the existence of relative lateral motions on Mars: Earth and Planetary Science Letters, v. 25, p. 279–285, doi:10.1016/0012-821X(75)90242-3.

Davis, P.A., and Golombek, M.P., 1990, Discontinuities in the shallow Martian crust at Lunae, Syria, and Sinai Plana: Journal of Geophysical Research, v. 95, p. 14,231–14,248, doi:10.1029/JB095iB09p14231.

Davis, P.A., Tanaka, K.L., and Golombek, M.P., 1995, Topography of closed depressions, scarps, and grabens in the north Tharsis region of Mars: Implications for shallow crustal discontinuities and graben formation: Icarus, v. 114, p. 403–422, doi:10.1006/icar.1995.1071.

Dohm, J.M., and Tanaka, K.L., 1999, Geology of the Thaumasia region, Mars: Plateau development, valley origins, and magmatic evolution: Planetary and Space Science, v. 47, p. 411–431, doi:10.1016/S0032-0633(98)00141-X.

Dohm, J.M., Ferris, J.C., Baker, V.R., Anderson, R.C., Hare, T.M., Strom, R.G., Barlow, N.G., Tanaka, K.L., Klemaszewski, J.E., and Scott, D.H., 2001a, Ancient drainage basin of the Tharsis region, Mars: Potential source for outflow channel systems and putative oceans or paleolakes: Journal of Geophysical Research, v. 106, p. 32,943–32,958.

Dohm, J.M., Tanaka, K.L., and Hare, T.M., 2001b, Geologic Map of the Thaumasia Region of Mars: U.S. Geological Survey Map I-2650.

Dohm, J.M., Baker, V.R., Maruyama, S., and Anderson, R.C., 2007, Traits and evolution of the Tharsis superplume, Mars, *in* Yuen, D.A., Maruyama, S., Karato, S.-I., and Windley, B.F., eds., Superplumes: Beyond Plate Tectonics: Dordrecht, The Netherlands, Springer, p. 523–537.

Dohm, J.M., Williams, J.P., Anderson, R.C., Ruiz, J., McGuire, P.C., Komatsu, G., Davil, A.F., Ferris, J.C., Schulze-Makuch, D., Baker, V.R., Boynton, W.V., Fairen, A.G., Hare, T.M., Miyamoto, H., Tanaka, K.L., and Wheelock, S.J., 2009, New evidence for a magmatic influence on the origin of Valles Marineris, Mars: Journal of Volcanology and Geothermal Research, v. 185, p. 12–27, doi:10.1016/j.jvolgeores.2008.11.029.

Flahaut, J., Quantin, C., Allemand, P., and Thomas, P., 2010, Morphology and geology of the ILD in Capri/Eos Chasma (Mars) from visible *Icarus* and infrared data: Icarus, v. 207, p. 175–185, doi:10.1016/j.icarus.2009.11.019.

Flahaut, J., Mustard, J.F., Quantin, C., Clenet, H., Allemand, P., and Thomas, P., 2011, Dikes of distinct composition intruded into Noachian-aged crust exposed in the walls of Valles Marineris: Geophysical Research Letters, v. 38, L15202, doi:10.1029/2011GL048109.

Forsythe, R.D., and Zimbelman, R., 1988, Is the Gordii Dorsum escarpment on Mars an exhumed transcurrent fault?: Nature, v. 336, p. 143–146, doi:10.1038/336143a0.

Frey, H., 1979, Martian canyons and African rifts: Structural comparisons and implications: Icarus, v. 37, p. 142–155, doi:10.1016/0019-1035(79)90122-2.

Fueten, F., Stesky, R.M., and MacKinnon, P., 2005, Structural attitudes of large scale layering in Valles Marineris, Mars, calculated from Mars Orbiter Laser Altimeter data and Mars Orbiter Camera imagery: Icarus, v. 175, p. 68–77, doi:10.1016/j.icarus.2004.11.010.

Fueten, F., Stesky, R.M., MacKinnon, P.G., Hauber, E., Gwinner, K., Scholten, F., Zegers, T., and Neukum, G., 2006, A structural study of an interior layered deposit in southwestern Candor Chasma, Valles Marineris, Mars, using high resolution stereo camera data from *Mars Express*: Geophysical Research Letters, v. 33, L07202, doi:10.1029/2005GL025035.

Fueten, F., Stesky, R.M., MacKinnon, P., Hauber, E., Zegers, T., Gwinner, K., Scholten, F., and Neukum, G., 2008, Stratigraphy and structure of interior layered deposits in west Candor Chasma, Mars, from High Resolution Stereo Camera HRSC stereo imagery and derived elevations: Journal of Geophysical Research, v. 113, E10008, doi:10.1029/2007JE003053.

Fueten, F., Racher, H., Stesky, R.M., MacKinnon, P., Hauber, E., McGuire, P.C., Zegers, T., and Gwinner, K., 2010, Structural analysis of interior layered deposits in Northern Coprates Chasma, Mars: Earth and Planetary Science Letters, v. 294, p. 343–356, doi:10.1016/j.epsl.2009.11.004.

Fueten, F., Flahaut, J., Le Deit, L., Stesky, R., Hauber, E., and Gwinner, K., 2011, Interior layered deposits within a perched basin, southern Coprates Chasma, Mars: Evidence for their formation, alteration, and erosion: Journal of Geophysical Research, v. 116, E02003, doi:10.1029/2010JE003695.

Garfunkel, Z., 1981, Internal structure of the Dead Sea leaky transform (rift) in relation to plate kinematics: Tectonophysics, v. 80, p. 81–108, doi:10.1016/0040-1951(81)90143-8.

Garfunkel, Z., and Zvi Ben-Avraham, Z., 1996, The structure of the Dead Sea basin: Tectonophysics, v. 266, p. 155–176, doi:10.1016/S0040-1951(96)00188-6.

Golombek, M.P., and Phillips, R.J., 2010, Mars tectonics, *in* Watters, T.R., and Schultz, R.A., eds., Planetary Tectonics: New York, Cambridge University Press, p. 183–232.

Jackson, M.P.A., Adam, J.B., Dooley, T.P., Gillespie, A.R., and Montgomery, D.R., 2011, Modeling the collapse of Hebes Chasma, Valles Marineris, Mars: Geological Society of America Bulletin, v. 123, p. 1596–1627, doi:10.1130/B30307.1.

Karasozen, E., Andrews-Hanna, J.C., Dohm, J.M., and Anderson, R.C., 2012, The formation mechanism of the south Tharsis Ridge belt, Mars: Houston, Texas, Lunar and Planetary Institute, Lunar Planetary Science Conference XXXXIII, abstract 2592 (CD-ROM).

Lillis, R.J., Dufek, J., Bleacher, J.E., and Manga, M., 2009, Demagnetization of crust by magmatic intrusion near the Arsia Mons volcano: Magnetic and thermal implications for the development of the Tharsis province, Mars: Journal of Volcanology and Geothermal Research, v. 185, p. 123–138, doi:10.1016/j.jvolgeores.2008.12.007.

Lucchitta, B.K., 1979, Landslides in Valles Marineris, Mars: Journal of Geophysical Research, v. 84, p. 8097–8113.

Lucchitta, B.K., 1999, Geologic Map of Ophir and Central Candor Chasmata of Mars: U.S. Geological Survey Miscellaneous Investigation Series Map, I-2568, scale 1:500,000.

Lucchitta, B.K., McEwen, A.S., Clow, G.D., Geissler, P.E., Singer, R.B., Schultz, R.A., and Squyres, S.W., 1992, The canyon system of Mars, *in* Kieffer, H.H., et al., eds., Mars: Tucson, University of Arizona Press, p. 453–492.

Lucchitta, B.K., Isbell, N.K., and Howington-Kraus, A., 1994, Topography of Valles Marineris: Implications for erosional and structural history: Journal of Geophysical Research, v. 99, p. 3783–3798.

Malin, M.C., and Edgett, K.S., 2001, *Mars Global Surveyor* Mars Observer Camera: Interplanetary cruise through primary mission: Journal of Geophysical Research, v. 106, p. 23,429–23,570, doi:10.1029/2000JE001455.

Malin, M.C., Bell, J.F., III, Cantor, B.A., Caplinger, M.A., Calvin, W.M., Clancy, R.T., Edgett, K.S., Edwards, L., Haberle, R.M., James, P.B., Lee, S.W., Ravine, M.A., Thomas, P.C., and Wolff, M.J., 2007, Context Camera Investigation on board the *Mars Reconnaissance Orbiter*: Journal of Geophysical Research, v. 112, E05S04, doi:10.1029/2006JE002808.

Mangold, N., Quantin, C., Ansan, V., Delacourt, C., and Allemand, P., 2004, Evidence for precipitation on Mars from dendritic valleys in the Valles Marineris area: Science, v. 305, p. 78–81, doi:10.1126/science.1097549.

Mangold, N., Ansan, V., Masson, P., Quantin, C., and Neukum, G., 2008, Geomorphic study of fluvial landforms on the northern Valles Marineris plateau, Mars: Journal of Geophysical Research, v. 113, E08009, doi:10.1029/2007JE002985.

Masek, J.G., Isacks, B.L., Fielding, E.J., and Browaeys, J., 1994, Rift flank uplift in Tibet: Evidence for a viscous lower crust: Tectonics, v. 13, p. 659–667.

Masson, P., 1977, Structure pattern analysis of Noctis Labyrinthus–Valles Marineris regions of Mars: Icarus, v. 30, p. 49–62, doi:10.1016/0019-1035(77)90120-8.

Masson, P., 1985, Origin and evolution of Valles Marineris region of Mars: Advances in Space Research, v. 5, p. 83–92, doi:10.1016/0273-1177(85)90244-3.

McEwen, A.S., 1989, Mobility of large rock avalanches: Evidence from Valles Marineris: Marine Geology, v. 17, p. 1111–1114.

McEwen, A.S., Eliason, E.M., Bergstrom, J.W., Bridges, N.T., Hansen, C.J., Delamere, W.A., Grant, J.A., Gulick, V.C., Herkenhoff, K.E., Keszthelyi, L., Kirk, R.L., Mellon, M.T., Squyres, S.W., Thomas, N., , and Weitz, C.M., 2007, *Mars Reconnaissance Orbiter*'s High Resolution Imaging Science Experiment (HiRISE): Journal of Geophysical Research, v. 112, E05S02, doi:10.1029/2005JE002605.

McEwen, A.S., Banks, M.E., Baugh, N., Becker, K., Boyd, A., Bergstrom, J.W., Beyer, R.A., Bortolini, E., Bridges, N.T., Byrne, S., Castalia, B., Chuang, F.C., Crumpler, L.S., Daubar, I., Davatzes, A.K., Deardorff, D.G., DeJong, A., Delamere, W.A., Dobrea, E.N., Dundas, C.M., Eliason, E.M., Espinoza, Y., Fennema, F., Fishbaugh, K.E., Forrester, T., Geissler, P.E., Grant, J.A., Griffes, J.L., Grotzinger, J.P., Gulick, V.C., Hansen, C.J., Herkenhoff, K.E., Heyd, R., Jaeger, W.L., Jones, D., Kanefsky, B., Keszthelyi, L., King, R., Kirk, R.L., Kolb, K.L., Lasco, J., Lefort, A., Leis, R., Lewis, K.W., Martinez-Alonsom, S., Mattson, S., McArthur, G., Mellonm, M.T., Metz, J.M., Milazzo, M.P., Milliken, R.E., Motazedian, T., Okubo, C.H., Ortiz, A., Philippoff, A.J., Plassmann, J., Polit, A., Russell, P.S., Schaller, C., Searlsm, M.L., Spriggs, T., Squyres, S.W., Tarr, S., Thomas, N., Thomson, B.J., Tornabene, L.L., Van Houten, C., Verba, C., Weitz, C.M., and Wray, J.J., 2010, The High Resolution Imaging Science Experiment (HiRISE) during MRO's Primary Science Phase (PSP): Icarus, v. 205, p. 2–37, doi:10.1016/j.icarus.2009.04.023.

McKenzie, D., and Morgan, W.J., 1969, Evolution of triple junctions: Nature, v. 224, p. 125–133, doi:10.1038/224125a0.

McKenzie, D., and Nimmo, F., 1999, The generation of Martian floods by the melting of ground ice above dykes: Nature, v. 397, p. 231–233, doi:10.1038/16649.

Mège, D., and Masson, P., 1996a, Amounts of crustal stretching in Valles Marineris, Mars: Planetary and Space Science, v. 44, p. 749–781, doi:10.1016/0032-0633(96)00013-X.

Mège, D., and Masson, P., 1996b, A plume tectonics model for the Tharsis province, Mars: Planetary and Space Science, v. 44, p. 1499–1546.

Mège, D., Cook, A.C., Garel, E., Lagabrielle, Y., and Cormier, M.H., 2003, Volcanic rifting at Martian grabens: Journal of Geophysical Research, v. 108, doi:10.1029/2002JE001852.

Melosh, H.J., 1989, Impact Cratering: A Geologic Process (Oxford Monographs on Geology and Geophysics): Oxford, UK, Oxford University Press, 396 p.

Metz, J., Grotzinger, J., Okubo, C., and Milliken, R., 2010, Thin-skinned deformation of sedimentary rocks in Valles Marineris, Mars: Journal of Geophysical Research, v. 115, E11004, doi:10.1029/2010JE003593.

Montgomery, D.R., and Gillespie, A., 2005, Formation of Martian outflow channels by catastrophic dewatering of evaporite deposits: Geology, v. 33, p. 625–628, doi:10.1130/G21270.1.

Montgomery, D.R., Som, S.M., Jackson, M.P.A., Schreiber, B.C., Gillespie, A.R., and Adams, J.B., 2009, Continental-scale salt tectonics on Mars and the origin of Valles Marineris and associated outflow channels: Geological Society of America Bulletin, v. 121, p. 117–133.

Nahm, A.L., and Schultz, R.A., 2010, Evaluation of the orogenic belt hypothesis for the formation of the Thaumasia Highlands, Mars: Journal of Geophysical Research, v. 115, E04008, doi:10.1029/2009JE003327.

Naylor, M.A., Mandl, G., and Sijpesteijn, C.H.K., 1986, Fault geometries in basement-induced wrench faulting under different initial stress states: Journal of Structural Geology, v. 8, p. 737–752, doi:10.1016/0191-8141(86)90022-2.

Neukum, G., Jaumann, R., and the HRSC Co-Investigator and Experiment Team, 2004, The High Resolution Stereo Camera of *Mars Express*, *in* Wilson, A., and Chicarro, A., eds., *Mars Express*: The Scientific Payload: ESA SP-1240, Noordwijk, The Netherlands, European Space Agency Publications Division, p. 17–35.

Okubo, C.H., 2010, Structural geology of Amazonian-aged layered sedimentary deposits in southwest Candor Chasma, Mars: Icarus, v. 207, p. 210–225, doi:10.1016/j.icarus.2009.11.012.

Okubo, C.H., and McEwen, A.S., 2007, Fracture-controlled paleo-fluid flow in Candor Chasma, Mars: Science, v. 315, p. 983–985, doi:10.1126/science.1136855.

Okubo, C.H., and Schultz, R.A., 2006, Variability in Early Amazonian Tharsis stress state based on wrinkle ridges and strike-slip faulting: Journal of Structural Geology, v. 28, p. 2169– 2181.

Okubo, C.H., Lewis, K.L., McEwen, A.S., Kirk, R.L., and the HiRISE Team, 2008, Relative age of interior layered deposits in southwest Candor Chasma based on high-resolution structural mapping: Journal of Geophysical Research, v. 113, doi:10.1029/ 2008JE003181.E12002.

Oskin, M., Stock, J., and Martín-Barajas, A., 2001, Rapid localization of Pacific–North America plate motion in the Gulf of California: Geology, v. 29, p. 459–462, doi:10.1130/0091-7613(2001)029<0459:RLOPNA>2.0.CO;2.

Pelkey, S.M., Mustard, J.F., Murchie, S., Clancy, R.T., Wolff, M., Smith, M., Milliken, R., Bibring, J.-P., Gendrin, A., Poulet, F., Langevin, Y., and Gondet, B., 2007, CRISM multispectral summary products: Parameterizing mineral diversity on Mars from reflectance: Journal of Geophysical Research, v. 112, E08S14, doi:10.1029/2006JE002831.

Peulvast, J.P., and Masson, P.L., 1993, Melas Chasma: Morphology and tectonic patterns in Central Valles Marineris (Mars): Earth, Moon, and Planets, v. 61, p. 219–248, doi:10.1007/BF00572246.

Peulvast, J.P., Mège, D., Chiciak, J., Costard, F., and Masson, P.L., 2001, Morphology, evolution and tectonics of Valles Marineris wall slopes (Mars): Geomorphology, v. 37, p. 329–352, doi:10.1016/S0169-555X(00)00085-4.

Plescia, J.B., and Saunders, R.S., 1982, Tectonic history of the Tharsis region: Journal of Geophysical Research, v. 87, no. 9, p. 775–779, 791.

Purucker, M., Ravat, D., Frey, H., Voorhies, C., Sabaka, T., and Acuña, M., 2000, An altitude-normalized magnetic map of Mars and its interpretation: Geophysical Research Letters, v. 27, p. 2449–2452.

Quantin, C., Allemand, P., Mangold, N., and Delacourt, C., 2004, Ages of Valles Marineris (Mars) landslides and implications for canyon history: Icarus, v. 172, p. 555–572, doi:10.1016/j.icarus.2004.06.013.

Schultz, R.A., 1989, Strike-slip faulting of ridged plains near Valles Marineris, Mars: Nature, v. 341, p. 424–426, doi:10.1038/341424a0.

Schultz, R.A., 1991, Structural development of Coprates Chasma and western Ophir Planum, central Valles Marineris rift, Mars: Journal of Geophysical Research, v. 96, p. 22,777–22,792, doi:10.1029/91JE02556.

Schultz, R.A., 1995, Gradients in extension and strain at Valles Marineris, Mars: Planetary and Space Science, v. 43, p. 1561–1566.

Schultz, R.A., 1998, Multiple-process origin of Valles Marineris basins and troughs, Mars: Planetary and Space Science, v. 46, p. 827–834, doi:10.1016/S0032-0633(98)00030-0.

Schultz, R.A., 2000, Fault-population statistics at the Valles Marineris extensional province, Mars: Implications for segment linkage, crustal strains, and its geodynamical development: Tectonophysics, v. 316, p. 169–193, doi:10.1016/S0040-1951(99)00228-0.

Schultz, R.A., and Lin, J., 2001, Three-dimensional normal faulting models of the Valles Marineris, Mars, and geodynamic implications: Journal of Geophysical Research, v. 106, p. 16,549–16,566, doi:10.1029/2001JB000378.

Schultz, R.A., and Tanaka, T.L., 1994, Lithospheric-scale buckling and thrust structures on Mars: The Coprates Rise and south Tharsis ridge belt: Journal of Geophysical Research, v. 99, no. 8, p. 371–378, 385.

Schultz, R.A., Hauber, E., Kattenhorn, S.A., Okubo, C.H., and Watters, T.R., 2010, Interpretation and analysis of planetary structures: Journal of Structural Geology, v. 32, p. 855–875, doi:10.1016/j.jsg.2009.09.005.

Sengör, A.M.C., and Jones, I.C., 1975, A new interpretation of Martian tectonics with special reference to the Tharsis region: Geological Society of America Abstracts with Programs, v. 7, p. 1264.

Sharp, R.P., 1973, Mars: Troughed terrain: Journal of Geophysical Research, v. 78, p. 4063–4072.

Sieh, K.E., and Jahns, R.H., 1984, Holocene activity on the San Andreas fault at Wallace Creek, California: Geological Society of America Bulletin, v. 95, p. 883–896, doi:10.1130/0016-7606(1984)95<883:HAOTSA>2.0.CO;2.

Sleep, N.H., and Phillips, R.J., 1985, Gravity and lithospheric stress on the terrestrial planets with reference to the Tharsis region of Mars: Journal of Geophysical Research, v. 90, p. 4469–4489.

Spagnuolo, M.G., Rossi, A.P., Hauber, E., and van Gasselt, S., 2011, Recent tectonics and subsidence on Mars: Hints from Aureum Chaos: Earth and Planetary Science Letters, v. 312, p. 13–21, doi:10.1016/j.epsl.2011.09.052.

Spencer, J.R., and Fanale, F.P., 1990, New models for the origin of Valles Marineris closed depressions: Journal of Geophysical Research, v. 95, p. 14,301–14,313, doi:10.1029/JB095iB09p14301.

Sylvester, A.G., 1988, Strike-slip faults: Geological Society of America Bulletin, v. 100, p. 1666–1703, doi:10.1130/0016-7606(1988)100<1666:SSF>2.3.CO;2.

Tanaka, K.L., and Davis, P.A., 1988, Tectonic history of the Syria Planum province of Mars: Journal of Geophysical Research, v. 93, p. 14,893–14,917, doi:10.1029/JB093iB12p14893.

Tanaka, K.L., and MacKinnon, D.K., 2000, Pseudokarst origin for Valles Marineris [abs.]: Houston, Texas, Lunar and Planetary Institute, Lunar and Planetary Space Science Conference 1780.

Tanaka, K.L., Skinner, J.A., Crumpler, L.S., and Dohm, J.M., 2009, Assessment of planetary geologic mapping techniques for Mars using terrestrial analogues: The SP Mountain area of the San Francisco volcanic field, Arizona: Planetary and Space Science, v. 57, p. 510–532, doi:10.1016/j.pss.2008.06.012.

Webb, B.M., and Head, J.W., 2001, Noachian tectonics of Syria Planum and the Thaumasia Plateau: GSA Annual Meeting, November 5–8, 2001 Boston, Massachusetts, paper number 132-0.

Webb, B.M., and Head, J.W., 2002, Noachian tectonics of Syria Planum and the Thaumasia Plateau: Houston, Texas, Lunar and Planetary Institute, Lunar and Planetary Science Conference XXXIII, p. 1358.

Wilkins, S.J., and Schultz, R.A., 2003, Cross faults in extensional settings: Stress triggering, displacement localization, and implications for the origin of blunt troughs at Valles Marineris, Mars: Journal of Geophysical Research, v. 108, 5056, doi:10.1029/2002JE001968.

Williams, J.P., Paige, D.A., and Manning, C.E., 2003, Layering in the wall rock of Valles Marineris: Intrusive and extrusive magmatism: Journal of Geophysical Research, v. 30, doi:10.1029/2003GL017662.

Williams, J.P., Nimmo, F., Moore, W.B., and Paige, D.A., 2008, The formation of Tharsis on Mars: What the line-of-sight gravity is telling us: Journal of Geophysical Research, v. 113, E10011, doi:10.1029/2007JE003050.

Wise, D.U., Golombek, M.P., and McGill, G.E., 1979, Tharsis province of Mars: Geologic sequence, geometry, and a deformation mechanism: Icarus, v. 38, p. 456–472, doi:10.1016/0019-1035(79)90200-8.

Witbeck, N.E., Tanaka, K.L., and Scott, D.H., 1991, The Geologic Map of the Valles Marineris Region, Mars: U.S. Geological Survey Miscellaneous Investigations Series Map I-2010, scale 1:2,000,000.

Yeats, R.S., Sieh, K., and Allen, C.R., 1997, The Geology of Earthquakes: New York, Oxford University Press, 568 p.

Yin, A., 2006, Cenozoic evolution of the Himalayan orogen as constrained by along-strike variations of structural geometry, exhumation history, and foreland sedimentation: Earth-Science Reviews, v. 76, p. 1–131, doi:10.1016/j.earscirev.2005.05.004.

Yin, A., 2010a, Cenozoic tectonics of Asia: A preliminary synthesis: Tectonophysics, v. 488, p. 293–325, doi:10.1016/j.tecto.2009.06.002.

Yin, A., 2010b, Evidence for a crustal-scale thrust belt along the northwestern margin of the Tharsis Rise: Implications for possible plate subduction on Mars: Abstract EP21A-0734 presented at 2010 Fall Meeting, American Geophysical Union, San Francisco, Calif., 13–17 Dec.

Yin, A., 2011, Impact-induced subduction and slab rollback for the tectonic origin of the Tharsis Rise on Mars: Houston, Texas, Lunar and Planetary Institute, Lunar and Planetary Science Conference XLII, p. 1525.

MANUSCRIPT RECEIVED 14 DECEMBER 2011
REVISED MANUSCRIPT RECEIVED 1 APRIL 2012
MANUSCRIPT ACCEPTED 3 APRIL 2012

Printed in the USA